

Generation and Characterization of Spred-2 Knockout Mice

Dissertation zur Erlangung des
naturwissenschaftlichen Doktorgrades
der Bayerischen Julius-Maximilians-Universität Würzburg

vorgelegt von

**Dr. med. Karin Andrea Bundschu
(geb. Geis)**

aus Frankfurt/Main

Würzburg 2005

Eingereicht am:

Mitglieder der Promotionskommission:

Vorsitzender:

Gutachter: Prof. Dr. U. Walter

Gutachter: Prof. Dr. G. Krohne

Betreuer: Dr. Kai Schuh

Tag des Promotionskolloquiums:

Doktorurkunde ausgehändigt am:

The present study was performed under supervision of Dr. Kai Schuh in the group of Prof. Dr. med. Ulrich Walter in the Institute of Clinical Biochemistry and Pathobiochemistry at the Julius-Maximilians-University of Würzburg. The dissertation was part of the MD/PhD program, organized by the IZKF of the University of Würzburg.

Declaration:

Hereby, I declare that the submitted dissertation was completed by myself and no others and that I have not used any sources or materials other than those enclosed.

Moreover, I declare that the following dissertation has not been submitted further in this form or any other form and has not been used for obtaining any other equivalent qualification in any other organization.

Additionally, other than this degree I have not applied or will attempt to apply for any other degree or qualification in relation to this work.

Würzburg,

(Dr. med. Karin Andrea Bundschu)

In love
for
my husband

Christoph

and
our son

Sebastian

TABLE OF CONTENTS

1. SUMMARY	5
2. ZUSAMMENFASSUNG	7
3. INTRODUCTION.....	9
3.1. EVH-1 (ENA/VASP HOMOLOGY-1) DOMAIN PROTEINS.....	9
3.1.1. <i>Ena/VASP proteins</i>	9
3.1.2. <i>WASP proteins</i>	10
3.1.3. <i>Homer/Vesl proteins</i>	10
3.2. SPROUTY PROTEINS.....	11
3.3. SPRED PROTEINS.....	13
3.4. THE MAP KINASE SIGNALING PATHWAY	15
3.5. KNOCKOUT STRATEGIES IN MICE	16
3.6. BONE GROWTH AND FGF-MEDIATED ENDOCHONDRAL OSSIFICATION	19
3.7. AIM OF THE WORK.....	21
4. MATERIAL AND METHODS	22
4.1. MOLECULAR-BIOLOGICAL METHODS.....	22
4.1.1. <i>Database analyzes of the mouse genome</i>	22
4.1.2. <i>Isolation of plasmid DNA</i>	22
4.1.3. <i>Isolation of genomic DNA of mouse tails and ES cells</i>	22
4.1.4. <i>DNA gel electrophoresis</i>	22
4.1.5. <i>DNA purification of agarose gels</i>	22
4.1.6. <i>Purification of PCR products</i>	23
4.1.7. <i>Cutting DNA by endonucleases</i>	23
4.1.8. <i>Dephosphorylation of DNA 5' overhangs</i>	23
4.1.9. <i>Ligation/cloning of DNA fragments in a plasmid vector</i>	23
4.1.10. <i>T/A-cloning</i>	23
4.1.11. <i>Generation of competent bacterias</i>	23
4.1.12. <i>Transformation of competent bacterias</i>	24
4.1.13. <i>Verification of inserts</i>	24
4.1.14. <i>LA- (long and accurate) PCR</i>	25
4.1.15. <i>Sequencing (Sanger method)</i>	25
4.1.16. <i>Southern blot analyzes</i>	25

4.1.17.	<i>Cloning of Spred-1 and Spred-2 full length cDNA in TOPO2.1</i>	26
4.1.18.	<i>Cloning of Spred-1 and Spred-2 cDNA in pcDNA3.1/Myc-His</i>	27
4.1.19.	<i>RNA extraction of mouse tissues</i>	27
4.1.20.	<i>DNA removal of RNA extracts</i>	28
4.1.21.	<i>RT- (Reverse Transcription) PCR</i>	28
4.1.22.	<i>Northern blot analyzes</i>	28
4.2.	HISTOLOGICAL METHODS	29
4.2.1.	<i>Paraffin sections and HE staining</i>	29
4.2.2.	<i>Immunohistochemistry</i>	29
4.2.3.	<i>X-Gal staining</i>	30
4.2.4.	<i>Toluidine staining</i>	30
4.3.	CELL CULTURE	31
4.3.1.	<i>Transfection of HEK 293 cells</i>	31
4.3.2.	<i>Primary mouse chondrocyte culture</i>	31
4.4.	PROTEIN BIOCHEMICAL METHODS	31
4.4.1.	<i>Protein isolation of mouse tissues</i>	31
4.4.2.	<i>Western blot analyzes</i>	32
4.4.3.	<i>Coomassie-blue protein staining of SDS gels</i>	32
4.5.	GENERATION AND AFFINITY PURIFICATION OF POLYCLONAL SPRED-1 AND SPRED-2 SPECIFIC ANTIBODIES	33
4.5.1.	<i>Expression and preparation of GST-Spred-1 and GST-Spred-2 fusion proteins</i>	33
4.5.2.	<i>Coupling of proteins to NHS-HiTrap columns</i>	35
4.5.3.	<i>Immunization of rabbits</i>	35
4.5.4.	<i>Affinity purification of antisera</i>	35
4.6.	GENERATION OF SPRED-2 KNOCKOUT MICE USING A GENE TRAP MODEL	37
4.6.1.	<i>Gene trapping and Southern blot analysis</i>	37
4.6.2.	<i>Mouse breeding</i>	38
4.6.3.	<i>Genotyping of mice</i>	38
4.7.	GENERATION OF SPRED-1 AND SPRED-2 KNOCKOUT MICE USING GENE TARGETING VECTORS	39
4.7.1.	<i>General strategy</i>	39
4.7.2.	<i>Cloning of Spred-1 and Spred-2 gene targeting vectors</i>	40
4.7.3.	<i>Optimization of the embryonic stem (ES) cell screening PCR</i>	45

Table of Contents

4.7.4. <i>Electroporation and selection of ES cells</i>	46
4.7.5. <i>PCR screening of ES cells for homologous recombination events</i>	46
4.7.6. <i>Cre-recombinase treatment of ES cells and PCR screening of different Cre-recombinase events for complete and conditional knockouts</i>	47
4.8. MOUSE PHYSIOLOGY	48
4.8.1. <i>Hormone measurements in mice</i>	48
4.8.2. <i>Blood glucose measurements in mice</i>	48
4.8.3. <i>Blood cell counts in mice</i>	48
4.8.4. <i>Bleeding time measurements in mice</i>	48
4.8.5. <i>Bleeding volume measurements in mice</i>	48
4.8.6. <i>Heart parameter measurements in mice</i>	49
4.8.7. <i>Estimation of bone lengths</i>	49
4.8.8. <i>Statistical analyzes</i>	49
4.9. ADDITIONAL MATERIALS AND EQUIPMENT.....	49
5. RESULTS	50
5.1. GENERATION OF SPRED-2-DEFICIENT MICE USING A GENE TRAP APPROACH.....	50
5.2. SPRED-2-DEFICIENCY IN KNOCKOUT MICE ON RNA AND PROTEIN LEVEL	52
5.3. GENE DISRUPTION OF SPRED-2 CAUSES ACHONDROPLASIA-LIKE DWARFISM	54
5.4. UNALTERED HORMONE AND BLOOD TESTS IN SPRED-2 ^{-/-} MICE.....	56
5.5. SPRED-2 PROMOTER ACTIVITY IN BONES.....	57
5.6. EXPRESSION OF ENDOGENOUS SPRED-2 IN CHONDROCYTES.....	59
5.7. NARROWER GROWTH-PLATE AND REDUCED TIBIA LENGTH IN SPRED-2 ^{-/-} MICE	59
5.8. INCREASED AND EARLIER ERK PHOSPHORYLATION IN SPRED-2 ^{-/-} CHONDROCYTES AFTER FGF STIMULATION.....	61
5.9. INCREASED BLEEDING IN SPRED-2 ^{-/-} MICE	63
5.10. TISSUE-SPECIFIC SPRED-2 PROMOTER ACTIVITY CHARACTERIZED BY A GENE TRAP APPROACH.....	64
5.10.1. <i>Physiological Spred-2 promoter activity in newborn mice</i>	65
5.10.2. <i>Physiological Spred-2 promoter activity in adult mice</i>	68
5.11. SPRED-1 AND SPRED-2 RNA EXPRESSION PATTERN IN MICE.....	72
5.12. SPRED-1 AND SPRED-2 PROTEIN EXPRESSION PATTERN IN MICE.....	74
5.12.1. <i>Generation of Spred-1- and Spred-2-specific antibodies</i>	74
5.12.2. <i>Spred-1/-2 protein expression pattern in fetal and adult mice</i>	75

Table of Contents

5.13. GENERATION OF SPRED-1 AND SPRED-2 KNOCKOUT MICE USING GENE TARGETING VECTORS	76
6. DISCUSSION	81
6.1. DOMAIN STRUCTURE OF SPRED-2	81
6.2. PHYSIOLOGICAL FUNCTION OF SPRED.....	81
6.3. THE SPRED-2 GENE TRAP MODEL	82
6.4. SPRED-2 KNOCKOUT MICE	83
6.5. SPRED-2 LOSS OF FUNCTION CAUSES DWARFISM.....	84
6.6. <i>SPRED-2</i> PROMOTER ACTIVITY	86
6.7. ENHANCED BLEEDING OF <i>SPRED-2</i> ^{-/-} MICE.....	88
6.8. OUTLOOK.....	89
7. REFERENCES.....	91
8. ABBREVIATIONS.....	100
9. ACKNOWLEDGMENTS	102
10. CURRICULUM VITAE	103
11. PUBLICATIONS.....	104

1. Summary

Spreds are a new Sprouty-related family of membrane-associated proteins inhibiting the MAPK signaling pathway by interacting with Ras and Raf-1. Different studies have already demonstrated the inhibitory function of Spreds in cell culture systems, but the in vivo function of Spreds in the whole organism was still unclear.

Therefore, **Spred-2 knockout mice** were generated using a gene trap approach. The Spred-2 deficiency was verified on RNA and protein levels and the lack of functional Spred-2 protein in mice caused a **dwarf phenotype** similar to achondroplasia, the most common form of human dwarfism. Spred-2^{-/-} mice showed reduced growth and body weight, they had a shorter tibia length and showed narrower growth plates as compared to wildtype mice. Spred-2 promoter activity and protein expression were detected in chondrocytes, suggesting an important function of Spred-2 in chondrocytes and bone development. Furthermore, stimulation of chondrocytes with different FGF concentrations showed earlier and augmented ERK phosphorylation in Spred-2^{-/-} chondrocytes as compared to Spred-2^{+/+} chondrocytes. These observations suggest a model, in which loss of Spred-2 inhibits bone growth by inhibiting chondrocyte differentiation through upregulation of the MAPK signaling pathway.

An additional observation of Spred-2^{-/-} mice was an increased **bleeding phenotype** after injuries, whereas the bleeding volume was extremely enlarged and the bleeding time was significantly prolonged. So far, hypertension as cause could be excluded, but to discover the physiological reasons for this phenotype, the different steps of the clotting cascade have to be investigated further. As the Spred-2 promoter activity studies demonstrated a high and specific Spred-2 expression in vascular smooth muscle cells and previous studies showed an interaction of Spreds with RhoA, a key regulator of vascular smooth muscle contraction, the regulation of smooth muscle contractility seems to be a good candidate of this phenomenon.

Moreover, **Spred-1 and Spred-2 specific antibodies** were generated as important tools to study the protein expression patterns in mice.

Furthermore, nothing was known about the **Spred-2 promoter** region and its regulation. Here, a detailed in situ analysis of the physiological promoter activity profile in the gene trapped Spred-2-deficient mouse strain was shown. In these mice, the beta-galactosidase and neomycin fusion gene (β -geo) of the gene trap vector

was brought under control of the endogenous *Spred-2* promoter, giving the opportunity to monitor *Spred-2* promoter activity in practically every organ and their corresponding sub-compartments. X-Gal staining of sections of newborn and adult mice revealed 1) a very high *Spred-2* promoter activity in neural tissues and different glands; 2) a high activity in intestinal and uterine smooth muscle cells, and kidney; 3) a low activity in heart, testis, lung, and liver; 4) an almost lacking activity in skeletal muscle and spleen, and 5) very interestingly, a very distinct and strong activity in vascular smooth muscle cells. Moreover, comparison of newborn and adult mouse organs revealed a nearly congruent *Spred-2* promoter activity. These detailed data provide valuable information for further studies of the physiological functions of *Spred-2* in organs showing strong *Spred-2* promoter activity, which are in most of these organs still unclear.

Finally, gene targeting vectors for *Spred-1* and *Spred-2* were cloned, to generate **ES cells with a floxed exon 2 of the *Spred-1* and *Spred-2* gene**, respectively. Now, these ES cells are valuable tools to establish conditional knockout mice. This is of major interest to investigate the physiological tissue specific functions of *Spred-1* and *Spred-2*, especially if the double knockout mice are not viable.

2. Zusammenfassung

Spreds gehören zu einer neuen Sprouty-verwandten Familie Membran-assoziiierter Proteine, welche den MAPK Signalweg hemmen, indem sie mit Ras und Raf-1 interagieren. In Zellkultur-Systemen haben mehrere Studien bereits die hemmende Funktion von Spred gezeigt, aber die in vivo Funktion im Gesamtorganismus blieb bisher noch ungeklärt.

In dieser Arbeit wurden deshalb **Spred-2 Knockout Mäuse** mithilfe eines Gene-trap Ansatzes generiert. Die Spred-2 Eliminierung konnte auf RNA- und Protein-Ebene bestätigt werden, und der Verlust des funktionsfähigen Spred-2 Proteins führte zu einem Achondroplasie-ähnlichen **Zwergenwuchs**, der häufigsten Form des menschlichen Zwergenwuchses. Die Spred-2^{-/-} Mäuse waren insgesamt kleiner und hatten ein vermindertes Körpergewicht. Im Vergleich zu Wildtyp Mäusen war die Tibia-Länge verkürzt und die Wachstumsfugen verschmälert. In Knorpelzellen wurde sowohl die Aktivität des *Spred-2* Promoters, als auch eine Spred-2 Proteinexpression detektiert, was auf eine wichtige Funktion in Knorpelzellen und bei der Knochenentwicklung schließen lässt. Im Vergleich zu Spred-2^{+/+} Knorpelzellen zeigte die Stimulierung von Spred-2^{-/-} Knorpelzellen mit verschiedenen FGF-Konzentrationen eine frühere und verstärkte ERK-Phosphorylierung. Diese Beobachtungen deuten auf einen Mechanismus hin, bei dem der Verlust von Spred-2 das Knochenwachstum hemmt, indem die Knorpel-Differenzierung durch eine Hochregulation des MAPK Signalweges gehemmt wird.

Spred-2^{-/-} Mäuse zeigten nach Verletzungen eine **erhöhte Blutungsneigung**, wobei das verlorene Blutvolumen extrem vergrößert und die Blutungszeit signifikant verlängert war. Bisher konnte Bluthochdruck als Ursache ausgeschlossen werden, aber die verschiedenen Stufen der Blutstillung und Gerinnungskaskade müssen noch weiter untersucht werden, um die physiologischen Ursachen dieses Phänotyps ausfindig machen zu können. Untersuchungen der *Spred-2* Promotoraktivität zeigten eine starke und spezifische Expression von Spred-2 in glatten Gefäßmuskelzellen. Außerdem zeigten vorhergehende Studien eine Interaktion von Spreds mit RhoA, einem Hauptregulator der Kontraktion glatter Gefäßmuskelzellen. Diesen Beobachtungen zufolge scheint die Regulation der Kontraktilität glatter Gefäßmuskelzellen ein guter Kandidat für dieses Phänomen zu sein.

Weiterhin wurden **Spred-1 und Spred-2 spezifische Antikörper** hergestellt, die als elementares Werkzeug zur Untersuchung der Proteinexpression in der Maus notwendig waren.

Bisher gab es noch keine Informationen über die Region und Regulation des **Spred-2 Promotors**. In dieser Arbeit wurde eine detaillierte in situ Analyse des physiologischen Promotoraktivitätsprofils in der Spred-2 defizienten Mauslinie gezeigt, die mit Hilfe des Gene-trap Vektors generiert wurde. In diesen Mäusen wurde das beta-Galaktosidase/Neomycin-Resistenz Fusionsgen (β -geo) des Gene-trap Vektors unter die Kontrolle des endogenen *Spred-2* Promotors gebracht, und lieferte damit die Möglichkeit, die *Spred-2* Promotoraktivität in praktisch jedem Organ und den zugehörigen Teilstrukturen beobachten zu können. X-Gal Färbungen von Gewebeschnitten neugeborener und erwachsener Mäuse zeigten 1) eine sehr starke *Spred-2* Promotoraktivität in Nervengeweben und verschiedenen Drüsen; 2) eine starke Aktivität in glatten Muskelzellen des Uterus und Verdauungstraktes, sowie der Nieren; 3) eine geringe Aktivität in Herz, Hoden, Lunge und Leber; 4) eine fast fehlende Aktivität in Skelettmuskeln und Milz; und 5) interessanterweise eine starke und eindeutige Aktivität in glatten Gefäßmuskelzellen. Außerdem zeigte der Vergleich zwischen Organen von neugeborenen und erwachsenen Mäusen ein fast identisches Aktivitätsmuster. Diese detaillierten Daten liefern hilfreiche Informationen für weitere Untersuchungen der physiologischen Funktionen von Spred-2 vor allem in Organen mit starker *Spred-2* Promotoraktivität, die in den meisten dieser Organe bisher noch immer ungeklärt sind.

Zuletzt wurden in dieser Arbeit noch Gene-targeting Vektoren für Spred-1 und Spred-2 kloniert, die zur Generierung von **embryonalen Stammzellen mit gefloxtem Exon 2 des Spred-1 bzw. Spred-2 Gens** genutzt wurden. Diese embryonalen Stammzellen stehen nun als wertvolle Grundlage zur Etablierung von konditionalen Knockout Mäusen zur Verfügung. Dies ist von großem Interesse, um die physiologischen gewebespezifischen Funktionen von Spred-1 und Spred-2 zu untersuchen, vor allem wenn die Doppel-Knockout Mäuse nicht lebensfähig sein sollten.

3. Introduction

3.1. EVH-1 (Ena/VASP homology-1) domain proteins

So far, various protein families harboring an N-terminal EVH-1 domain have been described. The EVH-1 domain is a homologous region of 110 amino acids, first described in proteins of the Ena/VASP family (Gertler et al., 1996). It was presented that the EVH-1 domain specifically binds proteins with proline-rich sequences (Ball et al., 2002; Niebuhr et al., 1997; Reinhard et al., 1995; Reinhard et al., 1996). Moreover, this domain plays an important role in the integrity of the cytoskeleton, actin-based cell motility, and postsynaptic signal transduction. The four known EVH-1 families are: 1) Ena/VASP proteins, 2) Wiskott-Aldrich-Syndrome proteins (WASP), 3) Homer/Vesl proteins, and 4) Spred proteins. SMIF (Smad4-interacting transcriptional co-activator), a regulator of the TGF- β signaling pathway, is an additional protein with an N-terminal EVH-1 domain, but not directly connected to one of these four families (Bai et al., 2002; Callebaut, 2002).

3.1.1. Ena/VASP proteins

VASP (vasodilator stimulated phosphoprotein), a 46 KDa membrane associated protein, was first characterized in platelets as proline-rich substrate of cAMP- and cGMP-dependent protein kinases (Halbrugge and Walter, 1989). Beside the high expression in platelets, VASP is present in almost all mammalian cell-types (Halbrugge and Walter, 1989; Reinhard et al., 1999). VASP is associated to actin filaments and localized in focal adhesion complexes, dynamic membrane regions, leading membrane areas of non-epithelial cells, and cell/cell contacts of MDCK cells (Haffner et al., 1995). Biochemical and functional analyzes observed Ena/VASP proteins as important regulators of actin filament structures and associated processes like cell adhesion and cell motility (Machesky, 2000; Reinhard et al., 1999). During different biological processes, Ena/VASP proteins seem to act not only as positive but also as negative regulators (for review see (Machesky, 2000; Reinhard et al., 2001).

Additional members of the Ena/VASP family are the Drosophila gene product **enabled** (ena), its mammalian homologue **Mena** (mammalian enabled), and the Caenorhabditis elegans homologue **unc34**; because all their domains show high sequence similarities compared to the VASP protein (Gertler et al., 1996; Haffner et

al., 1995; Lanier and Gertler, 2000). *Drosophila* *ena* is important to build axonal structures, and homozygous *ena* mutations are lethal with defects in the embryonic CNS (Gertler et al., 1996). *Mena* and *unc34* are as well localized in axonal growing cones, and therefore, probably –like *ena*– important during neuronal development (Colavita and Culotti, 1998; Gertler et al., 1996). Another *Ena/VASP* family member is the murine **Evl** (Enabled/Vasodilator-stimulated phosphoprotein like) (Gertler et al., 1996).

The EVH-1 domain of the *Ena/VASP* family recognizes an E/DFPPPPXD/E (FP₄) binding motif (Niebuhr et al., 1997), which is different compared to the other EVH-1 domains (Klostermann et al., 2000). This motif is established as functional protein binding site, present in the focal adhesion proteins vinculin (Niebuhr et al., 1997; Reinhard et al., 1996) and zyxin (Niebuhr et al., 1997), the axon guidance protein roundabout (*Robo*) (Bashaw et al., 2000), lipoma preferred partner (*LPP*) (Petit et al., 2000), semaphorin 6A-1 (*Sema6A-1*) (Klostermann et al., 2000), T-cell signaling protein Fyn-binding protein/SLP-76-associated protein (*Fyb/SLAP*) (Krause et al., 2000), and the surface protein *ActA* of *Listeria* (Niebuhr et al., 1997).

3.1.2. WASP proteins

In most of the *WASP* family members, the conserved N-terminal EVH-1 domain begins just after 40 amino acids and is usually named WH1 (*WASP* homology 1) domain. *WASP* is a cytoplasmic protein and is suggested to regulate the actin cytoskeleton structure (Snapper et al., 1998). Direct interaction with the small GTPase *Cdc42* enables *WASP* proteins to stimulate actin polymerization by activating the *Arp2/3* complex (Zigmond, 2000). After injection of *WASP* in adherent cells, it localizes at focal adhesion contacts, suggesting recognition of different binding motifs of the *WASP* WH1-domain as compared to the *VASP* EVH-1 domain (Niebuhr et al., 1997; Symons et al., 1996). Nevertheless, it is known that the WH1-domain binds to proline-rich regions of *WIP* (*WASP* interacting proteins) and different mutations of the *WASP* WH-1-domain cause the *Wiskott-Aldrich* syndrome, an X-chromosomal immunodeficiency (Martinez-Quiles et al., 2001; Ramesh et al., 1997).

3.1.3. Homer/Vesl proteins

Vesl 1S, *Vesl 1L*, and *Vesl 2* (*Vesl*: VASP/ena related gene up-regulated during seizure and LTP) are members of the *Homer/Vesl* family, whereas “*Homer*” is sometimes used as a synonym for *Vesl 1S* (Kato et al., 1998). *Homer/Vesl* proteins

contain an N-terminal EVH-1 domain as well and are localized at specialized actin-rich postsynaptic sites of neuronal dendritic cells (Xiao et al., 2000). Even if the EVH-1 domains of Mena, EVL, and Homer are structurally very similar, Homer rather binds ligands with the PPSPF motif than with the (F/L/W/Y)PPPP motif (Beneken et al., 2000). The EVH-1 domain of Homer interacts with metabotropic glutamate receptors, IP3 (Inositol-3-phosphate)-receptors and Shank, and has therefore an adapter role in connecting different molecules that regulate the crosstalk of synapses. Moreover, the Homer-Shank complex could play a major role in dendritic cell formation, which is an important process for learning and memory and is at least partly regulated by F-actin (Sala et al., 2001) (for detailed review see (Renfranz and Beckerle, 2002)).

3.2. Sprouty proteins

All known Sprouty proteins (one *Drosophila*, three human, four murine, and two avian Sproutys) contain a highly conserved cysteine-rich 110 amino acids domain at the C-terminus (Chambers and Mason, 2000; de Maximy et al., 1999; Hacohen et al., 1998; Minowada et al., 1999; Tefft et al., 1999). This Sprouty domain harbors a central tyrosine (Tyr 55 in Sprouty2, and Tyr 53 in Sprouty1 and -4), and mutations of this tyrosine lead to a dominant-negative form (Sasaki et al., 2001). The N-terminal regions of Sprouty proteins have no homologous areas, but they contain a common serine-rich region with a PEST domain (proline (P), glutamic acid (E), serine (S), and threonine (T)), which directs proteins to a faster degradation process (Rechsteiner and Rogers, 1996).

The *Drosophila* Sprouty (dSprouty) gene was found by genetic screens and is a known inhibitor of FGF-receptor-signaling (Hacohen et al., 1998). dSprouty, a 63 kDa protein, inhibits not only FGF-receptor-signaling, but also other receptor-tyrosine-kinases (RTKs) like EGF-receptor, Torso and Sevenless (Casci et al., 1999; Kramer et al., 1999; Reich et al., 1999). Additionally, dSprouty interacts with two different signaling molecules upstream of Ras in the Ras/Raf/MAPK signaling pathway. These interaction partners are Gap1, a GTPase activating protein, and Drk, the *Drosophila* homologue of the adapter molecule Grb2 (Casci et al., 1999). In the fruit fly, Sprouty seems to play an important role during lung (Hacohen et al., 1998), eye, and ovary development (Reich et al., 1999).

Sequence analyzes identified four mammalian Sproutys (de Maximy et al., 1999; Hacohen et al., 1998; Minowada et al., 1999). A conserved function of dSprouty and

mammalian Sprouty during organogenesis (Minowada et al., 1999; Tefft et al., 1999) and angiogenesis (Lee et al., 2001) was suggested. The four mammalian Sproutys are small phosphoproteins, which build oligomers by their C-terminal domain. The C-terminus is also necessary for the translocation to and anchoring in the plasma membrane by palmitoylation (Hanafusa et al., 2002; Impagnatiello et al., 2001; Yigzaw et al., 2001).

Murine Sprouty1, -2, and -4 are expressed in embryonic and adult tissues like brain, heart, kidney, lung, limbs, and skeletal muscles (de Maximy et al., 1999; Minowada et al., 1999; Tefft et al., 1999). Sprouty3 mRNA expression is limited to adult brain and testis (Leeksma et al., 2002; Minowada et al., 1999).

Mammalian Sproutys are selective inhibitors, blocking FGF- (fibroblast growth factor) but not EGF- (epidermal growth factor) induced ERK activation, whereas the molecular mechanisms of this selective inhibition are not clarified yet (Egan et al., 2002; Impagnatiello et al., 2001; Sasaki et al., 2001; Wong et al., 2001). Multiple studies have demonstrated that Sproutys act upstream of Ras, because they are not able to inhibit ERK activation induced by constitutive activated Ras (Egan et al., 2002; Gross et al., 2001; Hanafusa et al., 2002; Lee et al., 2001). But Sproutys can inhibit FGF-induced activation of Raf, without influencing Ras. Therefore, it seems to be possible, that Sproutys inhibit ERK activation by a Ras-independent signaling pathway (Yusoff et al., 2002). In HEK 293 cells, Sprouty2 and -4 are quickly induced by EGF, FGF, and PDBu (phorbol 12,13-dibutyrate) in an ERK-signaling-dependent manner (Sasaki et al., 2001). The increased expression of mSprouty2 and -4 inhibits the FGF-induced, but not the EGF- and PDBu-induced ERK activation (Sasaki et al., 2001).

In unstimulated cells, Sprouty proteins are distributed throughout the whole cytoplasm, except of human Sprouty2, which is additionally colocalized with microtubules. Following EGF stimulation, all Sproutys are quickly shifted to the plasma membrane (Lim et al., 2000).

Interestingly, Sprouty family members can regulate the RTK-signaling not only negative, but also positive by interacting with different signaling molecules (Egan et al., 2002; Hall et al., 2003; Hanafusa et al., 2002; Rubin et al., 2003; Sasaki et al., 2003; Wong et al., 2002) (for detailed review see (Christofori, 2003). Known interaction partners of Sproutys are c-Cbl, Grb2, Raf1, FRS2, Shp2, caveolin-1,

TESK1, the protein-tyrosine-phosphatase PTP1B, and the *Drosophila* Ras-GAP, Gap1 (Tefft et al., 2002) (for review see (Dikic and Giordano, 2003)).

Sprouty is directly associated with the EGF-receptor and phosphorylated after growth factor stimulation. Sprouty1 and -2, but not Sprouty4 can interact with the E3 ubiquitin-ligase c-Cbl (Wong et al., 2001). Hereby, the phosphorylated Tyr55 acts as binding site for the SH2 domain of c-Cbl (Rubin et al., 2003). The binding of Sprouty2 with c-Cbl leads to ubiquitinylation and degradation of the protein in the 26S proteasom, and limits the inhibitory function of Sprouty2 (Egan et al., 2002; Hall et al., 2003; Rubin et al., 2003).

Another Sprouty binding partner is the adapter molecule Grb2 that connects the RTK activation with the Ras/Raf signaling pathway (Casci et al., 1999; Glienke et al., 2000). Sprouty might play its inhibitory role in this signaling pathway by binding to Grb2.

Sprouty4 blocks the VEGF-mediated ERK activation between the protein kinase C- δ (PKC- δ) and Raf1 (Sasaki et al., 2003). Under physiological conditions, Sprouty2 and -4 can bind Raf1 by a highly conserved region of the C-terminus, called the Raf-binding-motif (RBM). In this context, it was shown, that Sprouty1, -2, and -4 and Spred-2 suppress Raf1 phosphorylation at serine 338, without influencing Ras activation (Sasaki et al., 2003).

With these findings, three functional mechanisms of Sprouty proteins were postulated: First, binding to c-Cbl might cause degradation of Sprouty and, therefore, stabilization of the EGF-receptor, resulting in an increased ERK activation. Second, binding of Grb2 to tyrosin-phosphorylated Sprouty could interrupt the Ras/Raf/MAPK signaling pathway. And third, the binding of Raf to the C-terminus of Sprouty might inhibit Raf phosphorylation by PLC- γ -activated PKC- δ (Christofori, 2003).

3.3. Spred proteins

Spred family members contain an N-terminal EVH-1 domain, a central c-Kit binding domain (KBD), and a C-terminal Sprouty-like cysteine-rich domain (SPR-domain). The initially described member of the Spred family is the *Drosophila* homologue AE33. AE33 was identified as an insertion-bearing element in an enhancer-trap line, characterized by significant expression pattern changes in absence of rough and glass (DeMille et al., 1996; Freeman et al., 1992; Treisman and Rubin, 1996). Rough, a homeobox transcription factor, and glass, a zincfinger transcription factor, are

responsible for the appropriate differentiation of photo receptors during eye development in the fruit fly (Moses et al., 1989; Tomlinson, 1989; Tomlinson et al., 1988). Beside the *Drosophila* AE33, three mammalian Spred proteins were described (Kato et al., 2003; Wakioka et al., 2001). They have been described as a new Sprouty-related family of membrane-associated physiological inhibitors of the MAPK signaling pathway by interacting with Ras and Raf-1 (Wakioka et al., 2001). Spreds seem to inhibit MAP kinase activity by inhibiting the serin 338 phosphorylation and, therefore, the activation of Raf-1, but the interaction between Spred and Raf-1 increases at the same moment (Wakioka et al., 2001).

Drosophila's Sprouty was identified as a negative regulator of growth factor-induced ERK activation (Hacohen et al., 1998; Lee et al., 2001; Minowada et al., 1999) and Spred-1 and Spred-2 also inhibit different types of growth-factor-mediated ERK activation, including EGF, FGF, VEGF (vascular endothelial cell growth factor), PDGF, SCF (stem cell factor) and Serum (Kato et al., 2003; Miyoshi et al., 2004; Sasaki et al., 2001). The SPR (Sprouty-related) domains of Sprouty, and probably also of Spred, are palmitylated, localizing Sprouty and Spred to the membrane fraction (Impagnatiello et al., 2001). In Cos-1 and Swiss 3T3 cells, Sproutys and Spreds translocate to the plasma membrane after activation (Lim et al., 2002).

So far, three mammalian Spred family members have been identified. In mice, *Spred-1* is located on chromosome 2E5, *Spred-2* on chromosome 11A3-A4, and *Spred-3* on chromosome 7A3. In the human system, *Spred-1* was found on chromosome 15q13.2, *Spred-2* on 2p14, and *Spred-3* on 19q13.13 (Kato et al., 2003).

Like Spred-1 and Spred-2, Spred-3 harbors an N-terminal EVH-1 domain and a C-terminal SPR (sprouty related cysteine-rich region) domain. But Spred-3 has no functional c-Kit binding domain, because the critical amino acid arginine 247 is replaced by glycine. Nevertheless, Spred-3 also inhibits growth factor-mediated MAP kinase activity, but to a lower extent as compared to Spred-1 and Spred-2. The central c-Kit binding domain is responsible for the phosphorylation of Spred, but for effective suppression of ERK activation, the SPR domain is necessary (Kato et al., 2003).

Spred-1 was found to be expressed in fetal tissues, brain, heart and, to a minor extent, in other tissues. Spred-2 expression was found to be more ubiquitous, whereas Spred-3 expression was restricted to the brain (Engelhardt et al., 2004; Kato et al., 2003). During rat lung development, Spred-1 and Spred-2 mRNAs were shown

to be expressed predominantly in mesenchymal tissue from the onset of lung branching and coexpression of FGF-10 was demonstrated in the same region (Hashimoto et al., 2002).

Additionally, it was shown that Spred-1 plays a role as key regulator of RhoA-mediated cell motility and signal transduction. Spred-1 binds to activated RhoA and inhibits chemokine-induced RhoA activation and active RhoA-induced Rho-kinase activation. By this mechanism, Spred inhibits cell motility, metastasis and Rho-mediated actin reorganization (Miyoshi et al., 2004). Spred-1 is also highly expressed in hematopoietic cell lines and negatively regulates Interleukin-3-mediated ERK/MAPK activation (Nonami et al., 2004). Wildtype Spred-1 inhibits colony formation of bone marrow cells in the presence of cytokines, while a ΔC -Spred-1 dominant negative mutant enhances colony formation (Nonami et al., 2004). Moreover, Spred-1 is expressed in eosinophils and negatively regulates allergen-induced airway eosinophilia and hyperresponsiveness (Inoue et al., 2005).

Spred-2 was detected in the aorta-gonad-mesonephros (AGM) region of midgestation mouse embryos, and suppresses there hematopoiesis by inhibiting the MAP kinase activation (Nobuhisa et al., 2004). A specific function of Spred-3, which is expressed exclusively in brain, is not known yet.

3.4. The MAP kinase signaling pathway

The Ras/Raf/MAP kinase signaling pathway regulates cell proliferation and differentiation mediated by different extracellular signals like FGF and EGF. Following ligand binding, receptor tyrosin kinases (RTKs) are autophosphorylated and recruit different adapter molecules like Shc and Grb2. This binding then recruits the nucleotide exchange factor Sos to this signal complex (Schlessinger, 2000). Sos activates the GTPase Ras that interacts directly with the protein kinase Raf and leads in response Raf to the plasma membrane (Lowy and Willumsen, 1993; Robinson and Cobb, 1997). Raf is phosphorylated and activated by not well-defined kinases with complex regulatory mechanisms (Kerkhoff and Rapp, 2001; Morrison and Cutler, 1997; Sternberg and Alberola-Ila, 1998). Raf phosphorylates and activates MEK, which further phosphorylates and thereby activates MAP kinases including ERK1 (extracellular stimulus-activated protein kinases) and ERK2 (Kerkhoff and Rapp, 2001; Morrison and Cutler, 1997; Sternberg and Alberola-Ila, 1998). Activated MAP kinases phosphorylate different cytoplasmatic and nuclear proteins, leading to

different cellular changes (Fig. 1). In contrast to the quite well studied activating mechanisms of the Ras/MAPK cascade, the negative regulatory mechanisms have to be investigated further. Spred proteins seem to be one group of such negative regulators.

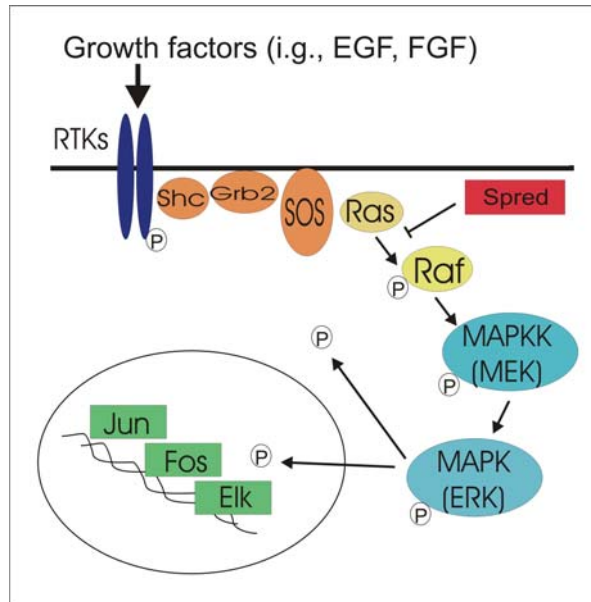


Figure 1. Putative Spred function in the Ras/Raf/MAP kinase signaling pathway.

Inhibitory function of Spreds in the MAPK signaling pathway, while binding to Ras and inhibiting the phosphorylation of Raf. (for detailed pathway description see text).

3.5. Knockout strategies in mice

Now, that the human and mouse genome sequences are known (Lander et al., 2001; Venter et al., 2001; Waterston et al., 2002), attention has turned to elucidate gene function and identify gene products, that might have therapeutic value. The laboratory mouse (*mus musculus*) has had a predominant role in the study of human disease mechanisms throughout the rich, 100-year history of classical mouse genetics, exemplified by the lessons learned from naturally occurring mutants such as agouti (Bultman et al., 1992), reeler (D'Arcangelo et al., 1995), and obese (Zhang et al., 1994). The large scale production and analysis of induced genetic mutations in worms, flies, zebrafish, and mice have greatly accelerated the understanding of gene function in these organisms. Among the model organisms, the mouse offers particular advantages for the study of human biology and disease: first, the mouse is a mammal and its development, body plan, physiology, behavior, and diseases have much in common with those of humans; second, almost all (99%) mouse genes have homologues in humans; and third, the mouse genome supports targeted mutagenesis in specific genes by homologous recombination in embryonic stem (ES) cells, allowing genes to be altered efficiently and precisely.

The ability to disrupt or “knockout” a specific gene in ES cells and mice was developed in the late 1980’s (Goldstein, 2001) and the use of knockout mice has led to many insights into human biology and diseases (Chen et al., 2001b; D’Orleans-Juste et al., 2003; Wallace, 2001). Current technology also permits insertion of “reporter” genes into the disrupted gene, which can then be used to determine the temporal and spatial expression pattern of the knocked-out gene in mouse tissues. Such marking of cells by a reporter gene facilitates the identification of new cell types according to their gene expression patterns and allows further characterization of marked tissues and single cells.

Recognition of the power of mouse genetics to inform the study of mammalian physiology and diseases, coupled with the advent of the mouse genome sequence and the ease of producing mutated alleles, has catalyzed public and private sector initiatives to produce mouse mutants on a large scale, with the goal of eventually knocking out a substantial portion of the mouse genome (Nadeau et al., 2001; Zambrowicz et al., 1998). Large-scale, publicly funded gene trap programs have been initiated in several countries, with the International Gene Trap Consortium coordinating certain efforts and resources (Hansen et al., 2003; Skarnes et al., 2004; Stryke et al., 2003; Wiles et al., 2000). Despite these efforts, the total number of knockout mice described in the literature is relatively modest, corresponding to only ~10% of the ~25,000 mouse genes. The curated Mouse Knockout and Mutation Database lists 2,669 unique genes, the curated Mouse Genome Database lists 2,847 unique genes, and an analysis at Lexicon Genetics identified 2,492 unique genes (Austin et al., 2004). Most of these knockouts are not readily available to scientists who may want to use them in their research; for example only 415 unique genes are represented as targeted mutations in the Jackson Laboratory’s Induced Mutant Resource Database.

Various methods can be used to create mutated alleles, including gene targeting, gene trapping, reporter gene insertion, and RNA interference.

Advantages of conventional and conditional gene targeting include flexibility in design of alleles, lack of limitation to integration hot spots, reliability for producing complete loss-of-function alleles, ability to produce reporter knock-ins and conditional alleles (using cis-elements, e.g., loxP or frt sites), and ability to target splice variants and alternative promoters. BAC-based targeting has the potential advantages of higher

recombination efficiencies and flexibility for producing complex mutated alleles (Valenzuela et al., 2003).

Gene trapping is rapid, cost-effective, and produces a large variety of insertional mutations throughout the genome, but can be somewhat less flexible (Chen et al., 2004; Skarnes et al., 2004; Stanford et al., 2001; Zambrowicz et al., 2003). There is uncertainty regarding the percentage of gene traps that produce a true null allele and the fraction of the genome that can ultimately be covered by gene trap mutations. Trapping is not entirely random but shows preference for larger transcription units and genes more highly expressed in ES cells. In recent studies, gene trapping was estimated to potentially produce null alleles for 50-60% of all genes, perhaps more, if a variety of gene trap vectors with different insertion characteristics is used (Skarnes et al., 2004; Zambrowicz et al., 2003). Large-scale trapping projects have already defined gene classes that probably cannot be knocked out by trapping (e.g., single exon GPCRs, genes that are not expressed in ES cells).

Moreover, inserting a **reporter gene** (e.g., β -galactosidase, green fluorescent protein, or luciferase) allows a rapid assessment of which cell types normally support the expression of that gene. Therefore, gene targeting or trapping constructs that utilize the *lacZ* gene encoding beta-galactosidase have become an increasingly important way to disrupt gene function and monitor gene expression in parallel. To monitor gene expression of mice in situ, X-Gal staining was established as an easy-to-use and convenient tool. This method allows cell-specific staining and the intensity of X-Gal staining is consistent with the level of beta-galactosidase expression. Therefore, this approach enables the detection of specific promoter activity e.g. in embryonic tissues, in subcompartments of organs, and also entire organs.

RNA interference offers enormous promise for analysis of gene function in mice (Kunath et al., 2003), but is not yet sufficiently developed, as the production of true null alleles is not completely reliable.

In the Knock Out Mouse Project (KOMP), important researchers of the field recommend that both gene targeting and gene trapping are suitable methods for producing large numbers of knockout alleles and, given their complementary advantages, a combination of these methods should be used to produce a genome-wide collection of null-reporter alleles most efficiently.

3.6. Bone growth and FGF-mediated endochondral ossification

Long bone growth is determined mainly by the process of endochondral ossification, a strictly regulated process that requires proliferation and differentiation of chondrocytes. During this process, chondrocytes in the reserve zone that arise from mesenchymal cells first undergo proliferation, they then exit the cell cycle, undergo terminal hypertrophic differentiation, and finally the synthesised cartilage matrix calcifies and is replaced by bone (Kronenberg, 2003). Various signaling molecules have been shown to regulate and coordinate this complex process of endochondral ossification. Fibroblast growth factor (FGF) signaling plays a major role in a variety of developmental processes and recent results have highlighted its function in the regulation of bone morphogenesis (for review see (Goldfarb, 1996). FGFs are a large family of at least 23 polypeptides that signal through their binding to specific tyrosine kinase receptors (FGFRs), which constitute a four-member gene family (Basilico and Moscatelli, 1992). FGF receptor 3 (FGFR3) is expressed in proliferating and prehypertrophic chondrocytes in the epiphyseal growth plates (Naski and Ornitz, 1998; Ohbayashi et al., 2002; Peters et al., 1993). Activating mutations in FGFR3 cause different forms of human dwarfism-like achondroplasia, hypochondroplasia, and thanatophoric dysplasia (Bellus et al., 1995; Rousseau et al., 1994; Shiang et al., 1994; Tavormina et al., 1995). The most common form of human dwarfism is achondroplasia with a prevalence at birth of about 1/26,000 (Oberklaid et al., 1979). Expression of activating FGFR3 mutants in mice reproduces the dwarf phenotype of these skeletal diseases (Chen et al., 2001a; Iwata et al., 2000; Iwata et al., 2001; Li et al., 1999; Naski and Ornitz, 1998; Segev et al., 2000; Wang et al., 1999). In contrast, lack of FGFR3 in mice causes skeletal overgrowth, indicating that FGFR3 signaling inhibits endochondral bone growth (Colvin et al., 1996; Deng et al., 1996). Similarly, transgenic mice overexpressing FGFs show dwarfism (Coffin et al., 1995; Garofalo et al., 1999), whereas mice homozygous for a targeted disruption of FGF18 exhibit a growth-plate phenotype similar to that of FGFR3 null mice (Liu et al., 2002; Ohbayashi et al., 2002). These observations indicate that FGFs and FGFR3 signaling play major roles in the regulation of bone growth. To date, four signaling pathways have been shown to propagate FGFR3 signals: the STAT, MAPK-extracellular signal-regulated kinase (ERK), phospholipase C- γ , and phosphatidylinositol 3-kinase-AKT pathways (Choi et al., 2001; Hart et al., 2000; Kanai et al., 1997; Kong et al., 2002; Legeai-Mallet et al., 1998; Liu et al., 2002; Murakami et al., 2000; Sahni et al., 1999;

Su et al., 1997; Weksler et al., 1999). Upregulation of Sox9, a HMG-box-containing transcription factor, which is essential for chondrocyte differentiation, is inhibited by a specific inhibitor of the MAPK pathway (Murakami et al., 2000). Recently, it has been shown that constitutive activation of MEK1 in chondrocytes causes STAT1-independent achondroplasia-like dwarfism in mice and rescues the FGFR3-deficient mouse phenotype (Murakami et al., 2004). Overexpression of C-type natriuretic peptide (CNP) in chondrocytes counteracts dwarfism in a mouse model of achondroplasia with activated FGFR3 in cartilage. CNP prevented the shortening of achondroplastic bones by correcting the decreased extracellular matrix synthesis in the growth plate through inhibition of the FGF-mediated MAPK pathway (Yasoda et al., 2004). Growth hormone (GH) therapy in achondroplasia patients has beneficial effects through IGF-1 by preventing chondrogenic cell apoptosis induced by an activating mutation in the FGFR3 (Koike et al., 2003). These results indicate that MAPK activity is a negative regulator of bone growth and suggest that the MAPK pathway plays an important role in bone development.

Despite recent advances in understanding the roles of FGFs and FGF receptors in skeletal development, the downstream events through which FGFs influence the proliferation or differentiation of osteogenic chondrocytes remain to be elucidated.

3.7. Aim of the work

Spreds have been described as a new Sprouty-related family of membrane-associated physiological inhibitors of the MAPK signaling pathway by interacting with Ras and Raf-1. Different studies demonstrate the inhibitory function of Spreds in cell culture systems, but the *in vivo* function of Spreds in the whole organism is still unclear.

Therefore, the main aim of this work was the generation and characterization of Spred-2-deficient mice. To establish a mouse strain with a disruption of the *Spred-2* gene, a gene trap approach was used.

So far, very rare data of the Spred-1 and Spred-2 RNA expression and no data of the protein expression in different mouse organs were available. Therefore, the second aim of this work was the examination of the Spred-1 and Spred-2 RNA and protein expression patterns in mice. In order to this, the generation of Spred-1 and Spred-2 specific antibodies was necessary.

Furthermore, nothing was known about the *Spred-2* promoter region and its regulation. Therefore, an additional aim of this work was to study the physiological promoter activity profile in mice. For this examination the Spred-2-deficient mouse strain with a *beta-geo* fusion gene harboring gene trap vector was used.

Moreover, to investigate the physiological tissue specific function of Spred-1 and Spred-2 in mice, conditional ES cells to generate knockout mice for Spred-1 and Spred-2 were established. This will be of major interest, if the single or double knockout mice of Spred-1 and Spred-2 are not viable.

4. Material and Methods

4.1. Molecular-biological methods

4.1.1. Database analyzes of the mouse genome

For database analyzes of the mouse genome the EBI database of the Sanger Institution (<http://www.ensembl.org>) and the NCBI database were used.

4.1.2. Isolation of plasmid DNA

Plasmid DNA preparations of bacteria cultures - "Mini/Midi/Maxi Preps" - were performed according to the manufacturer's instructions (Qiagen).

DNA concentrations were measured photometrically at 260 nm (Ultrospec 2000, Pharmacia). ($OD_{260}=1$ corresponds to 50 mg/ml of DNA).

4.1.3. Isolation of genomic DNA of mouse tails and ES cells

Genomic DNA of rodent tails and ES cells was isolated using the DNeasy preparation Kit (Qiagen) according to the manufacturer's instructions.

4.1.4. DNA gel electrophoresis

DNA fragments were diluted with 6x loading buffer (0.25% bromphenol-blue, 0.25% xylene cyanol FF, 15% Ficoll (Typ 400) in H₂O) and separated on 1-2% agarose gels by electrophoresis. Agarose was boiled in 1x TAE-buffer (50x TAE-buffer: 24.2 % (w/v) Tris, 5.71% (v/v) acetic acid, 10% (v/v) 0.5 M EDTA, pH 8.0), ethidiumbromide (0.5 mg/ml) added, and gels poured in appropriate chambers. After electrophoresis at 60-100 V, DNA separation and sizes were analyzed on a UV-light table ($\lambda=355$ nm) (BRL UV Transilluminator TFX-35M; Life Technologies/Gibco). DNA markers were derived from MBI Fermentas: 1K marker: (100 bp DNA ladder: 80, 100, 200, 300, 400, 500, 600, 700, 800, 900, 1031bp); 3K marker: (100 bp DNA ladder plus: 100, 200, 300, 400, **500**, 600, 700, 800, 900, 1031, 1200, 1500, 2000, 3000bp); 10K marker: (1 kb DNA ladder: 250, 500, 750, 1000, 1500, 2000, 2500, **3000**, 3500, 4000, 5000, 6000, 8000, 10000bp).

4.1.5. DNA purification of agarose gels

DNA in agarose gels, e.g. after gel electrophoresis, was isolated using the QIAquick column system (Qiagen) according to the manufacturer's instructions.

4.1.6. Purification of PCR products

DNA of PCR products can be purified directly using the QIAquick PCR Purification Kit (Qiagen) according to the manufacturer's instructions. This procedure was used to eliminate "unincorporated" dNTP's, primers, and salts.

4.1.7. Cutting DNA by endonucleases

Plasmid DNA or PCR fragments with an appropriate restriction site can be cut by restriction enzymes. Digests were performed in a volume of 10-100 µl using 1-10 Units of restriction enzyme with the recommended buffer and temperature for 1-15 hours. (Restriction enzymes were obtained from MBI Fermentas and New England Biolabs.)

4.1.8. Dephosphorylation of DNA 5' overhangs

To reduce immediate re-ligation of digested plasmids - prepared for cloning a DNA fragment - 5' ends of the plasmids can be dephosphorylated by "Shrimp Alkaline Phosphatase" (SAP, Roche) according to the manufacturer's instructions.

4.1.9. Ligation/cloning of DNA fragments in a plasmid vector

Cloning of a DNA fragment into a plasmid vector is possible if both parts are digested with restriction enzymes producing complementary overhangs. In this work, to ligate insert and vector, the TAKARA Ligation Kit (TAKARA) was used according to the manufacturer's instructions.

4.1.10. T/A-cloning

A fast and very efficient cloning of PCR fragments into plasmid vectors is derived by the T/A-cloning strategy. Amplification of PCR fragments by Taq polymerases generates A-overhangs at the 3' ends. Therefore, an already pre-cut T/A-vector can be used directly for cloning these fragments. In this work, the "pCR2.1-TOPO Vector" (3.9 kb; Invitrogen) and the "pDrive Cloning Vektor" (3.85 kb; Qiagen) were used according to the manufacturer's instructions.

4.1.11. Generation of competent bacterias

Bacterias are called „competent“, if they are able to incorporate external DNA. In this work, bacterias were chemically treated to obtain competent cells. 30 ml LB-medium were inoculated 1:100 with an overnight culture of XL1-blue cells and harvested at

the logarithmic growing phase at $OD_{550}=0.5$. Bacterias were centrifuged for 10 minutes, 2400 g, at 4°C, and in all further steps bacterias were treated on ice. The pellet was re-suspended in 5 ml ice-cold 50 mM $CaCl_2$ and centrifuged at 3000 rpm for 10 minutes. Then, the pellet was re-suspended in 7.5 ml ice-cold 50 mM $CaCl_2$, kept for 30 minutes on ice and again centrifuged at 3000 rpm for 10 minutes. The next pellet was re-suspended in 1.5 ml ice-cold 50 mM $CaCl_2/20\%$ glycerine, aliquots of 0.2 ml snap frozen in liquid nitrogen, and stored at -80°C.

An alternative were the commercially available and ready-to-use TOPO10 and TOPO10F' cells (Invitrogen).

4.1.12. Transformation of competent bacterias

Transformation of bacterias is called the process, if competent bacterias incorporate external plasmid DNA. This can be performed in self-made XL1-blue cells or commercially available TOPO10 or TOPO10F' cells (Invitrogen). In this work, the procedure was done according to the "TOPO protocol" (Invitrogen).

4.1.13. Verification of inserts

To check, whether the cloning of an insert into a plasmid vector was successful, three different methods were used:

1) Restriction digests of DNA Mini Preps (Qiagen):

After restriction digests of DNA, fragment sizes could be identified in an agarose gel.

2) PCR control of a DNA Mini Prep (Qiagen):

With this approach, not only the integration but also the correct orientation of the insert in the vector can be verified. In this case, one vector primer and a second insert primer with the appropriate orientation were used to identify only clones harboring the correct insert orientation in the vector.

3) PCR controls directly from a bacteria overnight culture:

A fast and efficient variant of the former PCR is to perform the PCR reaction directly of a 3-5 ml bacteria overnight culture. This is very convenient, because the previous DNA preparation of all cultures is not necessary any more. Only the PCR-positive overnight cultures have to be prepared for DNA isolation. For the PCR reaction, 1 µl of bacterial culture was sufficiently used as PCR template. In this work, the „PCR Taq Master Mix“(Qiagen) was used with a standard PCR protocol (volume: 20 µl; 30-35 cycles; denaturation: 95°C, 1 min; annealing: 50°C, 1 min; elongation: 72°C, 1 min).

(All Oligonucleotides were derived from Invitrogen. Stock solutions of 100 µM were stored at -20°C; working dilution for PCR primers: 10 µM; dNTPs were derived from Fermentas.)

4.1.14. LA- (long and accurate) PCR

To amplify long genomic DNA fragments for the cloning of the Cre-lox gene targeting vectors, the LA- (“long and accurate”) PCR Kit (TAKARA) was used according to the manufacturer’s instructions. As template 200-400 µl E14.1 derived genomic DNA was used, and an elongation time between 10-20 minutes was set. For very long and critical fragments, a previous touch-down PCR was performed to increase the specificity of the PCR reaction. An example of an often used PCR protocol is presented in Table 1.

	Touch down					
94°C	98°C	72-68°C (-0.5°C/cycle)	98°C	68°C	72°C	4°C
1min	20sec	15min	20sec	15min	10min	∞
	8 cycles		25 cycles			

Table 1.
Example of a LA- (“long and accurate”) PCR protocol.

4.1.15. Sequencing (Sanger method)

To sequence DNA fragments the „ABI PRISM Sequencer“(Perkin Elmer) and the „ABI PRISM Dye Terminator Cycle Sequencing Kit with AmpliTaq DNA Polymerase“(Perkin Elmer) was used according to the manufacturer’s instructions. Depending on the DNA quality, 300-600 bp were readable, whereas the first 30 bp directly after the primer were not detectable. (Working dilution for sequencing primers: 2.5 µM).

Alternatively, a commercially available sequencing service (MWG) was used.

4.1.16. Southern blot analyzes

DNA transfer: Approximately 10 µg of DNA fragments, for example after a restriction digest, were separated by agarose gel electrophoresis and documented on a UV-light table. After denaturation (1.5 M NaCl, 0.5 M NaOH) for 30 minutes, DNA transfer was performed with 20 x SSC (3 M NaCl, 0.3 M Na₃citrate) on HybondTM-N⁺-

membranes (Amersham). Membranes were air-dried and the DNA covalently bound to the membrane using a UV-linker (UV Stratalinker®1800, Stratagene).

Radioactive labeling of the probe: For radioactive labeling of the probe (template DNA concentration: 50-100 ng/μl), the Megaprime™ DNA labeling System (Amersham) and radioactive labeled ³²P-α-dATP (50 μCi; Amersham) were used according to the manufacturer's instructions. To reduce unspecific background signals, unincorporated nucleotides were removed by gel filtration with Sephadex G-50 columns (Pharmacia). The probe was ready for hybridization reaction after boiling at 95°C for 5 minutes.

Hybridization: To block unspecific bindings, the membrane was pre-hybridized with 500 μg herring sperm DNA in 25 ml hybridization buffer (6.25 ml 20x SSPE (3.6 M NaCl, 0.2 M sodium phosphate, 0.02 M EDTA, pH 7.7), 1.25 ml 100x Denhardt's solution (2% (w/v) BSA; 2% (w/v) Ficoll, 2% (w/v) PVP (polyvinylpyrrolidone)), 1.25 ml (10% w/v) SDS, 12.5 ml formamide (50%), 3.75 ml H₂O) at 42°C for 2 hours. Subsequently, hybridization was performed by adding the radioactive-labeled probe to the pre-hybridization buffer, and rotated at 42°C overnight. To remove the remaining free probe, the membranes were washed 3 times for 15 minutes with 2 x SSC buffer at 42°C and 3 times for 15 minutes with 0.2 x SSC buffer at 50°C. Signals were detected on X-ray films after an exposure time of a couple of hours until several days, depending on the strength of the signal.

4.1.17. Cloning of Spred-1 and Spred-2 full length cDNA in TOPO2.1

Total RNA extracts were isolated of various mouse tissues, treated with DNase, and RNA quality was tested by RT-PCR analyzes with GAPDH- and actin-specific primers. In order to clone the full length mouse cDNAs of Spred-1 and Spred-2, RT-PCRs were performed with the following gene specific primer pairs:

For Spred-1:

5' Spr.1 full-length (5'GTGAGGGAAAGatgAGCGAGGAGACGGC3') (start),

3' Spr.1 full-length (5'CTGGACTGCTtcaCCCAGCAGCCTTATG3') (stop).

For Spred-2:

5'm.cloningSpr2(1-28) (5'ATGACCGAAGAAACACACCCGGACGATG3') (start),

3'm.cloningSpr2(1233-1207) (5'TCACGCGGCGGCTTTGTGCTTCCCACC3') (stop).

RT-PCR products of liver (Spred-1) and brain (Spred-2) were purified by agarose gel electrophoresis, T/A-cloned into the TOPO2.1 vector (Invitrogen), and both constructs were verified by sequencing.

4.1.18. Cloning of Spred-1 and Spred-2 cDNA in pcDNA3.1/*Myc-His*

Full-length cDNAs of murine Spred-1 and Spred-2 were cloned into the *NotI*/*HindIII* sites of pcDNA3.1/*Myc-His* (-) (A) vector (5.5 kb, eukaryotic expression vector with CMV-promoter and ampicillin resistance; Invitrogen). The two Spred cDNAs were cloned either including their endogenous stop codons (generating a construct expressing the untagged full-length form) or using the in-frame stop codon of the vector (for a construct expressing the full-length 6xHis/c-myc-tagged version of the protein). All cDNAs were amplified using the proof-reading Advantage[®]2 PCR Kit (Clontech) and the TOPO2.1- Spred-1/Spred-2 cDNA plasmids as template. The final constructs were verified by sequencing. The following primers were used:

For Spred-1 (with stop/ without myc-His-tag):

5'CMV Spr.1,NotI (5'ATTAGCGGCCGCATGAGCGAGGAGACG3') (NotI)

3'CMV Spr.1,Hind, Stop (5'TAATAAGCTTTCACCCAGCAGCCTT3') (HindIII, *stop*)

For Spred-1 (without stop/ with myc-His-tag):

5'CMV Spr.1,NotI (5'ATTAGCGGCCGCATGAGCGAGGAGACG3') (NotI)

3'CMV Spr.1,Hind, ohne Stop (5'TAATAAGCTTCCCAGCAGCCTTATG3') (HindIII)

For Spred-2 (with stop/ without myc-His-tag):

5'CMV Spr.2,Not (5'ATTAGCGGCCGCATGACCGAAGAAACAC3') (NotI)

3'CMV Spr.2,Hind, Stop (5'TAATAAGCTTTCACGCGGCGGCTTTG3') (HindIII, *stop*)

For Spred-2 (without stop/ with myc-His-tag):

5'CMV Spr.2,Not (5'ATTAGCGGCCGCATGACCGAAGAAACAC3') (NotI)

3'CMV Spr.2,Hind, ohne Stop (5'TAATAAGCTTCGCGGCGGCTTTGTGC3') (HindIII)

4.1.19. RNA extraction of mouse tissues

To reduce RNase activity, mouse tissues were quickly prepared on ice, or immediately transferred and stored in „RNA later“ (Ambion) at 4°C for a maximum of 1 month. Total RNA was extracted using TriZol reagent (Gibco Life Technologies) and an Ultra Turrax (Kika) for homogenization of the samples. 1 ml TriZol reagent was used for 30 mg of tissue and RNA was isolated according to the manufacturer's instructions. Extracted RNA was solved in 100-300 µl RNase free H₂O in a 65°C water bath for 10 minutes and stored immediately at -80°C.

RNA concentrations were photometrically measured at 260 nm (Ultrospec 2000, Pharmacia). Samples were diluted 1:100, and then an OD₂₆₀=1 corresponds to 40 µg/ml of the RNA sample.

4.1.20. DNA removal of RNA extracts

To remove DNA residues out of RNA extracts, the DNA-free™ Kit (Ambion) was used according to the manufacturer's instructions.

4.1.21. RT- (Reverse Transcription) PCR

For RT-PCR analyses, 1 µg of total RNA was used with the OneStep RT-PCR Kit (Qiagen) according to the manufacturer's instructions. Furthermore, 0.2 µl RNase inhibitor („Superase“, Ambion) was added per reaction. To obtain a most specific amplification, it was useful to set some touch-down PCR cycles after the Pre-PCR. In this work, the following PCR protocol was used (Table 2).

Pre-PCR		Touch down					
50°C	95°C	94°C	72-68°C (-0.5°C/cycle)	95°C	68°C	72°C	4°C
30min	15min	30sec	1.30min	30sec	30sec	10min	∞
		8 cycles		25 cycles			

Table 2.
RT-PCR protocol.

Specific primer sequences for Spred-1:

5' Spr.1 full-length (5'GTGAGGGAAAGatgAGCGAGGAGACGGC3') (start),

3' Spr.1 full-length (5'CTGGACTGCTtcaCCCAGCAGCCTTATG3') (stop).

Specific primer sequences for Spred-2:

5'Spr2[1-28] (5'ATGACCGAAGAAACACACCCGGACGATG3') (start),

3'Spr2[1233-1207] (5'TCACGCGGCGGCTTTGTGCTTCCCACC3') (stop).

To test for RNA integrity, a control RT-PCR with GAPDH specific primers was amplified in parallel, using the following primers:

GAPDHforw (5'ACCACAGTCCATGCCATCAC3'),

GAPDHrev (5'TCCACCACCCTGTTGCTGTA3').

4.1.22. Northern blot analyzes

For Northern blot analyzes, 20 µg of each total RNA sample was separated on a formaldehyde-agarose gel, transferred to Hybond-N⁺ nylon membranes (Amersham Biosciences) and hybridized with a ³²P-labeled DNA probe (Megaprime DNA labeling system, Amersham). Hybridization signals were detected on X-ray films. In this study,

the full-length Spred-2 cDNA was used as probe and a beta-actin cDNA probe was used as loading control on a parallel prepared membrane.

Moreover, a commercially available Northern blot membrane (Message Map™ Northern Blot; Strategene) was examined for the RNA expression of Spred-1 and Spred-2. This membrane contained 2 µg poly-A (+) RNA of 8 different mouse tissues (brain, heart, kidney, liver, lung, skeletal muscle, spleen, and testis). Hybridization was performed with radioactive labeled full length cDNA probes of Spred-1 and Spred-2, respectively, using as well the Megaprime DNA labeling system (Amersham) according to the manufacturer's instructions. The full length cDNAs were T/A-cloned in the TOPO2.1 vector (Invitrogen) and isolated by EcoRI restriction enzyme digests.

4.2. Histological methods

4.2.1. Paraffin sections and HE staining

For histopathology, mouse tissues were dissected from sacrificed animals. Samples were fixed in 4% formaldehyde/PBS (140 mM NaCl, 2.7 mM KCl, 8.1 mM Na₂HPO₄, 1.5 mM KH₂PO₄) for 3 days, embedded in paraffin, and sections (7-10 µm) were stained with hematoxylin and eosin. Stained sections were mounted in Entellan (Merck) and images taken with a Nikon Eclipse E600 microscope.

4.2.2. Immunohistochemistry

For immunohistochemistry, mouse tissues were snap-frozen in 2-methyl-butane with liquid nitrogen. Tissues were fixed with „Tissue Tek“ (Sakura) on section blocks and cryosections (5-10 µm) cut with microtome blades (Carbon Steel, C35; Feather, Japan). Cryosections were put on Superfrost or Polysine-coated glass slides (Menzel-Gläser), fixed in 4% paraformaldehyde/PBS for 30 minutes, permeabilized with 0.1% TritonX-100/PBS for 20 minutes, and blocked with 5% goat serum in PBS for 1 hour to reduce non-specific binding. Sections were incubated with primary antibodies overnight at room temperature, washed 3 times in PBS/0.1% Tween20, followed by incubation with the secondary antibody. Stained sections were washed 3 times in PBS/0.1% Tween20 and mounted in Mowiol (2.4 g mowiol (4-88 Höchst), 6 g glycerol; stirred overnight; 6 ml H₂O added and kept for several hours at RT; 12 ml 0.2 M Tris-HCl (pH=8.5) added; stirred 10 minutes at 50°C; centrifuged (15 minutes, 5000 g); aliquots stored at -20°C).

The following antibodies were used: affinity-purified anti-Spred-2, polyclonal rabbit anti-ERK (CAT-#9102, Cell Signaling Technology), monoclonal rabbit anti-phospho-ERK (CAT-#4376, Cell Signaling Technology), and CyTM3-conjugated goat anti-rabbit IgG (Transduction Laboratories). To test for unspecific binding, the secondary CyTM3-labeled antibody was used alone.

4.2.3. X-Gal staining

For X-Gal staining, tissues of newborn and adult mice were snap frozen in 2-methylbutane. Cryosections (7-10 μ m) were fixed in X-Gal fixation buffer (0.1 M phosphate buffer, pH 7.3 (3.74 g NaH₂PO₄-H₂O, FW=137.99; 10.35 g Na₂HPO₄, FW=141.96; ad 1 l H₂O), 5 mM EGTA, 2 mM MgCl₂, 0.2% glutaraldehyde) for 15 minutes, washed 3 times with X-Gal wash buffer (0.1 M phosphate buffer, pH 7.3, 2 mM MgCl₂) and stained overnight at 37°C in X-Gal staining buffer (0.1 M phosphate buffer, pH 7.3, 2 mM MgCl₂, 5 mM K₄Fe(CN)₆-3H₂O, 5 mM K₃Fe(CN)₆, 1 mg/ml X-Gal). Stained sections were washed 3 times with X-Gal wash buffer and mounted in Aquatex (Merck).

ES cells and whole organs of adult mice were directly fixed, stained, and washed by the same protocol, whereas staining of whole organs was performed for 5-8 hours.

Images of ES cells and cryosections were taken with a Nikon Eclipse E600 microscope, overview sections with a Leica MZ 6 microscope. Wildtype littermates were co-analyzed to ensure that the beta-galactosidase expression was specific in Spred-2^{-/-} mice.

4.2.4. Toluidine staining

Skeletons were fixed in 3.7% formaldehyde for 18 hours at 4°C. After dehydration, the decalcified tibiae were embedded in methylmetacrylate and 5 μ m sections were cut in the sagittal plane on a rotation microtome (Cut 4060E, MicroTech, Munich, Germany). Sections were stained with toluidine blue and evaluated using a Carl Zeiss microscope (Carl Zeiss, Jena, Germany) as described (Amling et al., 1999). This work was done by Dr. T. Schinke (Hamburg).

4.3. Cell culture

4.3.1. Transfection of HEK 293 cells

HEK 293 cells were cultivated in 10% FCS (fetal calf serum)/DMEM/1% penicilline/streptomycine (Gibco) at 37°C in a CO₂-incubator to 50-80% confluency. DNA transfection into HEK 293 cells was efficiently performed using the Lipofectamine Plus™ Reagent (GIBCO) according to the manufacturer's instructions. For transfection, Spred-1 and Spred-2 full-length constructs with and without a myc/His-tag in the pcDNA3.1/ myc-His (-) A (5.5 kb) vector (eukaryotic expression vector with CMV-promoter and ampicillin resistance; Invitrogen) were used. After recommended incubation for 24-48 hours at 37°C and 5%- CO₂, cells were washed with PBS and harvested with 80-600 µl (dependent on well size and confluency) 3x SDS sample buffer (200 mM Tris-HCl pH 6.7, 6% SDS, 15% glycerine, 0.003% bromphenole-blue, 10% β-mercaptoethanol) for protein extracts. Protein samples were immediately boiled at 95°C for 5 minutes and stored at -20°C.

4.3.2. Primary mouse chondrocyte culture

Murine sterni and costal cartilage were dissected from pups at P1. Tissues were cut into small pieces and incubated in 1 mg/ml collagenase A (Roche) in DMEM for 3 hours at 37°C. Dissociated cells were counted (Coulter-counter) and 6 x 10⁵ cells/well were plated on 6-well plates in DMEM with 10% FCS. After 2 days, cells were starved in serum-free media for 20 hours and stimulated with serum-free media containing 1% FCS, 10% FCS, or 10 µg/ml heparin (Roth) with aFGF (Calbiochem, Cat. No. 341591) at indicated concentrations. For Western blot analyzes, cells were washed with PBS and harvested with 300 µl 3x SDS sample buffer. Samples were immediately boiled at 95°C for 5 minutes and stored at -20°C.

4.4. Protein biochemical methods

4.4.1. Protein isolation of mouse tissues

Mouse tissue lysates were homogenized with an Ultra Turrax mixer (T5 FU, Kika) in homogenization buffer (10 mM K₂HPO₄ at pH 7.4; 1 mM EDTA; 1 mM EGTA; Complete protease inhibitor cocktail; Roche Diagnostics) and protein concentrations were estimated by Lowry reagent (Sigma) according to the manufacturer's instructions. For Western blot analyzes, 3x SDS sample buffer (200 mM Tris-HCl pH

6.7; 6% SDS; 15% glycerine; 0.003% bromphenole-blue; 10% β -mercaptoethanol) was added, samples were immediately boiled at 95°C for 5 minutes, and stored at -20°.

4.4.2. Western blot analyzes

Protein samples (for mouse tissues: 30 μ g total protein/lane) were separated by SDS-polyacrylamide gel electrophoresis (Electrophoresis buffer (10x): 25 mM Tris pH 8.3, 192 mM glycine, 0.1% SDS) using 10% and 12% gels (Western blot gel buffer A: 0.5 M Tris-HCl, pH 6.8, 0.4% SDS; Western blot gel buffer B: 1.5 M Tris-HCl, pH 8.8, 0.4% SDS; APS 10%: 10% ammonium persulfate in bidest. H₂O), and transferred (Western blot transfer buffer: 25 mM Tris; 150 mM glycine; 10% methanol, pH 8.3) to nitrocellulose membranes using a semi-dry system (Trans Blot Cell, BioRad). Protein transfer and loading amount were verified by Ponceau S staining (0.1% Ponceau S; 5% acetic acid, in bidest. H₂O) of the membranes. To reduce unspecific antibody binding, membranes were blocked with PBS/0.05% Tween/4% fat-free dry milk for at least 3 hours. Then, membranes were incubated with the primary antibodies at 4°C overnight, washed three times (PBS/0.05% Tween), and incubated with the secondary antibodies at room temperature for 1-2 hours. For signal detection, ECL kit (Amersham) and X-ray films were used according to the manufacturer's instructions. For Western blot analyzes, the following antibodies were diluted in PBS/0.05% Tween/4% fat-free dry milk: affinity-purified polyclonal rabbit anti-Spred-2 (AS 96-415) (0.2 μ g/ml), affinity-purified polyclonal rabbit anti-Spred-1 (AS 124-233) (0.6 μ g/ml) (both were described in (Engelhardt et al., 2004), polyclonal goat anti-Actin (CAT-#sc-1616, SantaCruz Biotechnology), polyclonal rabbit anti-ERK (1:500; CAT-#9102, Cell Signaling Technology), monoclonal rabbit anti-phospho-ERK (1:500; CAT-#4376, Cell Signaling Technology), secondary peroxidase-conjugated goat anti-rabbit IgG (1:1000; Dianova), and peroxidase-conjugated donkey anti goat IgG (SantaCruz Biotechnology). As molecular weight marker, the BenchMark™ Protein Ladder (Invitrogen) was used.

4.4.3. Coomassie-blue protein staining of SDS gels

After SDS-PAGE, proteins in the gel can be stained directly with Coomassie-blue-G250 staining solution (10% isopropanole, 10% acetic acid, 0.04% (w/v) Coomassie-brilliant-blue R-250). Staining was performed for at least 3 hours and to remove unbound staining solution, gels were de-stained with de-staining solution (10%

isopropanole; 10% acetic acid) for at least 3 hours. For longer storage, gels were dried between cellophane foils using a vacuum gel dryer (Drygel Sr. Slab Gel Dryer Model SE 1160, Hoefer) at 60°C for 1-2 hours.

4.5. Generation and affinity purification of polyclonal Spred-1 and Spred-2 specific antibodies

To perform a Spred-1 specific polyclonal antibody, the most different intermediate region of Spred-1 (amino acids 124-233) - compared to Spred-2 - was used. To perform a Spred-2 specific polyclonal antibody, the intermediate region of Spred-2 (amino acids 123-196) was used.

4.5.1. Expression and preparation of GST-Spred-1 and GST-Spred-2 fusion proteins

The coding sequence representing amino acids 124-233 of Spred-1, and the coding sequence representing amino acids 123-196 of Spred-2 were cloned into the BamHI and EcoRI sites of the pGEX-4T-2 protein expression vector (prokaryotic GST-fusion vector, with glutathione-S-transferase coding sequence; Pharmacia Biotech). Therefore, the Spred-1/Spred-2 intermediate regions were amplified from the TOPO2.1- Spred-1/Spred-2 cDNA plasmids using the proof-reading Advantage[®]2 PCR Kit (Clontech) and the following primer pairs:

For Spred-1 (124-233): => PCR fragment: 350 bp:

5'MSpr.1,GST (5'CAGGATCCCCCTCTCTAGGGTGCCCAGCGTCA3')

(BamHI) (*proline=helix breaker*)

3'MSpr.1,GST (5'CGGAATTCTCACTTCAAAGGGACCCTAGTTTG3')

(EcoRI) (*Stop*)

For Spred-2 (123-196): => PCR fragment: 240 bp:

5'MSpr.2,GST (5'CAGGATCCCCCATAGAAGGTTCAACGACCTCC3')

(BamHI) (*proline=helix breaker*)

3'MSpr.2,GST (5'CGGAATTCTCACCGCGGCAACCGCTGGTCAGG3')

(EcoRI) (*Stop*)

The final constructs were verified by sequencing (ABI-PRISM) and transformed into E. coli BL21 (DE3) chemically competent cells for protein expression. All further procedures were done in parallel for both constructs, here described for the GST-Spred-1 fusion protein.

Overnight cultures of transformed BL21 cells were diluted 1:40 with 900 ml 2xYT medium (16 g tryptone, 10 g yeast-extract, 5 g NaCl ad. 1 l bidest. H₂O; ampicillin 100 µg/ml) and shaken at 37°C. In the late exponential growth phase (OD₆₀₀=0.8), fusion protein expression was induced with 1 mM IPTG. After 4 hours, the bacteria pellet was separated by centrifugation (5000 g, 10 minutes), and homogenized with 15 ml ice-cold lysis buffer (50 mM Tris-Cl, pH 8.5, 5 mM EDTA, 10 mM NaCl, 1 mg/ml lysozyme) for 45 minutes on ice. Then, 1% (v/v) Triton X-100 and 1 tablet protease inhibitor („Mini cocktail“, Roche) was added, the lysate vigorously mixed, and sonified on ice for 10 minutes (Branson sonifier 250: 50% duty cycle, 50% power output, level 2). After centrifugation at 14.000 rpm (Eppendorf microfuge 5415) for 10 minutes, the supernatant was used for glutathione (GSH) bead coupling to separate the GST-Spred-1 fusion protein. Previously, it was verified that the GST-Spred-1 fusion protein is soluble and localized in the supernatant. After pre-equilibration of 6 ml glutathione beads (Glutathione Sepharose-4B Beads; Amersham) with lysis buffer/1% Triton X-100, the bacteria supernatant was added and the suspension slowly rotated at 4°C for 3 hours. After centrifugation with 500 rpm at 4°C for 30 minutes (Rotanta/TRC centrifuge), the pellet with the GST-Spred-1 coupled beads was washed with 3 volumes of lysis buffer and again centrifuged with 500 rpm at 4°C for 10 minutes. The pellet was additionally washed 2 times with 3 volumes PBS. After the last centrifugation, the GST-Spred-1 fusion protein was eluted from the remaining pellet with 5 ml elution buffer (10 mM glutathione, 50 mM Tris, pH 8.0). The supernatant was collected after a final centrifugation (500 rpm, 4°C, 10 minutes) and a 5 µl sample of the GST-fusion protein was tested on a 12.5% SDS-gel (Fig. 2). Finally, the protein was dialysed in PBS or carbonate buffer at 4°C and stored at -80°C.

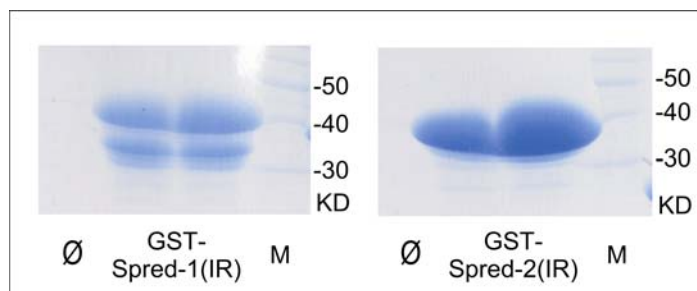


Figure 2.
Expression of purified GST-Spred fusion proteins.

GST-Spred-1(IR) (left) and GST-Spred-2(IR) (right) fusion proteins on a Coomassie-stained SDS gel. (IR: intermediate region, M: protein marker).

4.5.2. Coupling of proteins to NHS-HiTrap columns

The recombinant GST-Spred-1 was covalently coupled to an NHS-activated Hi-Trap[®] Sepharose column (Amersham Pharmacia Biotech). (The same procedure was performed in parallel with the GST-Spred-2 construct.) Therefore, the protein preparation was dialysed with coupling buffer (0.2 M NaHCO₃, 0.5 M NaCl; pH 8.3) at 4 °C, and the NHS-activated HiTrap columns (1 ml; Amersham) were prepared for the ligand coupling by injecting 6 ml ice-cold 1 mM HCl to remove the isopropanol containing storage buffer. One ml of the ligand (1-5 mg/ml) was injected in the column and incubated for 45 minutes at room temperature. To inactivate remaining active groups that have not reacted with the ligand and to wash out unbound ligands, the column was washed with 6 ml Buffer A (0.5 M ethanolamine, 0.5 M NaCl, pH 8.3) and 6 ml Buffer B (0.1 M Na-acetate, 0.5 M NaCl, pH 4). After an additional injection of 6 ml Buffer A, the column was incubated for 15 minutes at room temperature. Following three more alternating injections of 6 ml Buffer B and 6 ml Buffer A, the column was neutralized with 6 ml PBS. Then, the column was ready to be used or stored in PBS/0.1% NaN₃ at 4°C.

4.5.3. Immunization of rabbits

Recombinant GST-Spred-1 (GST-Spred-2) fusion protein was dialysed in PBS and concentrated with a Centricon column YM-3 (Amicon, Millipore) to a concentration of at least 1 mg/ml according to the manufacturer's instructions.

1 mg of recombinant GST-Spred-1 (GST-Spred-2) fusion protein was used as antigen for immunization of rabbits (BioGenes, Germany). Immunizations, boosts, and collections of antisera were performed by standard protocols of BioGenes (Berlin). Two rabbits for Spred-1 (4915 and 4916) and two rabbits for Spred-2 (6215 and 6216) were immunized and previously 20 ml pre-immune serum of each rabbit was collected for later control experiments. Two bleedings revealed 50 ml antiserum of each rabbit.

4.5.4. Affinity purification of antisera

The resulting antiserum of each rabbit was diluted 1:10 in PBS and run through the prepared Hi-Trap columns connected in series at a flow rate of 0.1 ml/min at 4°C.

For Spred-1:

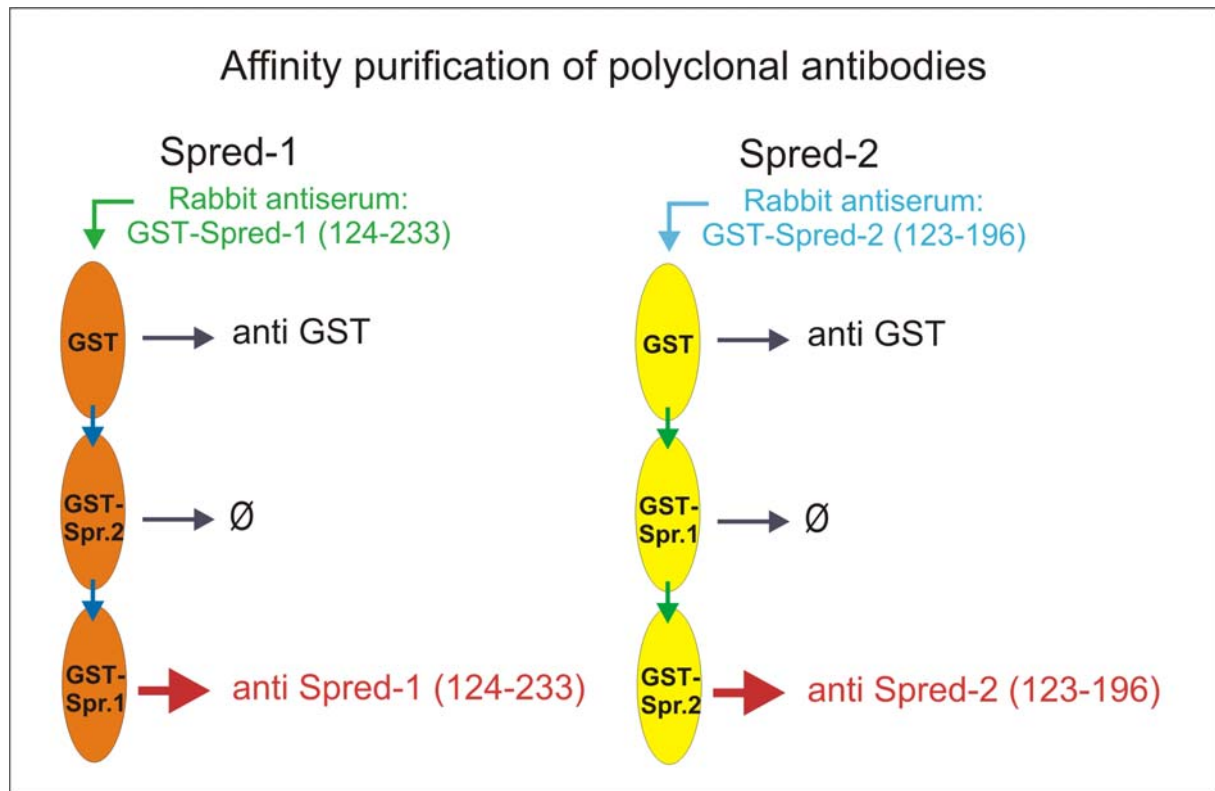
With a first column, coupled with GST antigen, GST-specific antibodies were depleted. With a second column, coupled with GST-Spred-2 (aa 123-196), cross-

reacting antibodies with Spred-2 were depleted. Then, the flow-through was affinity purified using a third column, coupled with GST-Spred-1 fusion protein (aa 124-233) (Fig. 3).

For Spred-2:

With a first column, coupled with GST antigen, GST-specific antibodies were depleted. With a second column, coupled with GST-Spred-1 (aa 124-233), cross-reacting antibodies with Spred-1 were depleted. Then, the flow-through was affinity purified using a third column, coupled with GST-Spred-2 fusion protein (aa 123-196) (Fig. 3).

The columns were washed with 20 ml PBS and 20 ml PBS/350 mM NaCl. Antibodies specifically binding to Spred-1 (Spred-2) were eluted from the third column with 100 mM glycine, pH 3.0 in six separate 1 ml fractions, and the resulting fractions were immediately neutralized with 40 μ l of 1 M Tris-HCl, pH 8.9, to avoid protein denaturation. All elution fractions were analyzed by a 12.5% SDS-PAGE gel to determine the fractions, containing the affinity purified antibodies. The two fractions with the highest antibody concentrations were pooled and glycerol added to a final concentration of 40%. Aliquots were stored at -20°C. Concentrations of antibodies were estimated by photometrical measurement at 280 nm (Ultrospec 2000, Pharmacia). ($OD_{280}=1.3$ corresponds to 1 mg/ml of antibody). In general, the antibodies were used with a concentration of 0.1 μ g/ml for Western blots, and 1 μ g/ml for immunohistochemical analyzes.

**Figure 3.****Affinity purification of polyclonal Spred-1/-2 antibodies.**

Column schemes for affinity purification of Spred-1 and Spred-2 specific antibodies. Rabbit antisera are depleted at the first column from GST antibodies, at the second column from Spred-2 (Spred-1, respectively) cross-reactive antibodies, and the Spred-1 (Spred-2, respectively) specific antibodies were eluted from the third column.

4.6. Generation of Spred-2 knockout mice using a gene trap model**4.6.1. Gene trapping and Southern blot analysis**

To disrupt the *Spred-2* gene in mice, I generated a mouse strain, using the XB228 embryonic stem cell line with the pGTO gene trap vector inserted between exons 4 and 5 (Baygenomics, San Francisco). Vector insertion was confirmed by X-Gal staining according to the protocol given by the Sanger Institute Gene Trap Resource (<http://www.sanger.ac.uk/PostGenomics/genetrapprotocols.shtml>) and single insertion of the gene trap vector was confirmed by Southern blot analysis. The Southern probe was a 630-bp fragment of the *engrailed2* intron 1 gene trap vector sequence, which was amplified with the following primers: forward (5'AGATGCCAGAGACTCAGTGAAGCC3') and reverse (5'TTCTTTGGTTTTTCGGGACCTGG3'). 10 µg of genomic XB228 DNA was digested with BglII, cutting once within the entire gene trap vector sequence, separated by conventional agarose gel electrophoresis, blotted, and hybridized with the radiolabeled probe.

4.6.2. Mouse breeding

After confirmation of single integration of the gene trap vector into the *Spred-2* gene, XB228 ES cells were used to generate germ line chimeras. Therefore, XB228 ES cells were injected into C57Bl/6 mouse blastocysts, transferred into pseudo-pregnant females, and offspring were examined for chimeras. In total, four blastocyst transfers were performed and eight chimeric males obtained. This work was done by K.P. Knobloch in the FMP (Forschungsinstitut für molekulare Pharmakologie in Berlin; Prof. Dr. Ivan Horak). Five of the eight chimeric males were mated to female C57Bl/6 wildtype mice to test for germ line transmission and to obtain heterozygous *Spred-2*^{+/-} mice.

4.6.3. Genotyping of mice

Genomic DNA was isolated of mouse tail tips (0.5 cm), using the DNeasy tissue Kit (Qiagen) according to the manufacturer's instructions. Offspring were genotyped by PCR analyzes, using the Taq Core Kit (+ Q-solution, Qiagen) and the following sets of primers: for wt PCR, amplifying a 1600 bp fragment, Pr.1 (5'XB228,Pr.3: 5'GCTTGACCGGCACCCCGGTGAG3') and Pr.3 (3'XB228,Spr.2 Exon 5 (wt): 5'TAGAAGAAGTGTCCGTAGCTGT3'), for ko PCR, amplifying a 2700 bp fragment, Pr.1 and Pr.2 (3'XB228,pGTO Vector/Exon: 5'TTCTTTGGTTTTTCGGGACCTGG3'). The following PCR protocol was used for both PCRs (Table 3).

94°C	94°C	72°C	68°C	72°C	4°C
3min	1min	1min	3min	10min	
40 cycles					

Table 3.
Genotype PCR protocol.

4.7. Generation of Spred-1 and Spred-2 knockout mice using gene targeting vectors

4.7.1. General strategy

To generate gene targeting vectors for *Spred-1* and *Spred-2*, the backbone vector „KO/lox/frt (pJB1; 9.44 kb)“ (a kind gift of Joachim Herz/Jochen Brich; Dallas) was used (Fig. 4). This vector includes a neomycin resistance cassette flanked by loxP and frt sites, followed by 2 HSV-TK (Herpes simplex virus- thymidine kinase) cDNAs. The four unique restriction sites (NotI, XhoI, PacI, and PmeI) and the vector size were verified by restriction digests. The integrity and orientation of the 2 loxP and 2 frt sites were verified by sequencing with T7 (5'GTAATACGACTCACTATAG3') and 5'neo (5'TATCGCCTTCTTGACGAGTTCTTCTGA3') primers.

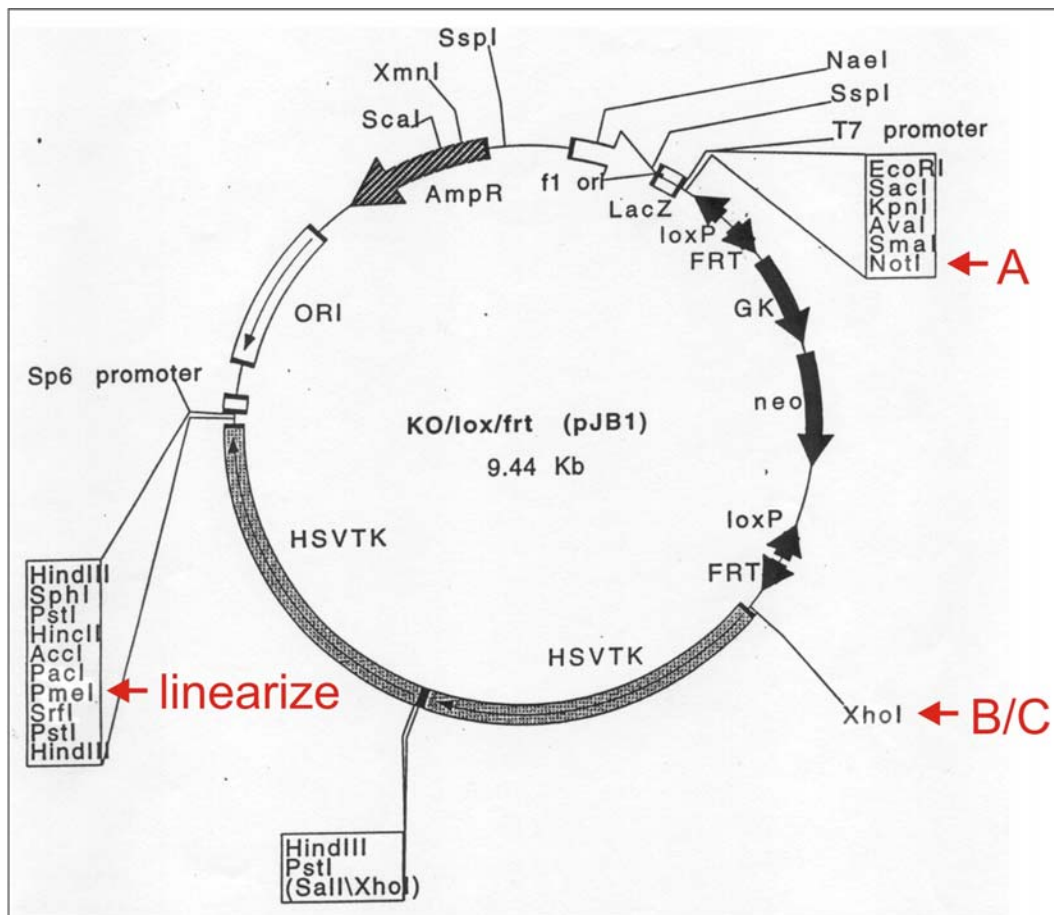


Figure 4.
KO/lox/frt (pJB1) vector map.

A-fragments were cloned in the NotI restriction site, B- and C-fragments, respectively, were cloned in the XhoI restriction site, and for linearization of the final vector the PmeI restriction site was used.

4.7.2. Cloning of Spred-1 and Spred-2 gene targeting vectors

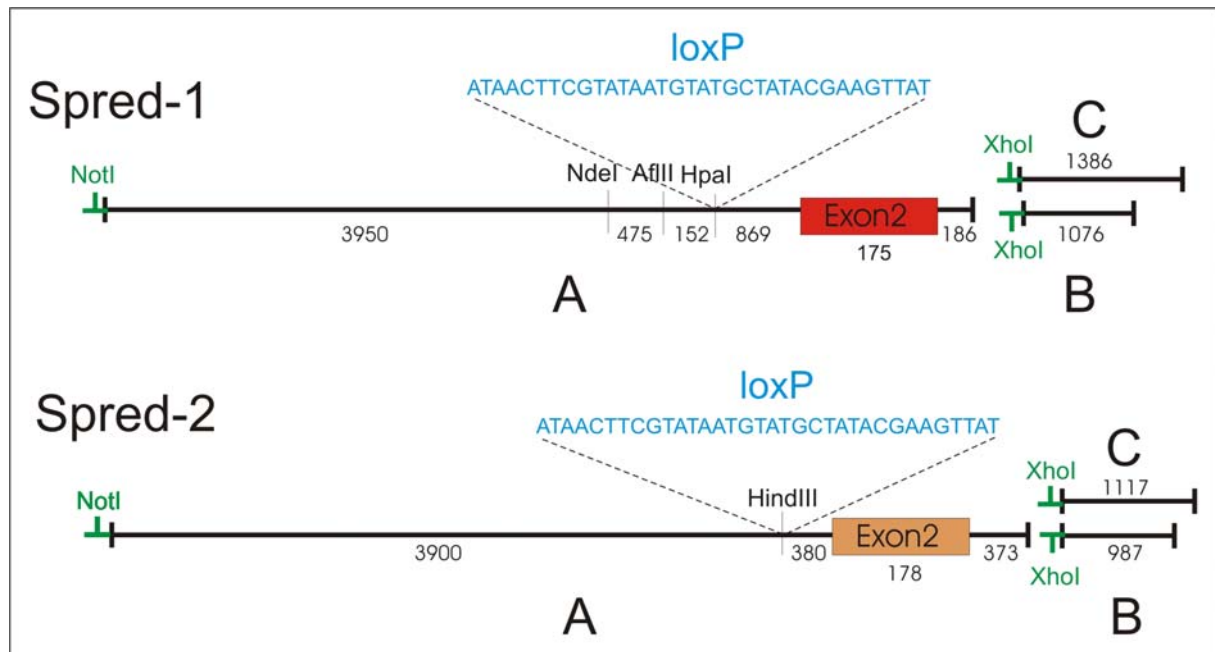


Figure 5.

Spred-1 and Spred-2 DNA fragments used for generating the gene targeting vectors.

For Spred-1 and Spred-2 the construct lengths of the A-, B-, and C-fragments with additional NotI and XhoI restriction sites (green) are demonstrated. The additional loxP site (blue) was inserted in the HpaI restriction site of Spred-1, and in the HindIII restriction site of Spred-2. (Numbers indicate the relevant basepair amounts for each section).

4.7.2.1. Cloning of A-fragments into TOPO2.1

First, the long homologous genomic sequences (further called “**A-fragments**”) were amplified by PCR (TAKARA) using genomic E14.1 DNA as template and T/A-cloned into the TOPO2.1 vector (Invitrogen). Only the T/A-cloning products with the right orientation (multiple cloning site at the 3’-end of the insert) were usable, because the NotI restriction site of the multiple cloning site was necessary for further cloning steps. Therefore, the right fragment orientation was verified by restriction digests, control PCRs, and sequencing of the vector/insert borders. The A-fragments contain exon 2 with flanking intronic sequences and at the 5’-end a NotI restriction site was added with the primers (Fig. 5). The following primer pairs were used:

For Spred-1 (-> 5750 bp PCR fragment):

5’Spr.1KO b+NotI: (5’GCGGCCGCTCAAGTTGGTAGAGGATACGTGCATTATGT3’)

(NotI)

3’ Spr.1KO A: (5’CTCAGACCCAGTTAGAAACAGTCACATCTT3’).

For Spred-2 (-> 4500 bp PCR fragment):

5' Spr.2KO b+NotI: (5'GCGGCCGCCTAATCTTAGGGATTCTTATTGTGGAATTG3')
(NotI)

3' Spr.2KO B: (5'CGAACACTCTTATGCTCTGGGCCACCTCCCAG3').

It was tested that no NotI and PmeI restriction sites were included in these A-fragment sequences, because this would have interfered with the further cloning and linearization processes.

4.7.2.2. Cloning of B-fragments into pDrive

Second, the short homologous genomic sequences (further called “**B-fragments**”) were amplified by PCR (Advantage 2 Polymerase Mix ;Clontech) using genomic E14.1 DNA as template and T/A-cloned into the pDrive Cloning Vektor (Qiagen). Only the T/A-cloning products with the right orientation (multiple cloning site at the 3'-end of the insert) were usable, because the XhoI restriction site of the multiple cloning site was necessary for further cloning steps. Therefore, the right fragment orientation was verified by restriction digests, control PCRs, and sequencing of the vector/insert borders. The B-fragments contain the intronic sequences following directly after the intronic sequence at the 3'-end of the corresponding A-fragments and at the 5'-end, a XhoI restriction site was added with the primers (Fig. 5). The following primer pairs were used:

For Spred-1 (-> 1076 bp PCR fragment):

5'Spr.1KOe+XhoI: (5'CTCGAGAGTAATGACAATATATTGCAAGGGGCTGCC3')
(XhoI)

3' Spr.1KO B: (5'TCGGATACTTAGTAGCTTTGGGCTCTCAGA3').

For Spred-2 (-> 987 bp PCR fragment):

5'Spr.2KOe+XhoI: (5'CTCGAGATGTGCAAACATGAAGAACTGAGTCAGATC3')
(XhoI)

3' Spr.2b* neu: (5'AGGTGTGCATGCACCAAGGTAC3')

It was tested that no XhoI, NotI, and PmeI restriction sites were included in these B-fragment sequences, because this would have interfered with the further cloning and linearization processes.

4.7.2.3. Cloning of C-fragments into TOPO2.1/ pDrive

Third, homologous genomic sequences for Spred-1 and Spred-2 test vectors, containing the B-fragment sequences plus an additional short following intronic sequence at the 3'-end (further called “**C-fragments**”), were amplified by PCR

(Advantage 2 Polymerase Mix; Clontech) using genomic E14.1 DNA as template and T/A-cloned into the TOPO2.1 cloning vector (Invitrogen) (Spred-1), or into the pDrive Cloning vector (Qiagen) (Spred-2), respectively. Only the T/A-cloning products with the right orientation (multiple cloning site at the 3'-end of the insert) were usable, because the XhoI restriction site of the multiple cloning site was necessary for further cloning steps. Therefore, the right fragment orientation was verified by restriction digests, control PCRs, and sequencing of the vector/insert borders. The C-fragments contain an additional XhoI restriction site at the 5'-end, which was added with the primers (Fig. 5). The following primer pairs were used:

For Spred-1 (-> 1386 bp PCR fragment):

5'Spr.1KOe+XhoI: (5'CTCGAGAGTAATGACAATATATTGCAAGGGGCTGCC3')
(XhoI)

3' Spr.1KO C: (5'GATCACTTAGGATAATTCTAACCATGGGAG3').

For Spred-2 (-> 1117 bp PCR fragment):

5'Spr.2KOe+XhoI: (5'CTCGAGATGTGCAAACATGAAGAACTGAGTCAGATC3')
(XhoI)

3' Spr.2KO C: (5'CTGCCTGCCTCAGCCTCCCACAGCTGGTAT3').

It was tested that no XhoI restriction sites were included in these C-fragment sequences, because this would have interfered with the further cloning process.

4.7.2.4. Insertion of an additional loxP site in the A-fragments before exons 2

To receive a floxed exon 2, it was necessary to integrate an additional loxP site in the same orientation like the 2 loxP sites in the final back bone vector. Therefore, suitable restriction sites were searched by database analyzes in the A-fragments and then tested by control restriction digests. For this cloning part, different strategies for the Spred-1 and Spred-2 constructs were necessary.

The following strategy was used for the **Spred-1** vector:

Three unique restriction sites - NdeI, AflII, and HpaI - were verified in the sequence in front of the Spred-1 A-fragment (Fig. 5). An insert with the additional loxP site and a HpaI restriction site at the 3'-end, and an AflII restriction site at the 5'-end was amplified by PCR using the Spred-1 A-fragment in the TOPO2.1 vector as template.

Therefore, the following primer pair was used to reveal a 188 bp PCR product:

5' Spred1A-Afl: (5'TAATCTTAAGTAAACCGTAATCTTACTACA3') (AflII),

3'Spred1A-Hpa+lox:

5'TAATGTTAACATAACTTCGTATAATGTATGCTATACGAAGTTATTAAGCGACTG
GAA3' (HpaI, *loxP*)

The A-fragment sequence between the AflII and HpaI restriction site in the TOPO2.1 vector was replaced by the PCR product with the additional loxP site by cloning and verified by a control PCR with 5'Kontr.Spr.1a+lox (5'TCCAGTCGCTTAATAACTTCGTATAGCAT3') and 3'Spr.1KOA (5'CTCAGACCCAGTTAGAAACAGTCACATCTT3') primers and by sequencing.

The following strategy was used for the **Spred-2** vector:

One unique restriction site – HindIII - was verified in the sequence in front of the Spred-2 A-fragment (Fig. 5). A replacement sequence with the additional loxP site and a HindIII restriction site at the 3'-end from the 5'-beginning of the Spred-2 A-fragment was amplified by PCR using the Spred-2 A-fragment in the TOPO2.1 vector as template.

Therefore, the following primer pair was used to reveal a 3660 bp PCR product:

5'M13 reverse: (5'AACAGCTATGACCATG3'), and 3'2aHindIII-loxP:
(5'TAATAAAGCTTATAACTTCGTATAATGTATGCTATACGAAGTTATTAACGTTTTAT
GAAGCTAAG3') (HindIII, *loxP*).

The A-fragment sequence between the HindIII restriction site of the vector multiple cloning site of the TOPO2.1 at the 5'-end and the HindIII restriction site in the Spred-2 sequence at the 3'-end was replaced by the PCR product with the additional loxP site by cloning and sequence orientation and integrity verified by a control PCR with 5'2aloxKontr. (5'AGTGAGAATGTGATTAATTT3'), and 3'Spr.2KOB (5'CGAACACTCTTATGCTCTGGGCCACCTCCCAG3') primers and by sequencing.

4.7.2.5. Re-cloning of the B-fragments from the pDrive cloning vector in the KO/lox/frt vector

The B-fragments of Spred-1 and Spred-2, respectively, were re-cloned from the T/A-cloning vector in the KO/lox/frt vector using the XhoI restriction sites. The ligation in the right orientation was verified by control PCRs with the following primer pairs:

For Spred-1:

5' NEO: (5'TATCGCCTTCTTGACGAGTTCTTCTGA3'),

3' Spr.1KO B: (5'TCGGATACTTAGTAGCTTTGGGCTCTCAGA3').

For Spred-2:

5' NEO: (5'TATCGCCTTCTTGACGAGTTCTTCTGA3'),

3' Spr.2b* neu: (5'AGGTGTGCATGCACCAAGGTAC3').

4.7.2.6. Re-cloning of the control C-fragments from the T/A-cloning vectors in the KO/lox/frt vector

The C-fragments of Spred-1 and Spred-2, respectively, were re-cloned from the T/A-cloning vector in the KO/lox/frt vector using the XhoI restriction sites. The ligation in the right orientation was verified by control PCRs with the following primer pairs:

For Spred-1:

5' NEO: (5'TATCGCCTTCTTGACGAGTTCTTCTGA3'),

3' Spr.1KO C: (5'GATCACTTAGGATAATTCTAACCATGGGAG3').

For Spred-2:

5' NEO: (5'TATCGCCTTCTTGACGAGTTCTTCTGA3'),

3' Spr.2KO C: (5'CTGCCTGCCTCAGCCTCCCACAGCTGGTAT3').

4.7.2.7. Re-cloning of the A-fragments with additional loxP site from the TOPO2.1 vector in the KO/lox/frt vector with the B-fragments.

The A-fragments with the additional loxP site of Spred-1 and Spred-2, respectively, were re-cloned from the TOPO2.1 vector in the KO/lox/frt vector with the corresponding B-fragment using the NotI restriction sites. The ligation in the right orientation was verified by control PCRs with the following primer pairs:

For Spred-1:

5'T7: (5'GTAATACGACTCACTATAG3'),

3' Kontr.1a in KO: (5'GTATTGGCAATGCTGCATTC3').

For Spred-2:

5'T7: (5'GTAATACGACTCACTATAG3'),

3' Kontr.2a in KO: (5'GAAATCCAGCTGCACAGGGT3').

4.7.2.8. Controls of the final gene targeting vectors

To verify the appropriate cloning processes, the Spred-1 and Spred-2 gene targeting vectors were tested by restriction digests (with NotI, XhoI, and PmeI) and sequencing.

For sequencing, the following primers were used:

For the Spred-1 gene targeting vector:

1) Sequence control of the A-fragment start:

T7: (5'GTAATACGACTCACTATAG3')

2) Sequence control of the 1. loxP site:

5' Spred1A-Afl: (5'TAATCTTAAGTAAACCGTAATCTTACTACA3') (AflIII)

3) Sequence control of the complete exon 2:

5' Seq Spr.1,Ex2: (5'GACCAACAGATTGACTTTCT3')

4) Sequence control of the 2. loxP and 1. frt site:

5' Ende 1a to loxP: (5'TATGTTAAAGATGTGACTGT3')

5) Sequence control of the 3. loxP, 2. frt site and start of the B-fragment:

3' 1b KO to Neo neu: (5'GACCTTTGGCCTAAGGAACA3')

6) Sequence control of the B-fragment end:

5' Spred1B to HSV: (5'TCTGAGAGCCCAAAGCTACT3').

For the Spred-2 targeting vector:

1) Sequence control of the A-fragment start:

T7: (5'GTAATACGACTCACTATAG3')

2) Sequence control of the 1. loxP site:

5' 2a lox Kontr.: (5'AGTGAGAATGTGATTAATTT3')

3) Sequence control of the complete exon 2:

5' Seq. Spr.2, Ex2: (5'CTTGCCCTGGGACACACGTT3')

4) Sequence control of the 2. loxP and 1. frt site:

5' Ende 2a to loxP: (5'CTGCAAGATGCTGGGGCTGG3')

5) Sequence control of the 3. loxP, 2. frt site and start of the B-fragment:

3' 2b in KO to Neo neu: (5'GGACGCTCCTGTCAATCACA3')

6) Sequence control of the B-fragment end:

5' 2b*in KO to HSV: (5'TCACAAATCGAGTAACTGAA3').

4.7.3. Optimization of the embryonic stem (ES) cell screening PCR

To optimize the ES cell screening PCR for homologous recombination events, control vectors (C-fragments in KO/lox/frt vector) for Spred-1 and Spred-2 were cloned. Because the amount and quality of genomic ES cell DNA is extremely low in the screening process, the PCR had to be optimized to a detection level of 100-10 fg (Fig. 6). The 5' primer was chosen as part of the neo-cassette, and the 3' primer external of the homologous sequence (B-fragment). To mimic the later background screening conditions, 100 ng of genomic ES cell DNA was added to each PCR reaction. The following primer pairs were used:

For Spred 1 (-> 1830 bp PCR product):

5' NEO: (5'TATCGCCTTCTTGACGAGTTCTTCTGA3'),

3' Spr.1KO C: (5'GATCACTTAGGATAATTCTAACCATGGGAG3').

For Spred2 (-> 1450 bp PCR product):

5' NEO: (5'TATCGCCTTCTTGACGAGTTCTTCTGA3'),

3' Spr.2KO C: (5'CTGCCTGCCTCAGCCTCCCACAGCTGGTAT3').

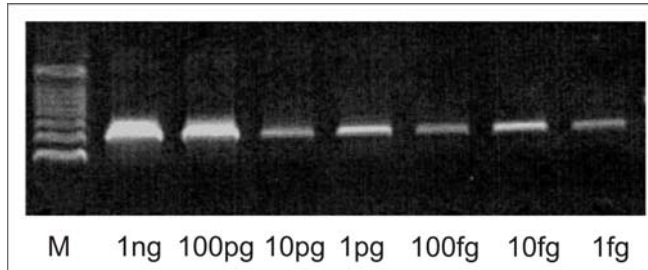


Figure 6.

Test PCR for ES cell screening.

Dilution row of the test vector to optimize the PCR conditions down to a level of 1 fg. (Example here for the Spred-1 construct).

4.7.4. Electroporation and selection of ES cells

To electroporate the gene targeting vectors in E14.1 ES cells, 25 µg vector DNA were linearized with PmeI, phenol/chloroform extracted, and dissolved in PBS (concentration 1 µg/µl). After electroporation, a positive and negative selection was performed to obtain as much positive clones - which have integrated the targeting vector by homologous recombination - as possible. Positive selection was performed by G418, a neomycin derivate, which selects only the clones with an (anywhere) integrated neo-cassette. Negative selection was done by Gancyclovir, which selects only the clones that have no HSV-TK (Herpes simplex virus- thymidine kinase) cassette integrated. The Herpes simplex thymidine kinase metabolises Gancyclovir into a cell toxic substance that kills all ES cells, which have only randomly integrated the targeting vector anywhere in the genome. By the process of homologous recombination, the HSV-TK cassette is eliminated, therefore, the ES cells are able to survive. After the selection period, half of each clone was cryo-conserved in liquid N₂, and the other half was used for DNA isolation and PCR screening for appropriate homologous vector recombination. For each construct, two electroporation rounds were performed. ES cell culture, electroporation, selection processes, and cryo-conservation were performed in the group of Prof. Sendtner/ Dr. Stefan Wiese, Institute of Neurobiology (University of Würzburg).

4.7.5. PCR screening of ES cells for homologous recombination events

To test large numbers of ES cell clones for homologous recombination events, the single clones were cultivated on 96-well-plates after the picking process. After lyses and Proteinase K digest at 70°C for 10 minutes, the cell lysates were boiled at 95°C

for 20 minutes to denature the Proteinase K. Within each electroporation round, 4-6 96-well-plates were picked, corresponding to 380-575 ES cell clones. A general problem of the ES cell PCR screening was the extremely low amount and poor quality of DNA, the use of different PCR machines, the outside temperature, and primer quality. Therefore, the screening PCRs were optimized as described before. For PCR screening, the Taq Core Kit (+Q-Solution, Qiagen) was used in a reaction volume of 50 µl with 5-7 µl of genomic ES cell DNA. PCRs could be evaluated only if the positive controls where in the range of 100-10 fg still positive. Otherwise, the PCR would not be sensitive enough and had to be repeated.

4.7.6. Cre-recombinase treatment of ES cells and PCR screening of different Cre-recombinase events for complete and conditional knockouts

To obtain ES cells for conventional and conditional knockouts, the homologous recombined ES cells for Spred-1 and Spred-2 can be further treated with a Cre-recombinase containing plasmid (pmc-Cre; Neurobiology) by electroporation. For PCR selection of the different recombination events, the following primer pairs can be used.

For Spred1:

5' Kontr. Spr.1Cre(lox): (5'GTTACTACTTTTTCCAGTCGCTTAATAAC3') (*loxP*),
3' 1b KO to Neo neu: (5'GACCTTTGGCCTAAGGAACA3').

For Spred2:

5'Spr.2 Cre-Kontrolle: (5'TAGCTTCATAAAACGTTAATAACTTC3') (*loxP*),
3' 2b in KO to Neo neu: (5'GGACGCTCCTGTCAATCACA3').

The following list shows the four possible events with the resulting PCR product lengths in the screening PCR (Spred-1/Spred2):

- | | |
|--|-----------------|
| 1) No recombination event (original clone): | 3300 bp/3060 bp |
| 2) Conventional knockout: | 240 bp/250 bp |
| 3) Conditional knockout: | 1400 bp/1200 bp |
| 4) Deleted exon 2, neo-cassette still present: | 2200 bp/2100 bp |

For further use, the ES cells clones for conventional and conditional knockouts are of major interest and can be injected directly in blastocysts to generate the mouse strain of interest.

Another alternative to obtain conditional knockout mice is the electroporation with a Flipase-recombinase (Flp) expressing vector. After successful recombination, the neo-cassette is deleted and a floxed exon 2 remains. Furthermore, the homologous recombinated ES cells can be used directly to generate mice, which are further mated with Flp-deleter mice to obtain conditional knockout mice.

4.8. Mouse physiology

4.8.1. Hormone measurements in mice

Blood was collected from the V. cava, clotted, and centrifuged to separate the serum. Steroid hormone levels - estrogen and testosterone - were measured in the Institute of Gynaecology (Würzburg). Thyroid hormone levels - TSH, T3, and T4 - were measured in the Department of Endocrinology (Würzburg).

4.8.2. Blood glucose measurements in mice

Blood glucose levels were measured by taking a blood drop from the mouse tail tip and analyzing it with Accu Check (Roche).

4.8.3. Blood cell counts in mice

To count the different blood cell numbers, blood was collected from the V. cava in appropriate EDTA tubes, and measured with standard cell counters in the Central laboratory (University of Würzburg).

4.8.4. Bleeding time measurements in mice

To measure the bleeding time, the mouse tail tip was cut and the forming blood drop removed with a filter paper every 20 seconds. The time, until no further drop had formed, was measured.

4.8.5. Bleeding volume measurements in mice

To measure the bleeding volume, the mouse tail tip was cut and the forming blood drops collected in a heparinized glass capillare (Kaba; 85µl capillares: 1 cm = 1 µl) until the bleeding stopped.

4.8.6. Heart parameter measurements in mice

Blood pressure, heart rate, and further heart parameters were measured by heart catheterizing through the A. carotis. This work was done by Dr. Kai Hu, Cardiology (Würzburg).

4.8.7. Estimation of bone lengths

To measure bone lengths, isolated mouse legs were exposed by soft X-ray.

4.8.8. Statistical analyzes

Statistical analyzes were calculated by Student's T-test (Excel).

4.9. Additional materials and equipment

General chemicals were derived from Ambion (Austin, USA), Gibco Lifesience (Eggenstein), Merck (Darmstadt), Roth (Karlsruhe), Serva (Heidelberg), and Sigma (Deisenhofen).

Additionally, the following equipment was used:

Electrophoresis chambers (BioRad, Wide Mini SUB® Cell; BioRad, Mini-SUB® Cell GT), heating block (Eppendorf, Thermomixer 5U36), CO₂-incubator (Heraeus Instruments type B 6060), magnet stirrer (IKA, Combimag REO), PCR machines (MWG Biotech, Primus 96 plus; Perkin Elmer, GeneAmp PCR System 2400), pH-meter (Radiometer/ Copenhagen, PHM 92 LAB pH Meter), UV-photometer (Pharmacia Biotech, Ultrospec 2000 UV/ Visible Spectrometer), power supply (Pharmacia, Gene Power Supply GPS 200/400), shaker (B.Braun, Certomat® H/Certomat® R), speed vac (Savant, Speed Vac Plus SC 110A; Savant, Universal Vacuum System Plus with VaporNet® UVS 400A), vacuum pump (type MZ 2C, Vacuubrand GmbH-Co; Wertheim), vortexer (Scientific Industries (SI) Vortex-Genie 2), scale (Sartorius, MC1 Laboratory LC 4800 P), and centrifuges (Personal Spin-Vortex Microspin FV-2400; Table centrifuge, Eppendorf centrifuge 5415; Sorvall RC 5 B Plus; Sorvall RC 5B Refrigerated Superspeed Centrifuge; Sorvall RT 6000D, Beckmann J-6B; Rotanta/ TRC centrifuge).

5. Results

5.1. Generation of Spred-2-deficient mice using a gene trap approach

In order to generate Spred-2-deficient mice, an embryonic stem cell clone with a disrupted *Spred-2* gene, XB228, Baygenomics, San Francisco (<http://baygenomics.ucsf.edu>), was used for blastocyst injection. Chimeric male offspring (Fig. 7) were then mated to wildtype C57Bl/6 mice to test for germ line transmission of the disrupted *Spred-2* allele. Inbreeding of heterozygous offspring resulted in a slightly altered Mendelian ratio of 33.33% wildtype, 41.03% heterozygous, and 25.64% knockout mice (n=195, in total).

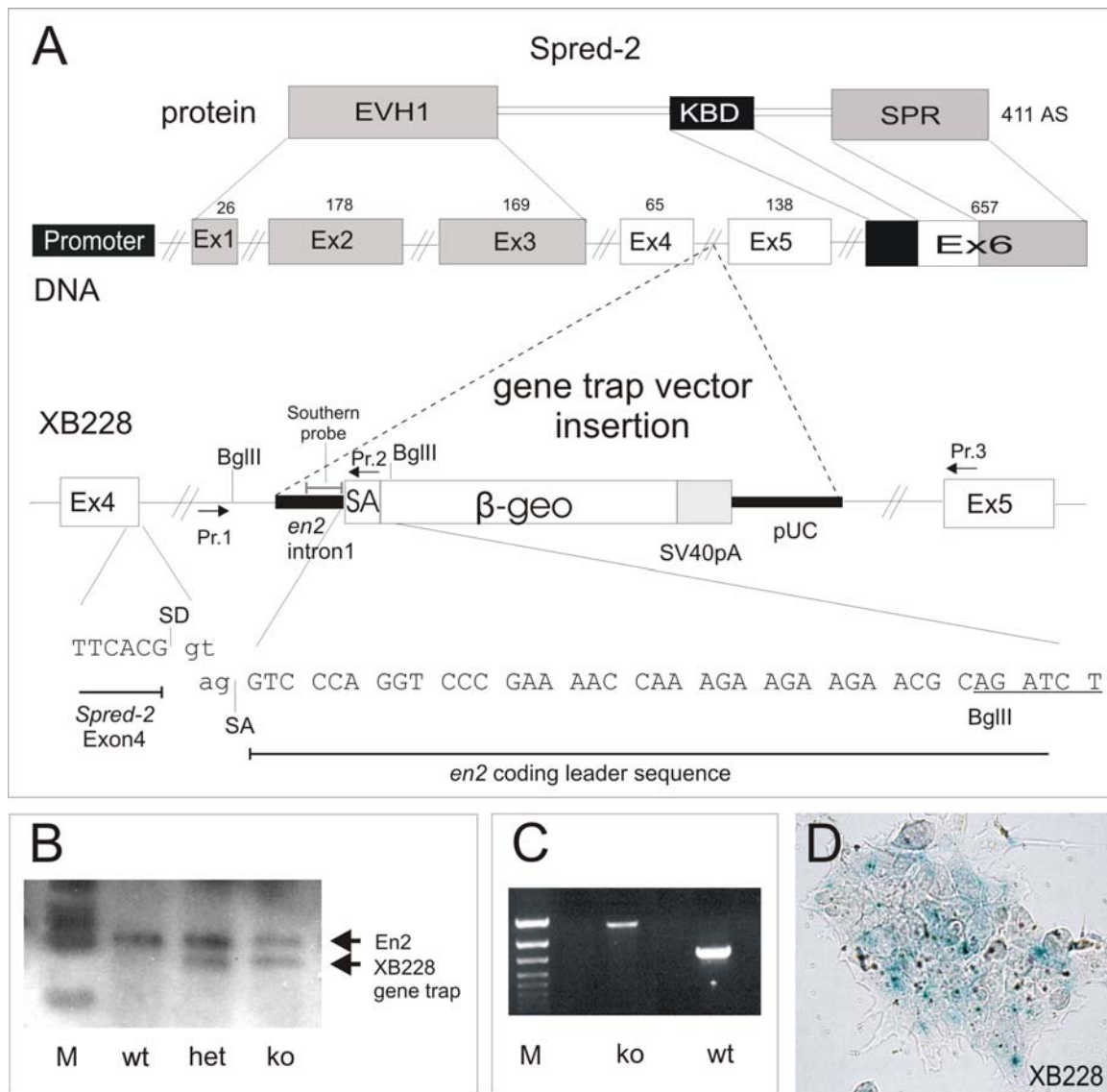


Figure 7.

Male chimera.

Example of the mixed ola/black coat colour of a male chimeric mouse.

The gene trap vector pGTO in the XB228 ES cell line was inserted between exons 4 and 5 of the *Spred-2* gene and the point of insertion was further defined by PCR and sequencing (Fig. 8A). Thereby, the artificial β -geo fusion cDNA of the pGTO gene trap vector was brought under control of the endogenous *Spred-2* promoter (Fig. 8A). Single integration of the gene trap vector into the genome was verified by Southern blotting. Therefore, genomic DNA was digested with BglII and part of the pGTO vector was used as radioactive probe (Fig. 8A). Appearance of only one additional band in knockout and heterozygous mice pointed towards a single integration of the gene trap vector. The upper band in the blot, which was also present in wildtype DNA, is related to the endogenous *engrailed2* gene, as the vector probe is part of the *en2* intron 1 (Fig. 8B). In XB228 ES cells, vector insertion and β -galactosidase expression was confirmed by X-Gal staining (Fig. 8D). Offspring were genotyped by PCR analyzes using primers Pr.1 and Pr.2 (Fig. 8A) for the knockout PCR and Pr.1 and Pr.3 (Fig. 8A) for the wildtype PCR (Fig. 8C).

**Figure 8.****Localization of the gene trap vector interrupting the *Spred-2* gene.**

(A) *Spred-2* protein structure with the corresponding genomic exon organization and a hypothetical promoter region. Exons 1, 2, and 3 are coding for the EVH-1 domain, exons 4 and 5 for the middle part and exon 6 for the KBD (c-Kit-binding domain) and the SPR (Sprouty related) domain. Numbers above exons correspond to the *Spred-2* cDNA. The gene trap vector, composed of a part of the *engrailed 2* intron 1 structure (*en2* intron1), a splice acceptor (SA), a β -galactosidase/neomycin resistance fusion gene (β -geo), an SV40 polyadenylation sequence (SV40pA), and a pUC backbone vector sequence, was inserted between exons 4 and 5 of the *Spred-2* gene. The nucleotide sequence near the splice junction joining the *Spred-2* exon 4 splice donor (SD) to the splice acceptor (SA) in the vector sequence is indicated below the diagram. Downstream of the splice acceptor, the first part of the *engrailed 2* (*en2*) coding leader sequence with the BgIII restriction site (underlined) is indicated. In the vector diagram, the Southern probe representing a part of the *engrailed 2* intron 1 sequence and the 3 primers (Pr.1, Pr.2, and Pr.3) used for genotyping PCRs are shown. The two relevant BgIII restriction sites, one in the *Spred-2* intron part and the other one in the gene trap vector sequence, are marked.

(B) Southern blot with DNA of wildtype (wt), heterozygous (het) and knockout (ko) mice, demonstrating single insertion of the gene trap vector in het and ko mouse DNA. The upper band - also present in wt DNA - corresponds to the endogenous *engrailed 2* (*en2*) gene.

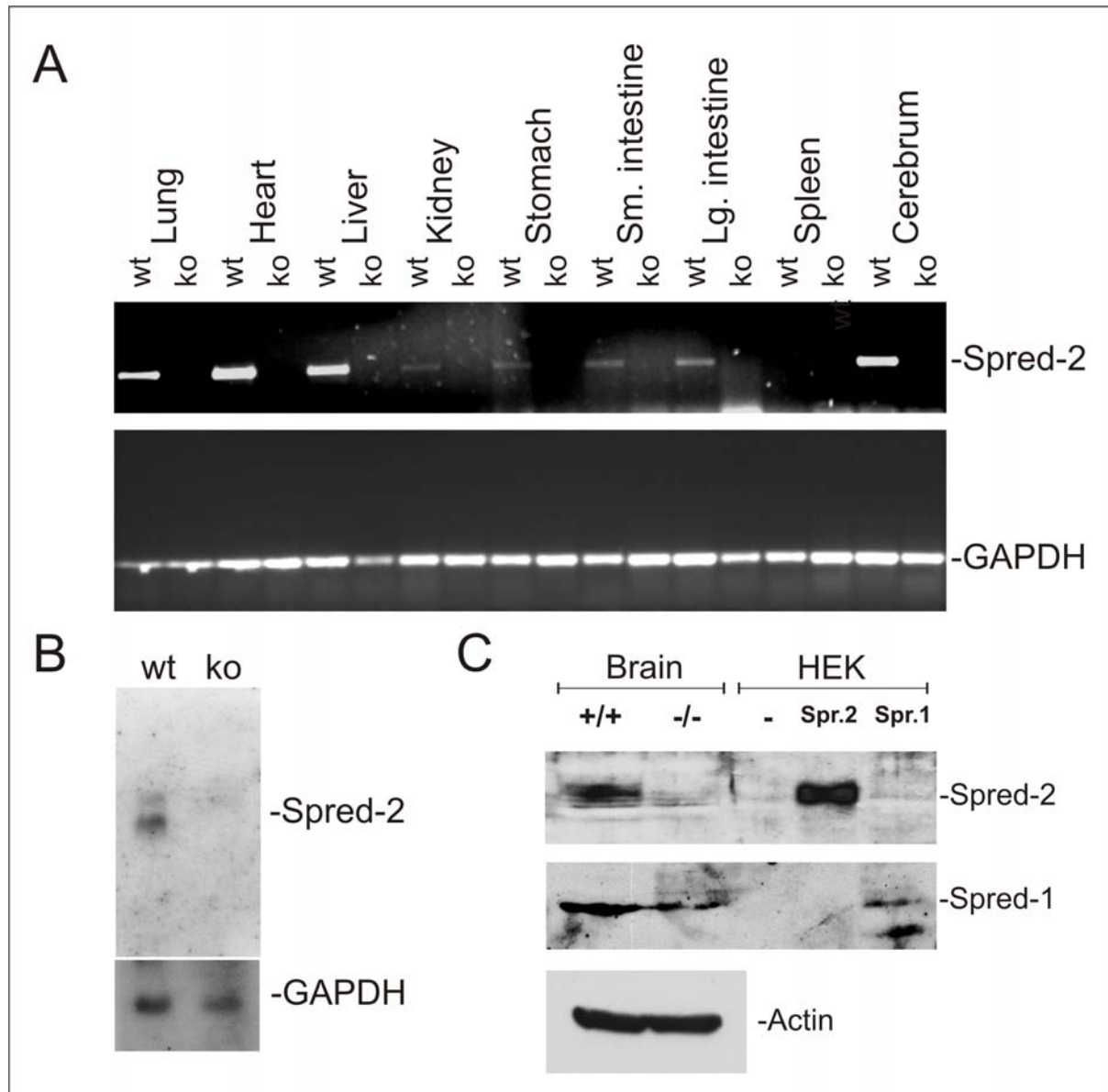
(C) Representative PCRs giving genotype of mice: knockout (ko) and wildtype (wt).

(D) X-Gal staining of cultured XB228 embryonic stem cells.

Male and female knockout mice were fertile and inbred matings resulted in viable offspring, although litters were smaller (average litter size 4.4 pups, ranging from 3-7), compared to litters of wildtype breeding pairs (average 8.4, ranging from 5-12). In general, life expectancy, nesting, and nursing behavior of knockout mice were inconspicuous as compared to their littermates.

5.2. Spred-2-deficiency in knockout mice on RNA and protein level

Successful disruption of the *Spred-2* gene in *Spred-2^{-/-}* mice was tested at both RNA and protein levels. Total RNA of different organs derived from *Spred-2*-deficient and wildtype mice was subjected to RT-PCR using specific primers for *Spred-2* and GAPDH. Loss of *Spred-2* mRNA was confirmed in all samples tested (Fig. 9A). Northern blot analyzes of brain - representing the organ with the strongest natural *Spred-2* expression - revealed no apparent forms of *Spred-2* mRNAs in total RNA preparations of *Spred-2^{-/-}* mice (Fig. 9B). To examine *Spred-2*-deficiency at the protein level, Western blots were performed with affinity-purified polyclonal rabbit anti-*Spred-2* antibodies. As above, brain lysates of wildtype and *Spred-2^{-/-}* mice were used as indicator tissues, since brain represents the organ with the highest *Spred-2* expression levels. Specificity of antiserum was confirmed with lysates of HEK293 cells transfected with expression constructs for *Spred-1* and *-2*. At the protein level, lack of *Spred-2* protein in *Spred-2^{-/-}* mice indicated functional loss of *Spred-2* (Fig. 9C). *Spred-1* expression in brain was determined by Western blot analyzes with affinity-purified polyclonal rabbit anti-*Spred-1* antibodies. Comparable amounts of *Spred-1* protein were detected in brain lysates of *Spred-2^{+/+}* and *Spred-2^{-/-}* mice, giving no evidence for a compensatory upregulation of *Spred-1* expression (Fig. 9C).

**Figure 9.****Loss of Spred-2 in XB228-derived mice.**

(A) RT-PCR showing loss of full-length Spred-2 mRNA in selected organs of knockout (ko) mice in comparison to wildtype controls (wt). (B) Northern blot using wildtype and knockout brain RNA. Note that no truncated or prolonged aberrant band was detectable in knockout mouse-derived RNA preparations. GAPDH levels indicate RNA integrity and equal loading. (C) Western blots demonstrating lack of Spred-2 protein in brain lysates of XB228-derived mice in comparison to lysates of control mice. Spred-1 levels seemed to be unaltered in Spred-2-deficient brain lysates. Lysates of Spred-1- and Spred-2-overexpressing HEK293 cells served as positive controls and actin levels indicate equal loading.

5.3. Gene disruption of Spred-2 causes achondroplasia-like dwarfism

Homozygous Spred-2-deficiency resulted in reduced body length and low body weight as compared to wildtype littermates (Fig. 10A). Soft X-ray exposures revealed a smaller skeleton of knockouts being in line with the observed growth retardation (Fig. 10B). Measurements of body weights of male (Fig. 10C) and female (Fig. 10D) wildtype and knockout mice at the age of 20 to 160 days demonstrated the trend towards dwarfism. Spred-2-deficient mice were already smaller at birth (Fig. 10A left panel) and remained smaller throughout the investigated lifetime (up to one year). Comparison of body weights of males (Fig. 10E) and females (Fig. 10F) at three different time points (25 days, 60 days, and 90 days) revealed statistically significant body weight differences between wildtype and knockout mice ($n \geq 10$ for each time point, *male $p < 0.01$, *female $p < 0.05$). Growth differences between male wildtype and knockout mice were more pronounced than that of their female counterparts. This might be due to an X-chromosomal compensatory effect in females which is not known yet and has to be investigated further. Organ weights in relation to whole body weights were compared at different time points: the organ weight to body weight ratio was not altered in knockout mice (lung: wt=0.6% \pm 0.137%, ko=0.8% \pm 0.081%, heart: wt=0.4% \pm 0.119%, ko=0.5% \pm 0.076%, kidney (average of both kidneys): wt=0.4% \pm 0.095%, ko=0.6% \pm 0.099%; liver: wt=4,6% \pm 0.436%, ko=5,0% \pm 0.707%; spleen: wt=0.3% \pm 0.091%, ko=0.3% \pm 0.117%; $n_{(wt)}=10$, $n_{(ko)}=7$), pointing towards a proportional dwarfism phenotype.

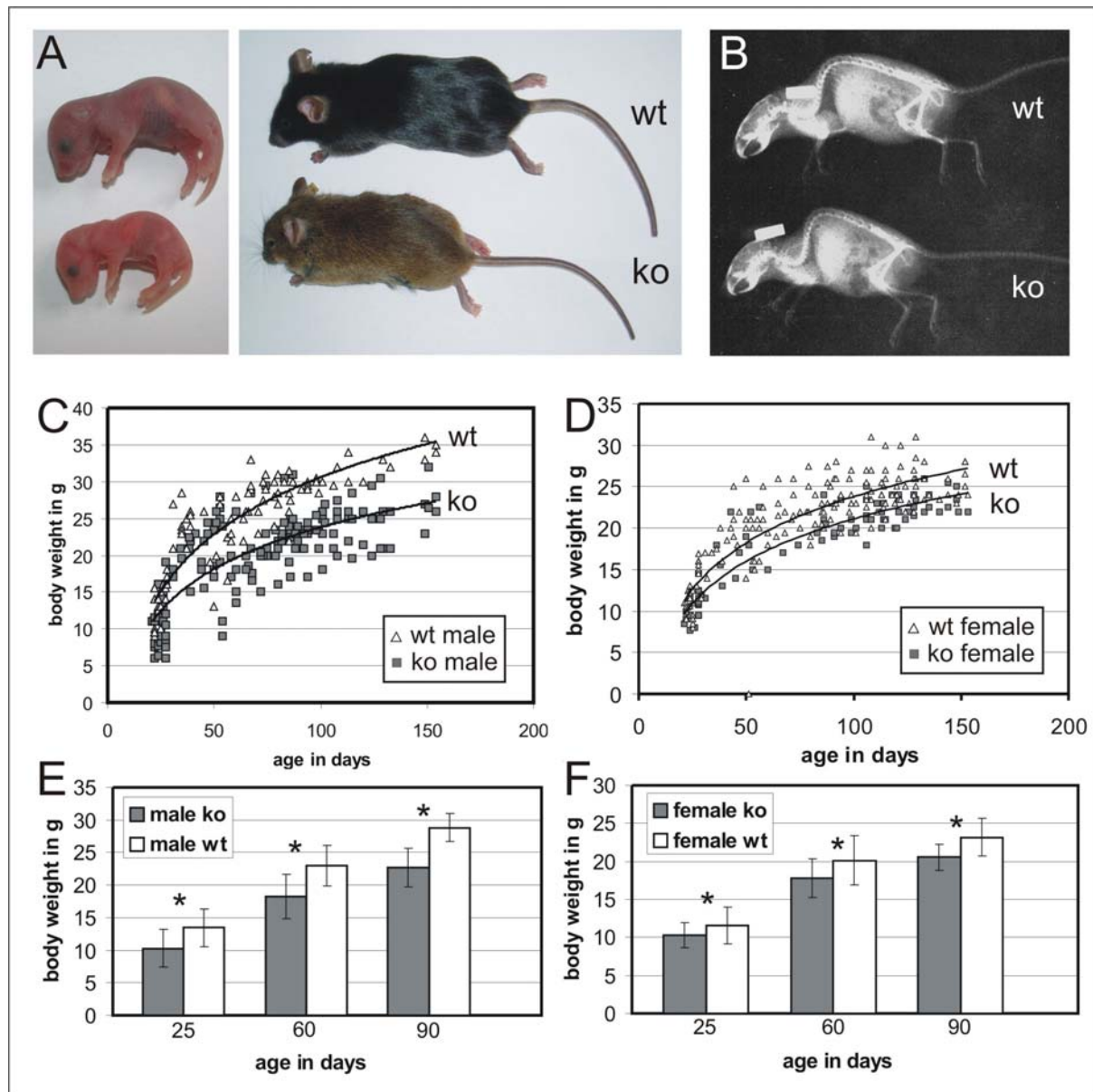


Figure 10.
Achondroplasia-like dwarfism.

(A) Knockout and wildtype littermates at P1 (left panel) and 8 weeks of age (right panel), demonstrating achondroplasia-like dwarf phenotype shortly after birth and in adulthood.

(B) X-rays of knockout and wildtype littermates at 8 weeks of age, showing generally reduced skeletal growth.

(C) Body weight trend curves of male knockout and wildtype mice showing development of body weight differences. Knockout mice are smaller at birth and stay smaller as wildtype mice.

(D) Body weight trend curves of female knockout and wildtype mice displaying similar body weight development differences, albeit female mice show a milder but also distinct weight difference as compared to male mice (C).

(E) Significant differences in body weights of male knockout and wildtype mice at the age of 25, 60, and 90 days ($*p < 0.01$; $n \geq 10$) and of female mice (F), showing smaller but still statistically significant differences of body weights at different time points ($*p < 0.05$; $n \geq 10$). (wt, wildtype; ko, knockout.)

5.4. Unaltered hormone and blood tests in *Spred-2^{-/-}* mice

To determine, whether the dwarf phenotype might be due to changed levels of steroid or thyroid hormones, serum levels of testosterone, estrogen, thyroid stimulating hormone (TSH), 3,5,3'-triiodothyronine (T3), and thyroxin (T4) were compared in female and male knockout and wildtype mice. None of these investigated hormone levels was found to be altered and, therefore, altered hormone production and secretion of steroid and thyroid hormones could be excluded (Fig. 11). As dwarfism could also be due to changed insulin metabolism, the blood glucose levels of *Spred-2^{+/+}* and *Spred-2^{-/-}* mice were tested at different times of the day. Since no significant alterations in glucose levels were detectable, a dysfunction of insulin metabolism seemed very unlikely (Fig. 11). Furthermore, except of an increased platelet amount, the cell counts of erythrocytes and white blood cells, as well as the hemoglobin and hematokrit levels were found to be unaltered in *Spred-2^{-/-}* mice (Fig. 11).

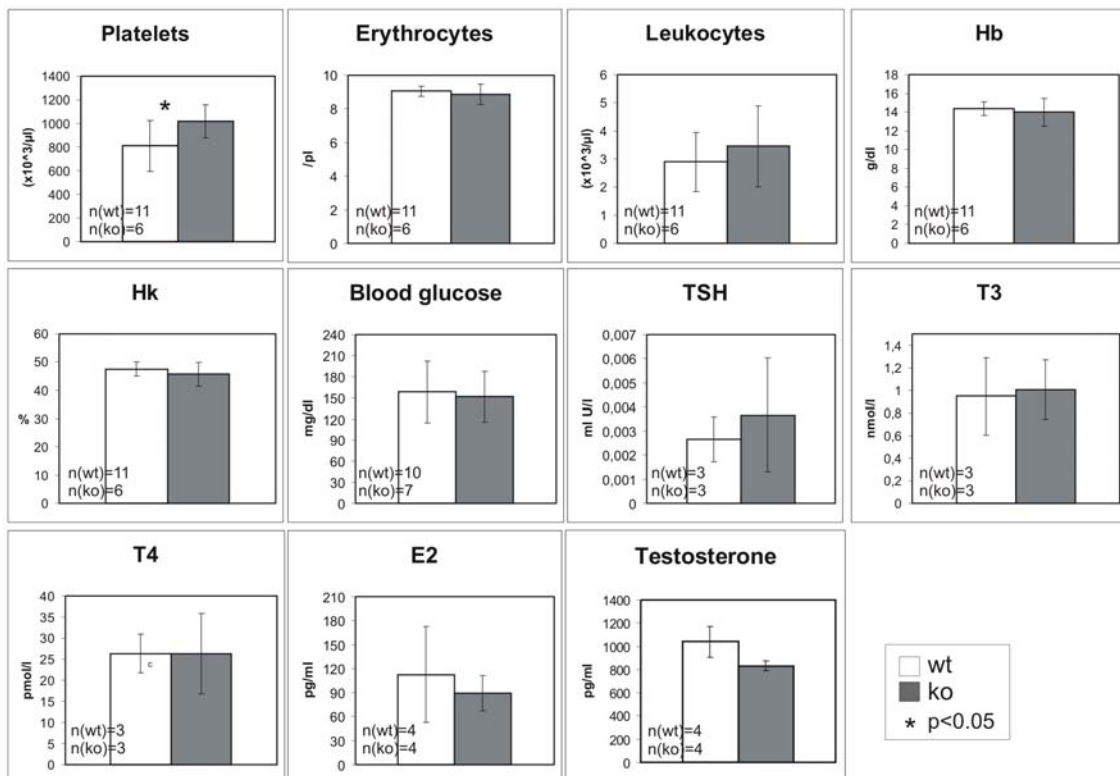


Figure 11.

Blood cell counts, blood glucose, and hormone levels.

Diagrams show the comparison of platelets, erythrocytes, leukocytes, hemoglobin (Hb), hematokrit (Hk), blood glucose, thyroid stimulating hormone (TSH), 3,5,3'-triiodothyronine (T3), thyroxin (T4), estrogen (E2), and testosterone between *Spred-2* knockout (ko) and wildtype (wt) littermates. Except of a significantly increased amount of platelets in *Spred-2^{-/-}* mice, all measured blood parameters are not altered.

To observe, whether the lack of a functional Spred-2 protein causes structural changes in organs of these mice, paraffin sections of several organs were stained with hematoxylin and eosin. Apart from a clear increase of megakaryocytes in the spleen of Spred-2 knockout mice as compared to wildtype littermates (Fig. 17), no obvious structural changes were observed in lung, heart, liver, kidney, stomach, small intestine, large intestine, thymus, testis, ovaries, uterus, skeletal muscle, salivary glands, and the prostate (data not shown).

5.5. Spred-2 promoter activity in bones

Assuming that the dwarf phenotype was due to a skeletal disorder, Spred-2 expression in bones and chondrocytes was determined. To visualize the expression pattern of Spred-2, the activity of the artificial β -geo fusion gene of the pGT0 gene trap vector, which is - following appropriate integration of the vector - brought under the control of the *Spred-2* gene promoter, was analyzed. X-Gal stainings of lower legs of P7 knockout and wildtype mice (Fig. 12A-L) revealed *Spred-2* promoter activity in chondrocytes of the whole growth plate of tibia, fibula, and femur. Very strong activity was also found in the periost (Fig. 12A, C). Spred-2 expression was seen in chondrocytes of all corresponding cartilage areas of the knee joint including the patella, tibia, and femur (Fig. 12E, G).

Remarkable Spred-2 expression was also seen in secondary ossification centers of long bones (Fig. 12I) and in distinct cells of bone marrow (Fig. 12K). As negative controls, corresponding wildtype sections were examined (Fig. 12B, D, F, H, J, and L). Additionally, cryosections of newborn knockout mice were stained with X-Gal and *Spred-2* promoter activity was detected in ribs (Fig. 12N), in chondrocytes of the acetabulum, the femur head in the hip joint (Fig. 12O), and in secondary ossification centers of the femur (Fig. 12M). In a higher magnification, X-Gal activity was clearly visible in chondrocytes of the growth plate (Fig. 12P). X-Gal staining of thoraxes of adult mice revealed Spred-2 expression at the cartilage areas of the ribs (Fig. 12Q).

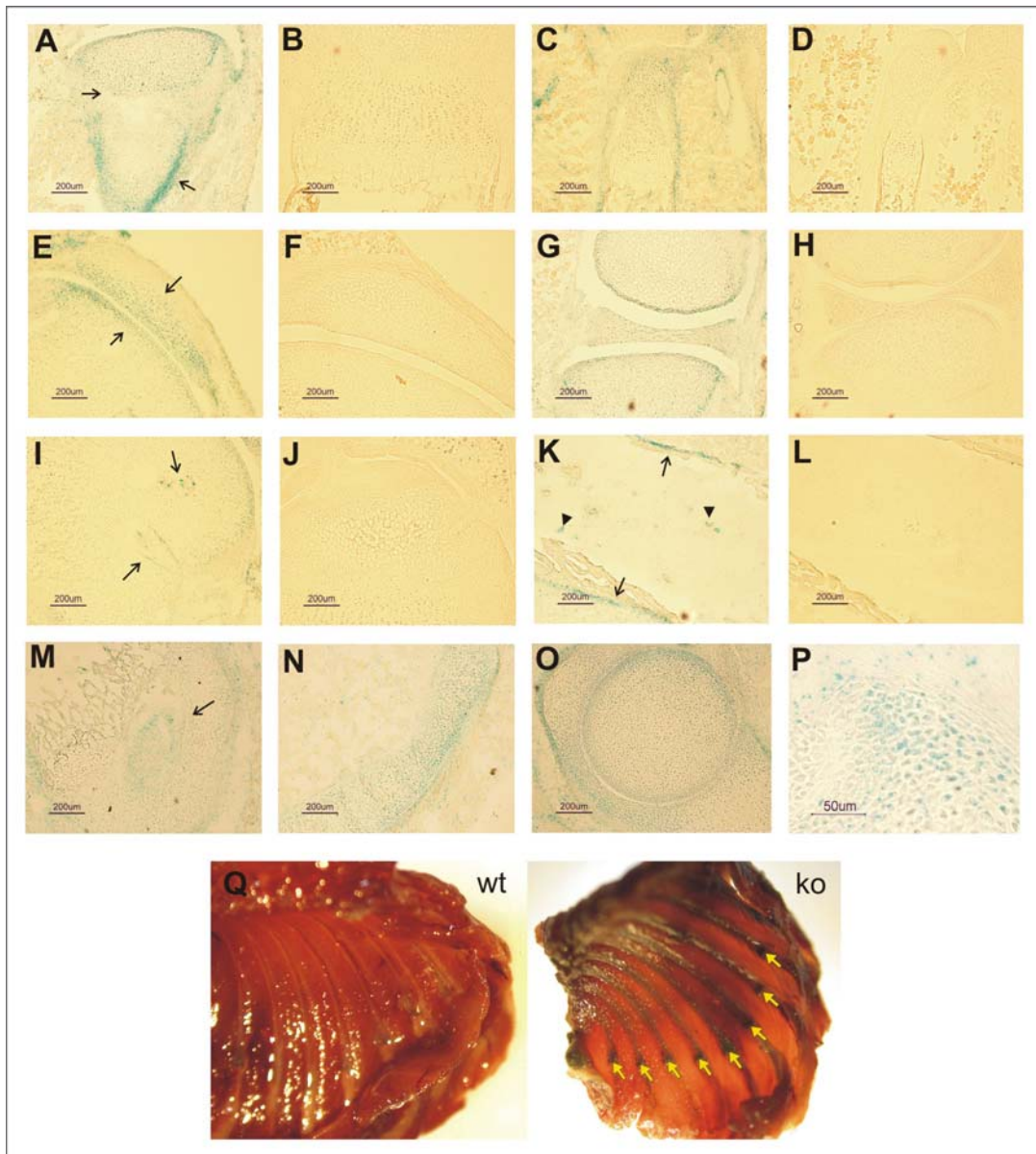


Figure 12.

Spred-2 promoter activity in bones.

X-Gal staining of cryosections of knockout (A, C, E, G, I and K) and wildtype (B, D, F, H, J, and L) lower legs at P7. Corresponding wildtype sections serve as negative controls for specific X-Gal staining in knockout mice. (A) X-Gal staining show Spred-2 promoter activity in chondrocytes of the growth plate and strong activity in the periost of proximal tibiae (arrows). (C) Spred-2 promoter activity in a proximal fibula demonstrating Spred-2 expression in the upper fibula pole, chondrocytes of the growth plate and the periost. Patella and the corresponding area of the tibia show Spred-2 activity in chondrocytes, as well (arrows in E). A knee joint with tibia and femur is shown in (G), in which chondrocytes are specifically stained in the distal areas. Arrows in (I) indicate expression of Spred-2 in secondary ossification centers of the tibia head. (K) Positive Spred-2 signal in the periost of the femur metaphyse is marked by arrows, the arrowheads indicate a strong signal in distinct cells in the bone marrow. (M-P) X-Gal staining of cryosections of newborn knockout mice. Spred-2 promoter activity was observed in a secondary ossification center of the distal femur (arrow in M). Longitudinal section through a rib (N) and a femur head in the acetabulum (O) show a strong signal in chondrocytes. Higher magnification of chondrocytes demonstrates distinct Spred-2 promoter activity in these cells (P). Scale bars 200 μ m (A-O), 50 μ m (P). (Q) Spred-2 promoter activity in cartilage areas of ribs of adult XB228-derived mice (arrows); wildtype thorax (left) as negative control.

5.6. Expression of endogenous Spred-2 in chondrocytes

To investigate endogenous Spred-2 protein expression, lower legs of P7 wildtype mice were dissected and immunostained with a polyclonal Spred-2-specific antibody. Thereby, it was confirmed that Spred-2 protein expression was congruent to the detected *Spred-2* promoter activity shown in Figure 12. Spred-2 was found to be expressed in chondrocytes of growth plates (Fig. 13E), the tibia head (Fig. 13F), secondary ossification centers (Fig. 13G), the periost, and distinct cells in the bone marrow (Fig. 13H). As negative controls corresponding sections were stained with secondary antibody (Fig. 13A-D).

5.7. Narrower growth-plate and reduced tibia length in *Spred-2*^{-/-} mice

In order to investigate the morphology of growth plates, the histology of epiphyseal growth plates was examined at P6 and P10 by HE stained sections and in 1 week, 4 weeks, and 12 weeks old knockout and control mice by toluidine staining (Data were obtained from a co-operation with T. Schinke and M. Amling, Hamburg). Growth plates of knockout tibiae showed narrower zones of hypertrophic chondrocytes and the proliferative and hypertrophic zone together was shorter in all stages in comparison to the wildtype tibiae (Fig. 13I-L; Fig. 14). Soft X-ray exposures of wildtype and knockout lower legs showed a highly significant reduction in tibia length of *Spred-2*-deficient mice (Fig. 13M, Fig. 13N; average wt=18.1 mm, ranging from 17-21 mm; average ko=16.1 mm, ranging from 14-18 mm; $n_{(wt)}=32$; $n_{(ko)}=26$; * $p<0.01$).

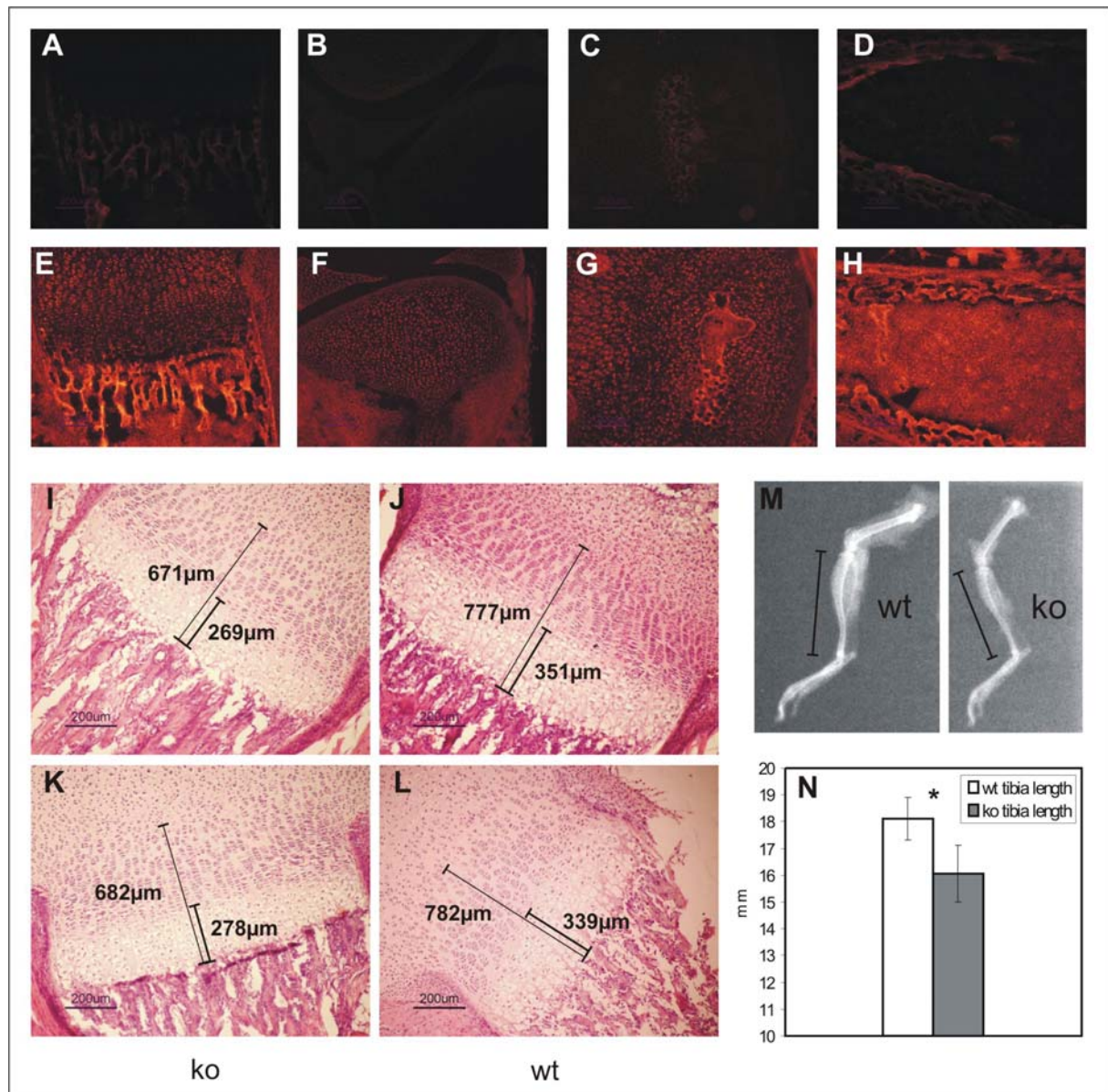


Figure 13.

Spred-2 deficiency causes bone growth defects.

(A-H) Immunohistochemistry of wildtype tibiae at P7. (A-D) Corresponding negative controls to the figures in the second row stained with the secondary antibody alone. (E-H) Spred-2 expression is demonstrated in different tibia areas. (E) shows a Spred-2 signal in chondrocytes of the growth plate, primary spongiosa, and the periost. In (F), the tibia part of the knee joint is shown with Spred-2 expressing chondrocytes of the tibia head. Spred-2 is also present in secondary ossification zones of the tibia head (G), in the periost, and the bone formation zone of the tibia metaphyse (H). Some cells in the bone marrow have a positive Spred-2 signal (H).

(I-L) HE staining of tibia growth plates of knockout (I and K) and wildtype (J and L) littermates at P6 (I and J) and P10 (K and L). Measured sections indicate lengths of growth plate zones. Thick lines mark lengths of hypertrophic chondrocyte zones, thin lines mark lengths of proliferative and hypertrophic chondrocyte zones together. At stage P6 and P10, the hypertrophic chondrocyte zone and the whole growth plate zone was smaller in knockout tibiae as compared to wildtypes. Scale bars, 200 μ m.

(M) Soft X-rays of wildtype and knockout lower legs, showing tibia lengths differences.

(N) Statistical significant differences of tibiae lengths of wildtype and knockout tibiae (* $p < 0.01$; $n_{(ko)} = 26$, $n_{(wt)} = 32$).

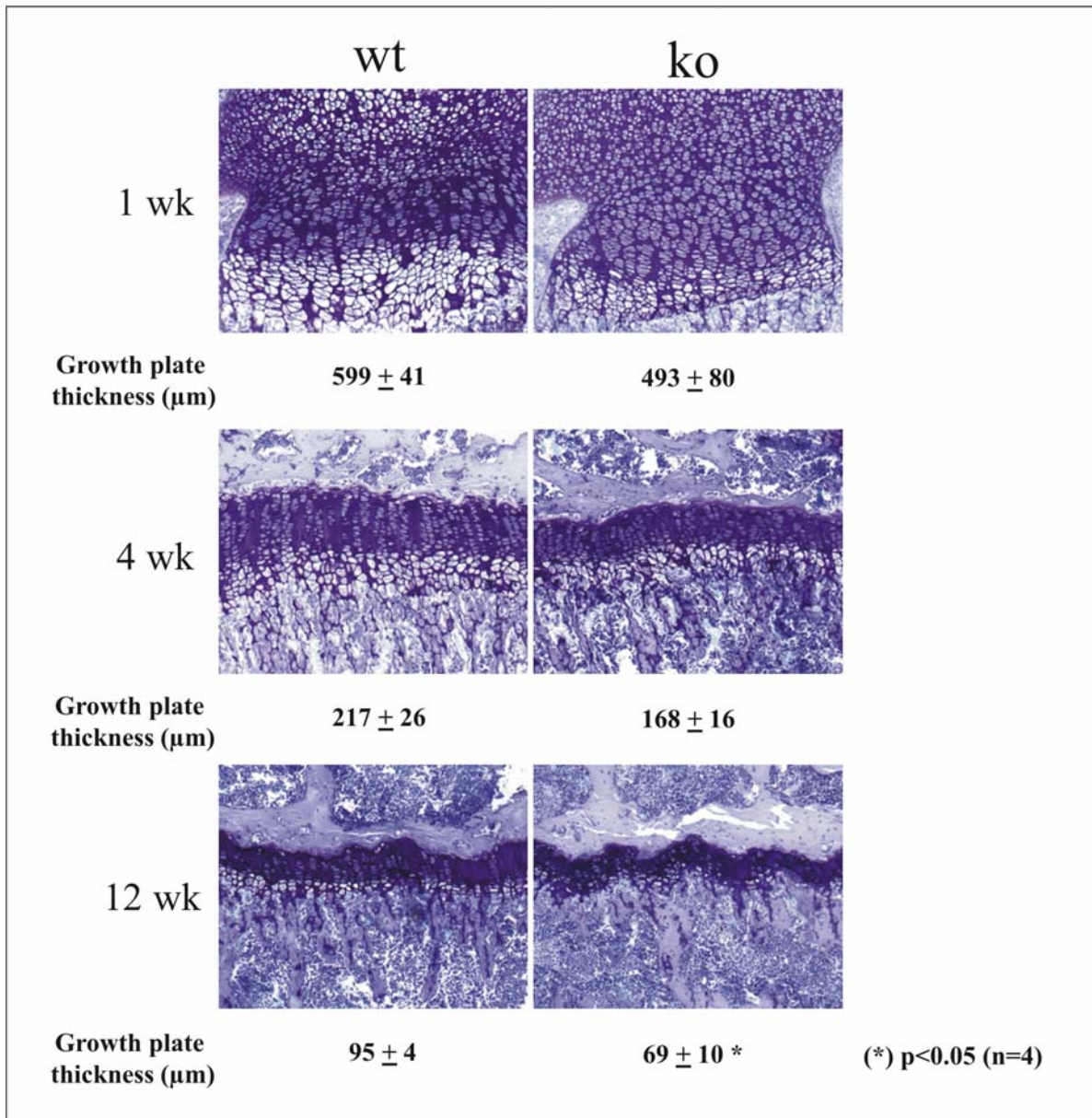


Figure 14.

Narrower growth plates in *Spred-2*^{-/-} mice.

Toluidine staining of tibia growth plates derived from 1 week, 4 weeks, and 12 weeks wildtype (wt) and knockout (ko) littermates. Measurements of growth plate thickness are marked below each figure. All stages of knockout mice demonstrate a narrower growth plate, especially with a reduction of the hypertrophic chondrocyte zone as compared to the wildtype controls. (wk, week(s); *p<0.05; n=4 animals for each time point). (These data are obtained from a co-operation with T. Schinke and M. Amling, Hamburg).

5.8. Increased and earlier ERK phosphorylation in *Spred-2*^{-/-} chondrocytes after FGF stimulation

Since *Spred-2* has been shown to be a negative regulator of the MAPK signaling pathway (Wakioka et al., 2001), ERK and phosphorylated ERK expression was examined in P7 knockout and wildtype lower legs by immunohistochemistry. ERK and phosphorylated ERK stainings were detected in both wildtype and knockout

tissue (Fig. 15). In particular, ERK and phosphorylated ERK was detected in chondrocytes of the tibia growth plate, primary spongiosa, chondrocytes of the knee joint, secondary ossification centers, and bone trabecules of the tibia metaphyse (Fig. 15).

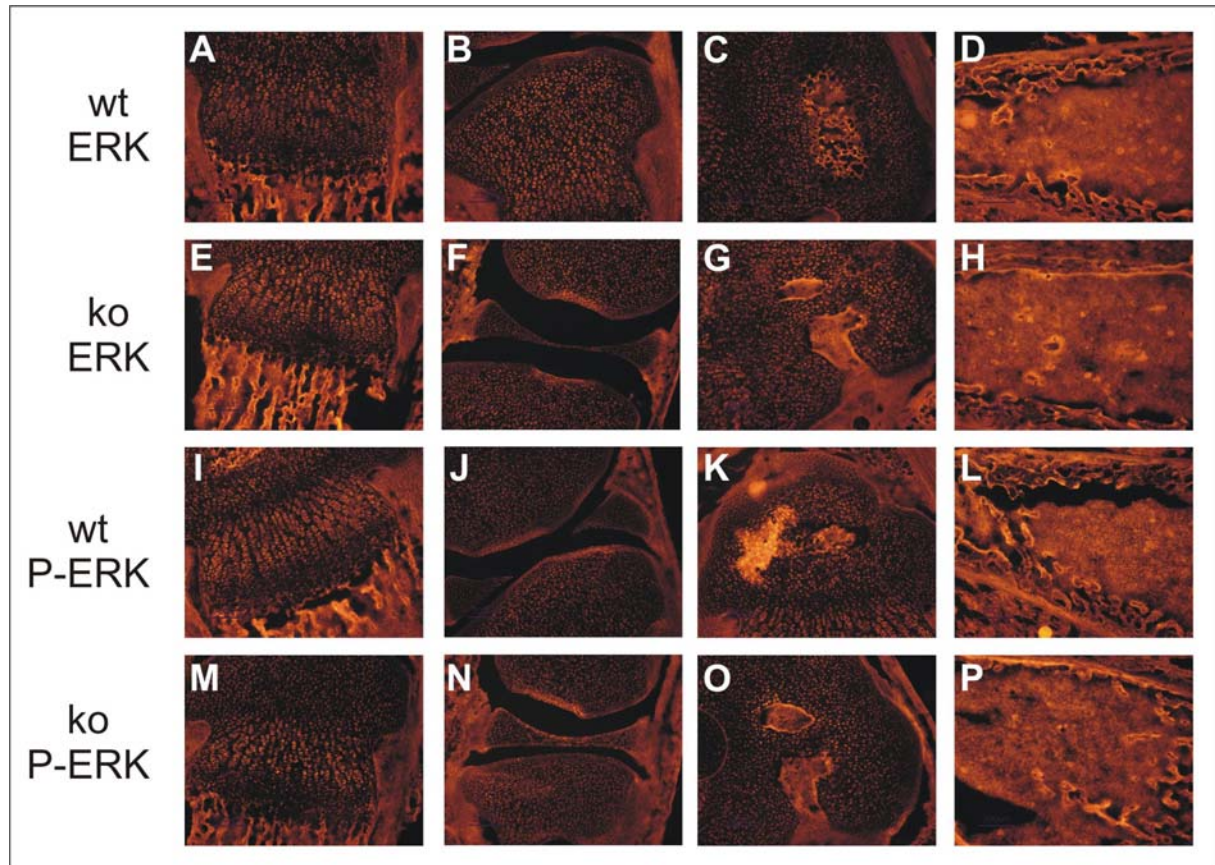


Figure 15.

Expression of ERK and phosphorylated ERK in tibiae at P7.

Immunohistochemistry of wildtype (A-D and I-L) and knockout (E-H and M-P) tibiae at P7. (A-H) are stained with anti-ERK antibody, (I-P) are stained with anti-phospho-ERK antibody. (A, E, I, and M) show tibia growth plates, (B, F, J, and N) show knee joints with the proximal tibia and distal femur, (C, G, K, and O) show proximal tibiae with secondary ossification centers, (D, H, L, and P) show a tibia metaphyse with bone marrow. ERK and phospho-ERK are expressed in chondrocytes of the growth plate, in primary spongiosa, in secondary ossification centers, and in some bone marrow cells (corresponding negative controls are seen in Figure 13 A-D).

Stimulation of cultured chondrocytes with different concentrations of FGF (5 ng, 10 ng, and 50 ng FGF/ml) revealed an earlier and increased ERK phosphorylation in *Spred-2^{-/-}* chondrocytes in comparison to *Spred-2^{+/+}* chondrocytes. Unspecific stimulation with fetal bovine serum (1% FCS or 10 % FCS) did not result in altered ERK phosphorylation in chondrocytes of wildtype and knockout chondrocytes (Fig. 16).

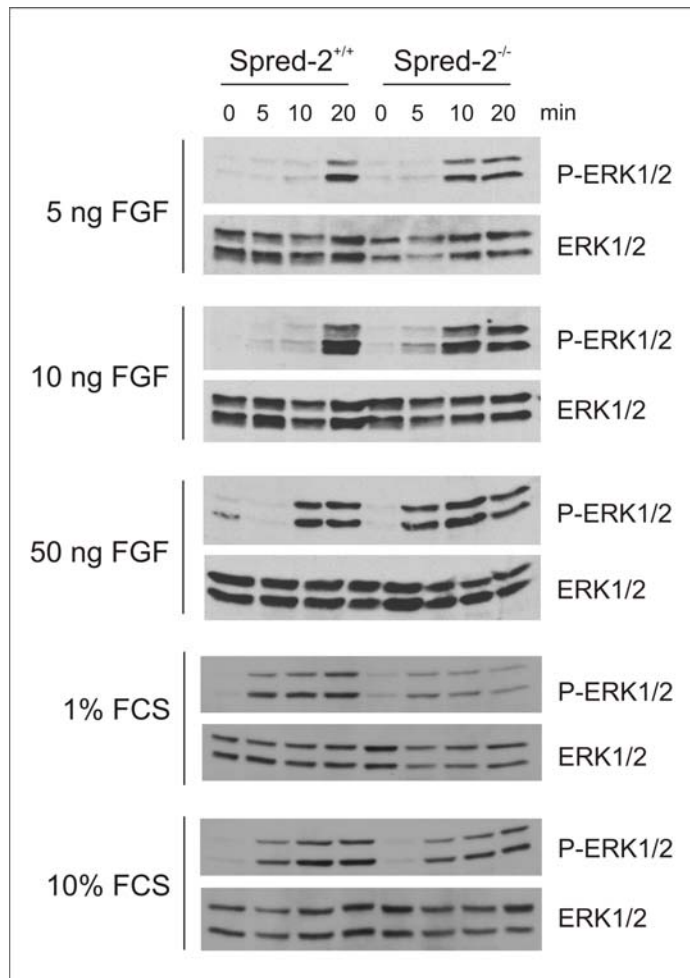


Figure 16.

Earlier and increased FGF-induced ERK phosphorylation in Spred-2^{-/-} chondrocytes.

Chondrocytes of Spred-2^{+/+} and Spred-2^{-/-} mice were stimulated with 5 ng FGF/ml, 10 ng FGF/ml, 50 ng FGF/ml, 1% FCS, and 10% FCS for indicated periods. Cell extracts were immunoblotted with anti-ERK1/2 or anti-phospho-ERK1/2 antibodies. Phosphorylation of ERK is earlier and increased in stimulated Spred-2^{-/-} chondrocytes with all tested FGF concentrations. (Chondrocyte stimulations were done in four different wt/ko pairs of mice.)

5.9. Increased bleeding in Spred-2^{-/-} mice

An additional phenotype of the Spred-2^{-/-} mice was an increased bleeding after injuries. The bleeding volume was extremely enlarged and the bleeding time was significantly prolonged (Fig. 17). So far, an increased bleeding resulted by hypertension was excluded by blood pressure measurements (Fig. 17). Interestingly, the amount of megakaryocytes in the spleen and the platelet amount in the peripheral blood of Spred-2^{-/-} mice were increased as compared to wildtype controls, suggesting an altered platelet function (Fig. 17). To further examine the physiological reasons of this phenotype, the different steps of the clotting cascade have to be investigated further.

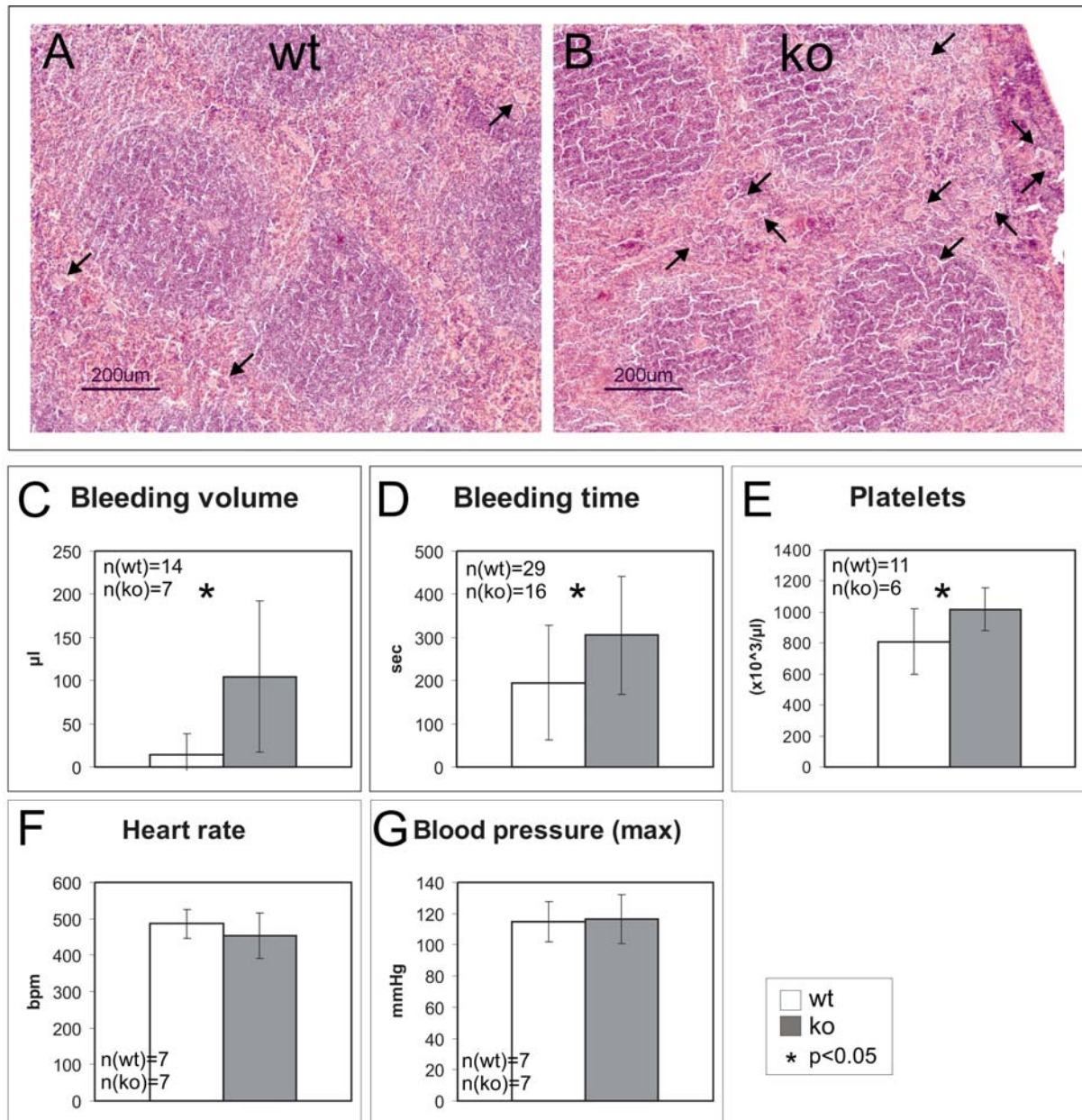


Figure 17.
Bleeding phenotype of *Spred-2* deficient mice.

(A, B) HE staining of the spleen demonstrates an increased number of megakaryocytes in (A) knockouts (ko) as compared to (B) wildtypes (wt). (C-G) Diagrams indicate a significantly increased bleeding volume (C), a prolonged bleeding time (D), and an increased amount of platelets (E) in *Spred-2*^{-/-} mice in comparison to wildtype mice. Heart rate (F) and blood pressure measurements (G) are unaltered in knockout and wildtype mice.

5.10. Tissue-specific *Spred-2* promoter activity characterized by a gene trap approach

This gene trap approach gives as well the opportunity to study the *Spred-2* promoter activity tissue-specific in situ of mice. Therefore, this tool was used to examine the physiological *Spred-2* promoter activity in various organs of newborn and adult mice.

5.10.1. Physiological *Spred-2* promoter activity in newborn mice

To visualize the physiological *Spred-2* promoter activity in newborn mice, the expression of the artificial β -*geo* fusion gene of the pGT0 gene trap vector was analyzed by X-Gal staining. As the β -*geo* fusion gene was brought under control of the *Spred-2* gene promoter, β -galactosidase expression was regarded as an appropriate indicator of the physiological *Spred-2* promoter activity (Fig. 8A).

X-Gal staining of cryosections of whole newborn mice gave a complete overview of the *Spred-2* promoter expression pattern in various organs (Fig. 18, and Fig. 19). Very high activity was detected in neural tissues like cerebrum (Fig. 18A, 18D, 19A, 19B), cerebellum (Fig. 18A, 19C), medulla oblongata (Fig. 19D), spinal cord (Fig. 18C, 19F), and spinal nerves (Fig. 18A, 18H, 19E). In particular, the frontoparietal cerebral cortex as well as Ammon's Horn (Fig. 18A and Fig. 19B) showed strong *Spred-2* promoter activity, while in cerebellum mainly the granular cell layer of the cerebellar cortex was positive (Fig. 19C). Furthermore, a very strong promoter activity was depicted in salivary glands (Fig. 18A) and kidneys, mainly in the cortex of kidneys (Fig. 18A, 18F, 18H, 19H). In organs of the intestinal tract, the *Spred-2* promoter was found to be predominantly active in smooth muscle cells and glandular cells of the mucus epithelium. This activity was investigated in stomach (Fig. 18A, 18G, 19N), small intestine (Fig. 18H, 19O, 19P), and colon (Fig. 18I, 19Q, 19R). Remarkable *Spred-2* promoter activity was also seen in the late developing eye with strong intensity in the retina and weaker staining in the episclera (Tenon's capsule) (Fig. 18A, 19G). In skin (Fig. 18A, 18J), the medulla (Fig. 18J, 19S) and the inner (Huxley's layer and Henle's layer) and outer root sheath of the hair follicles were stained, as well (Fig. 18A, 19T).

Additionally, the *Spred-2* promoter was active on a lower level in heart (Fig. 18E, 19K, 19L, 19M), lung (Fig. 18A, 18E, 19I, 19J), and cartilage tissues (trachea: Fig. 18C; bronchi: Fig. 19I; ribs: Fig. 18B, 19W; and hip joint: Fig. 19X). Almost no activity was detectable in skeletal muscle (Fig. 18A, 19U) and liver (Fig. 18A, 19V), except smooth muscle cells within the walls of blood vessels (Fig. 19V).

In other words, although the *Spred-2* promoter was found to be active in nearly all organs tested here, the activity levels were obviously different and revealed tissue- and cell-specific differences in *Spred-2* promoter activity.

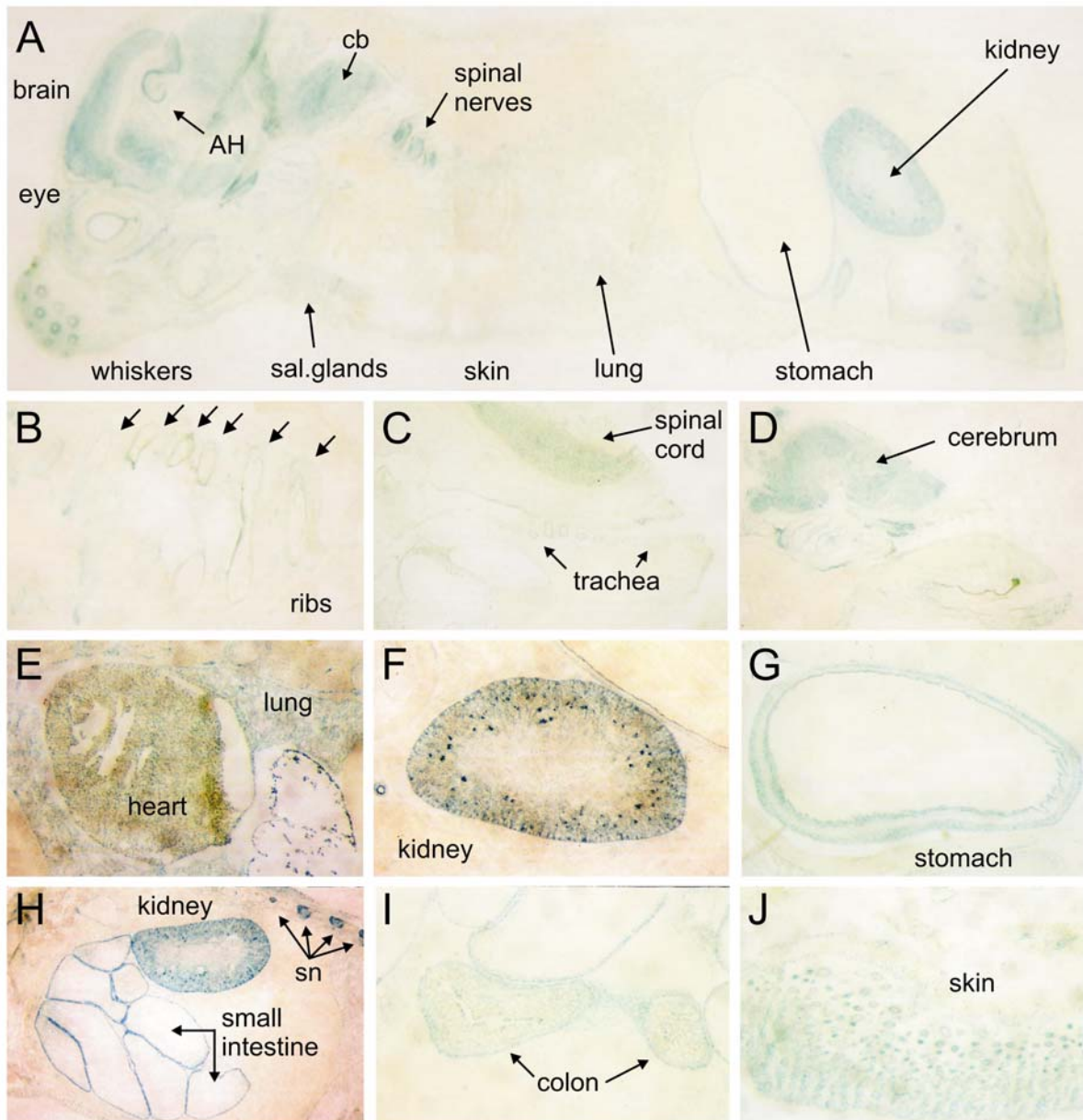


Figure 18.

***Spred-2* promoter activity in newborn mice; overviews.**

X-Gal stained cryosections of newborn *Spred-2*^{-/-} mice. (A) Sagittal overview of a whole animal section. Organs with high *Spred-2* promoter activity are marked (AH: Ammon's Horn; cb: cerebellum; sal. glands: salivary glands). In (B) ribs; (C) spinal cord and trachea; (D) cerebrum; (E) heart and lung; (F) kidney; (G) stomach; (H) spinal nerves (sn), small intestine, and kidney; (I) colon; and (J) skin are presented.

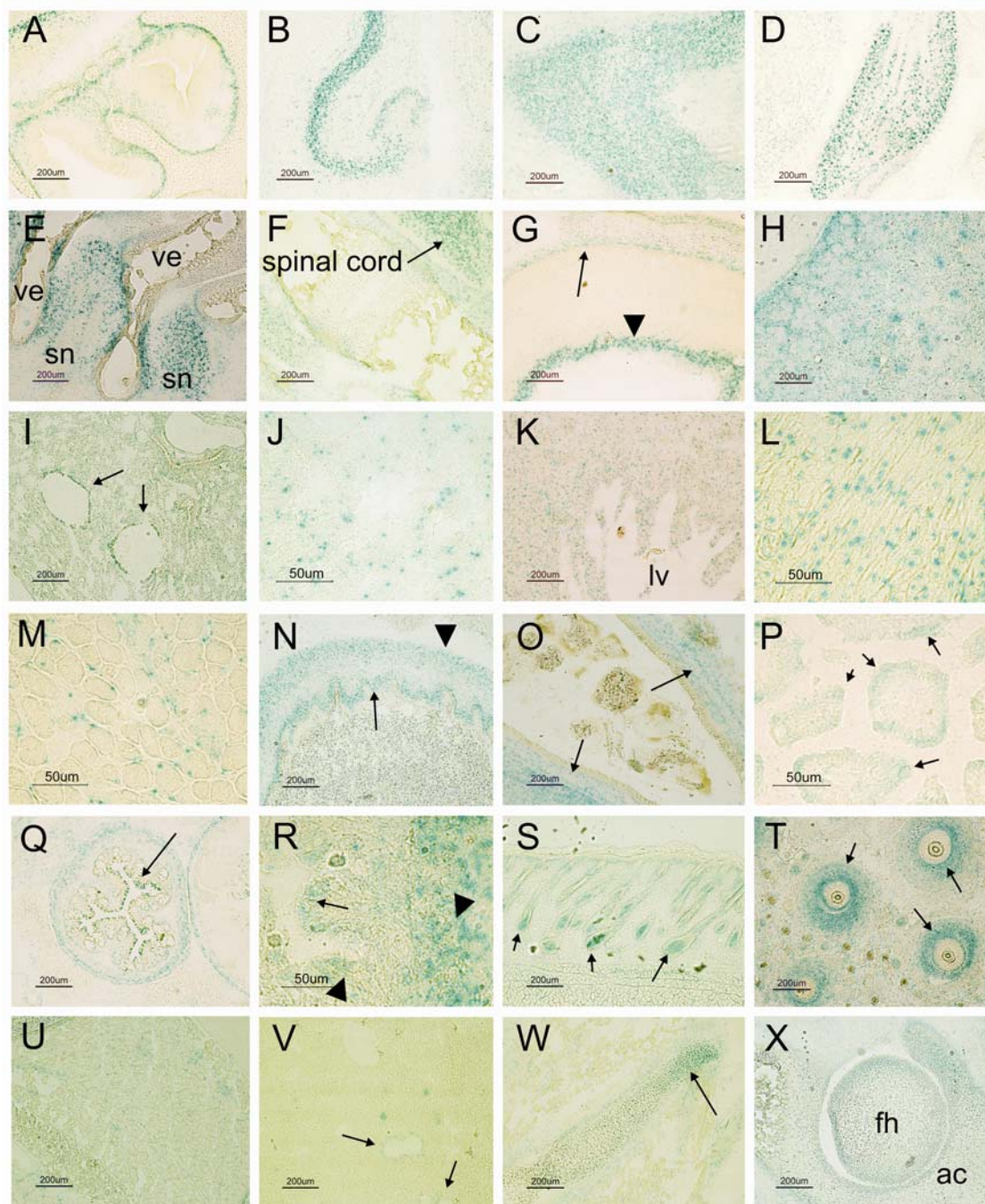


Figure 19.

***Spred-2* promoter activity in newborn mice; detailed illustrations.**

X-Gal stained cryosections of newborn *Spred-2*^{-/-} mouse organs. (A, B) cerebrum; (B) Ammon's Horn; (C) cerebellum; (D) medulla oblongata; (E) cervical spinal nerves (sn) and vertebrae (ve); (F) spinal cord; (G) eye (arrow: episclera (Tenon's capsule); arrowhead: retina), (H) kidney cortex; (I) lung (arrows: bronchi); (J) alveolar epithel; (K) heart (lv: left ventricle); (L) myocard longitudinal section; (M) myocard cross-section; (N) stomach (arrow: mucus membrane; arrowhead: tunica muscularis); (O) small intestine longitudinal section (arrows: tunica muscularis); (P) small intestine (arrows: intestinal villi cross-sections); (Q) colon cross-section (arrow: mucus membrane; arrowhead: tunica muscularis); (R) colon mucus membrane (arrow: goblet cells; arrowhead: tunica muscularis); (S) skin (arrows: hair follicles); (T) whiskers cross-sections (arrows indicate the inner (Huxley's and Henle's layer) and outer root sheath of the hair follicle); (U) skeletal muscle; (V) liver (arrows: Glisson trias); (W) rib cartilage (arrow: chondrocytes); (X) hip joint (fh: femur head, ac: acetabulum). Scale bars 200 μm and 50 μm, as indicated.

5.10.2. Physiological *Spred-2* promoter activity in adult mice

To examine the physiological *Spred-2* promoter activity not only in premature, but also in adult mice, β -galactosidase activity was detected in whole organs (Fig. 20) and organ sections (Fig. 21 and 22) of adult mice. The staining of whole mouse organs gave a general overview and impression of *Spred-2* promoter activity; whereas the staining of organ sections allowed detailed analyzes of the tissue- and cell-specific expression pattern.

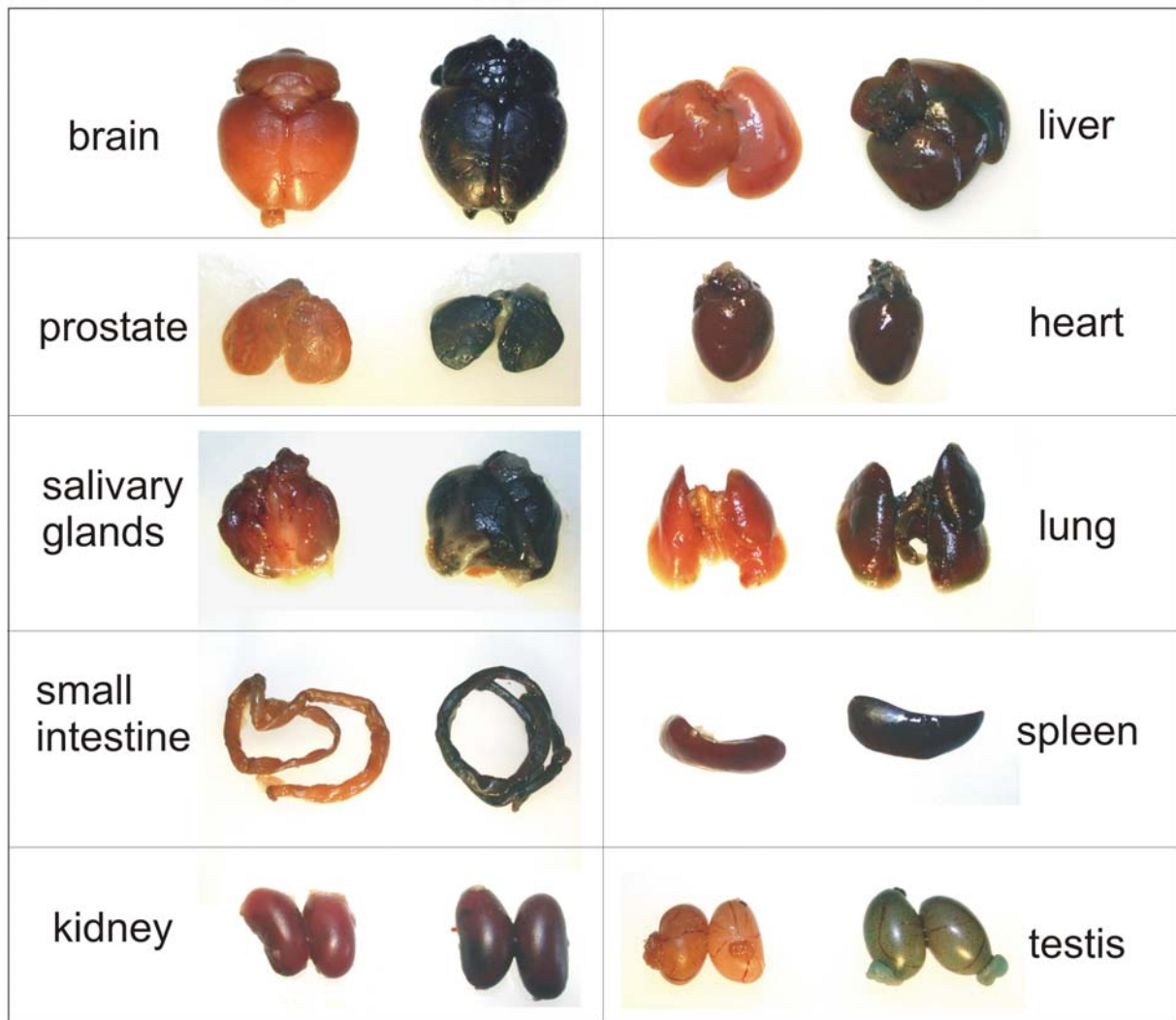
First, very high *Spred-2* promoter activity was detected in brain and various glands, including prostate (Fig. 20; Fig 21F, 21G), salivary glands (Fig. 20; Fig. 21H, 21I), and mucus epithelium glands in stomach (Fig. 21K) and colon (Fig. 21O, 21P, 21Q), respectively. In cerebrum (Fig. 20; Fig. 21A, 21B, 21C, 21D), the fronto-parietal cortex and the Ammon's Horn were strongly positive. Interestingly, an additional submeningeal, strongly positive cell layer of neuronal cells with strong *Spred-2* promoter activity was detected (Fig. 21D), reminding similar submeningeal neural cell populations found in the neonatal cerebral cortex. In cerebellum, the granular cell layer of the cerebellar cortex including Purkinje cells were also strongly positive (Fig. 20; Fig. 21B, 21C, 21E),

Second, high *Spred-2* promoter activity was observed in smooth muscle cells of the intestinal tract and uterus. In stomach (Fig. 21J), small intestine (Fig. 21L, 21M, 21N), and colon (Fig. 21O, 21P) smooth muscle cells of the tunica muscularis were stained, as well as the lamina muscularis mucosae in stomach (Fig. 21J, 21K). Moreover, smooth muscle cells in the myometrium of the uterus (Fig. 21R, 21S) were X-Gal positive.

Third, *Spred-2* promoter activity was examined in kidney, whereas the expression in the cortex was higher, compared to the mark zone (Fig. 22O, 22P, 22Q).

Fourth, very low promoter activity was detected in cardiac muscle cells (Fig. 22A, 22B, 22C), testis (Fig. 22F, 22G), liver (Fig. 22J, 22K), and lung (Fig. 22L, 22M, 22N); and almost no *Spred-2* promoter activity was seen in skeletal muscle (Fig. 22R, 22S) and spleen (Fig. 22T, 22U).

Finally, and very interestingly, distinct *Spred-2* promoter activity was explored in vascular smooth muscle cells. Impressive examples were detected in blood vessels of heart (Fig. 22D, 22E), testis (Fig. 22H, 22I), and liver (Fig. 22J, 22L).

**Figure 20.****Overview of *Spred-2* promoter activity in whole mouse organs.**

X-Gal stained whole mouse organs of *Spred-2*^{+/+} (left; negative control) and *Spred-2*^{-/-} (right) mice. X-Gal staining illustrates high *Spred-2* promoter activity in brain, prostate, salivary glands, and small intestine; and low activity in kidney, liver, heart, lung, spleen, and testis.

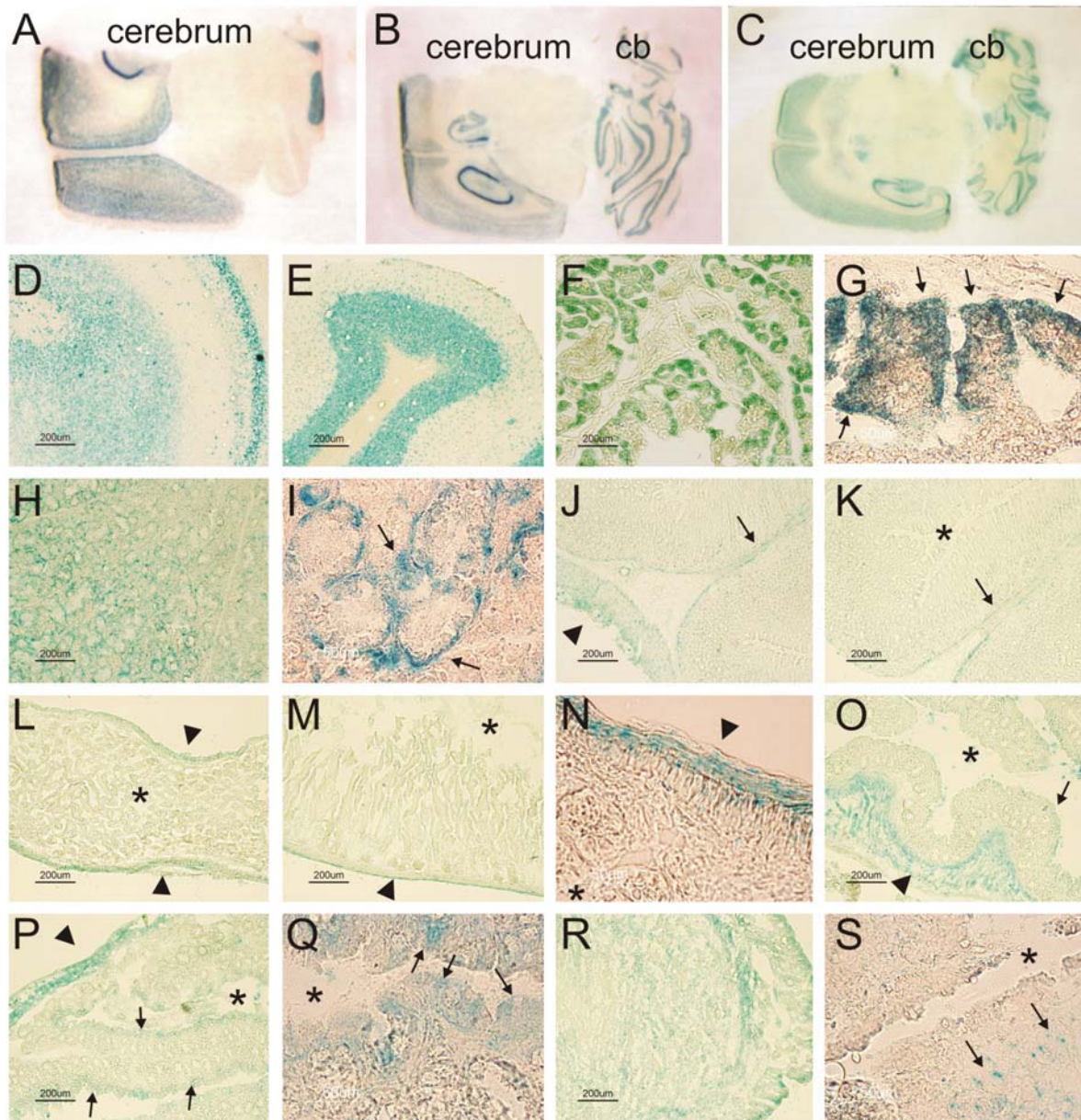


Figure 21.

***Spred-2* promoter activity in adult mice; organs with a high expression profile.**

X-Gal stained cryosections of adult *Spred-2*^{-/-} mouse organs.

(A, B, and C) Horizontal brain sections of three different levels (top to bottom, cb: cerebellum); (D) cerebrum; (E) cerebellum; (F, G) prostate (arrows: apical pole of glandular epithelial cells); (H, I) salivary glands (arrows: glandular epithelial cells); (J, K) stomach (arrows: lamina muscularis mucosae; arrowhead: tunica muscularis; asterisk: luminal side); (L, M, and N) small intestine (arrowheads: tunica muscularis; asterisk: luminal side); (O, P, and Q) colon (arrowheads: tunica muscularis; arrows: mucus membrane; asterisk: luminal side); (R, S) uterus (arrows: myometrium; asterisk: luminal side). Scale bars 200 μm and 50 μm, as indicated.

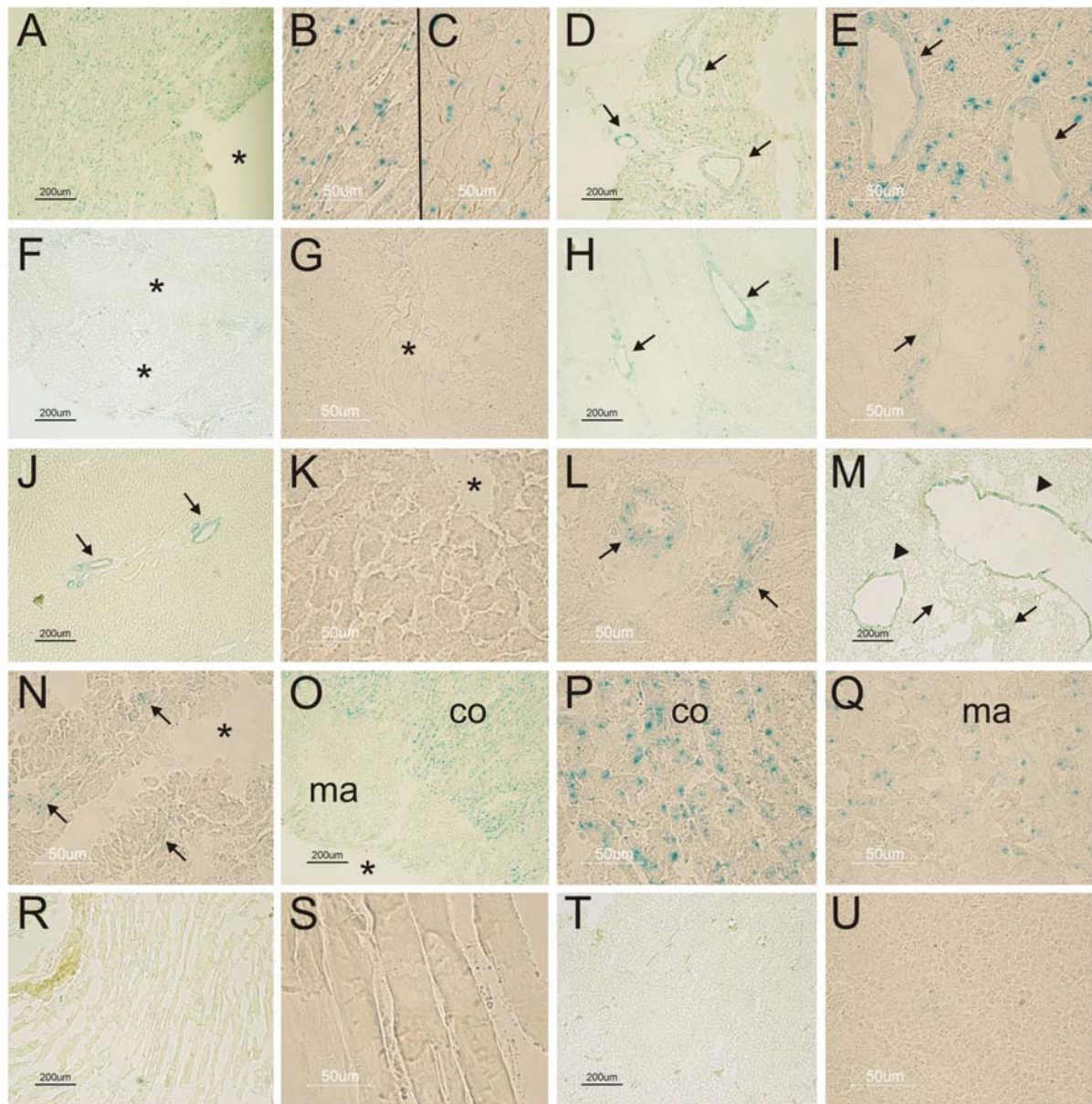


Figure 22.

***Spred-2* promoter activity in adult mice; organs with a low expression profile.**

X-Gal stained cryosections of adult *Spred-2*^{-/-} mouse organs.

(A-E) heart; (A) myocard (asterisk: left ventricle); (B) myocard longitudinal section; (C) myocard cross-section; (D, E) heart blood vessels (arrows: vascular smooth muscle cells); (F-I) testis (asterisk: lumina of tubuli seminiferi; arrows: vascular smooth muscle cells); (J, K, and L) liver (arrows: vascular smooth muscle cells of Glisson trias' blood vessels; asterisk: central vein); (M, N) lung (arrowheads: bronchi; arrows: blood vessels; asterisk: alveolar lumina); (O, P, and Q) kidney (co: cortex, ma: mark); (R, S) skeletal muscle; (T, U) spleen. Scale bars 200 μm and 50 μm, as indicated.

5.11. Spred-1 and Spred-2 RNA expression pattern in mice

The RNA expression patterns of Spred-1 and Spred-2 in various mouse organs were examined by RT-PCR analyzes using Spred-1 and Spred-2 specific primer pairs. As a control for RNA amount and quality, additional RT-PCRs with GAPDH primers (housekeeping gene) were performed in parallel.

The strongest Spred-1 RNA expression was found in brain (Fig. 23A). After 30 PCR cycles, a much weaker but detectable signal for the Spred-1 transcript was also observed in lung, heart, liver, kidney, intestine, spleen, testis, thymus, and ovaries (Fig. 23A). Although the expression levels varied over a broad range, with a very high signal in brain, RT-PCR analyses revealed the presence of the Spred-2 transcript in all investigated adult tissues (Fig. 23A).

Analyzes of Spred-1 and Spred-2 mRNA expression in fetal tissues (E16) showed substantial expression of both transcripts in heart, lung, liver, and brain. Weaker signals for both proteins were obtained in mRNA preparations from femoral bone and in placenta only Spred-1 mRNA expression was detected (Fig. 23B).

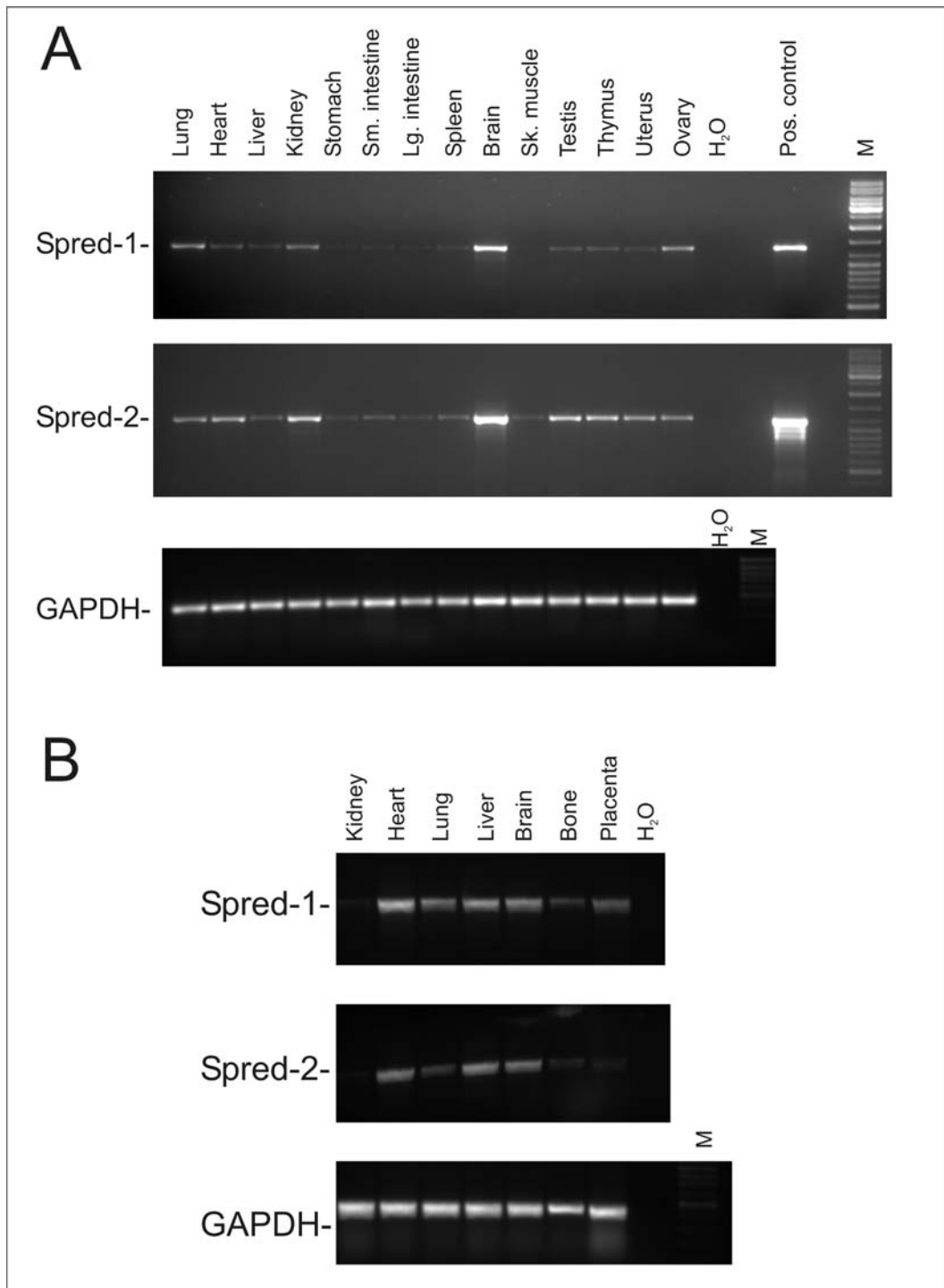


Figure 23.

Spred-1 and Spred-2 mRNA expression in various adult and fetal mouse tissues.

(A) RT-PCRs -using 2 μ g of total RNA per reaction and 30 amplification cycles- showed most prominent expression of mouse Spred-1 and -2 mRNA in brain and a weaker signal for Spred-1 in lung, heart, liver, kidney, testis, thymus, uterus, and ovaries. In contrast, mouse Spred-2 mRNA was detected in almost all adult tissues tested. RT-PCRs using GAPDH-specific primers were used as controls. Positive controls: 1 ng plasmids containing full-length Spred-1 and -2 cDNAs in reaction mixture.

(B) Expression of Spred-1 and -2 mRNA in different fetal mouse tissues. RT-PCRs with fetal RNA preparations showed expression of Spred-1 mRNA in heart, lung, liver, brain, placenta, and -to a minor extend- in femoral bone. Spred-2 mRNA was found to be expressed in fetal heart, lung, liver, and brain, and -also to a minor extend- in femoral bone. (H₂O: RT-PCR reaction mixture without RNA, M: DNA size marker.)

Moreover, the mRNA expression of Spred-1 and Spred-2 was studied in adult mouse organs by Northern blot analyzes using a commercial available Message Map™ Northern Blot (Stratagene) and the full-length cDNAs as radioactive labelled probes. In all tested organs (brain, heart, kidney, liver, lung, skeletal muscle, spleen, and testis) a similar Spred-1 and Spred-2 signal was detectable. The strongest signals were observed in brain, lung, and kidney and the lowest mRNA amount in skeletal muscle (Fig. 24).

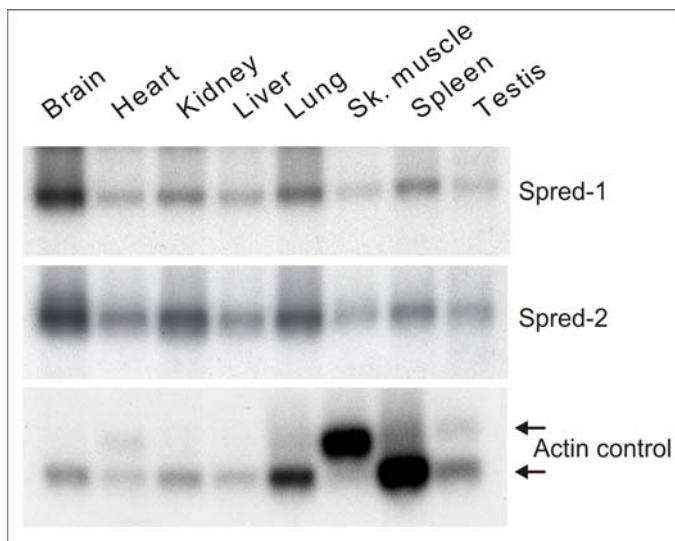


Figure 24.
Spred-1 and Spred-2 mRNA expression pattern.

Message Map Northern blot (Stratagene) with equal loading amounts of polyA⁺-RNA. Spred-1 and Spred-2 signals show a similar expression pattern, predominantly in brain. A membrane exposure with a actin probe demonstrate the control levels of the two actin isoforms (arrows) in all examined tissues.

5.12. Spred-1 and Spred-2 protein expression pattern in mice

5.12.1. Generation of Spred-1- and Spred-2-specific antibodies

In order to investigate the protein expression profile of Spred-1 and Spred-2, two specific polyclonal antibodies were raised for Spred-1 and Spred-2, respectively. Because of the high sequence homology of Spred-1 and Spred-2, especially between their EVH-1 (62% homology), SPR (76%) and the KBD (45%) domains, the Spred-1-specific antibody was raised and affinity-purified against an intermediate region between the C-terminal boundary of the EVH-1 domain and the N-terminal boundary of the KBD (aa 124-233). This region shows the lowest similarity between the two Spred family members.

The Spred-2-specific antibody, used for the Western blot (Fig. 25), was raised and affinity-purified against the region comprising the amino acids 96-415 of Spred-2. This antibody was generated by Dr. Catherine Engelhardt.

Crossreactivity and specificity of the two antibodies were tested by Western blotting (Fig. 25) and by immunofluorescence staining of Spred-1- and -2-overexpressing

cells (Engelhardt et al., 2004). The two affinity-purified antibodies, generated to detect Spred-1 and Spred-2, specifically recognized the corresponding protein and did not cross-react with the other family members (Fig. 25). They detected Spred-1, migrating at an molecular weight of approximately 49 kDa and Spred-2 at 47 kDa, respectively. As positive controls, Spred proteins were over-expressed in eukaryotic HEK 293 cells (a non-tagged full-length protein and a 6xHis/c-myc-tagged version of mouse Spred-1 and Spred-2).

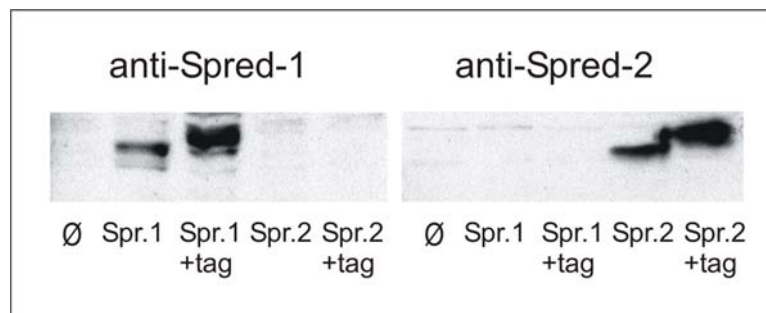


Figure 25.

Specificity of Spred-1- and Spred-2-specific antibodies.

(A) Western blots demonstrating specificity of Spred-1- and Spred-2-specific affinity-purified antibodies. Ø: untransfected HEK293 cells, Spr.1: Lysate of cells transfected with the full-length untagged Spred-1 expression vector, Spr.1+tag: cells transfected with the full-length 6xHis/c-myc-tagged Spred-1 expression vector, Spr.2: cells transfected with the full-length Spred-2 expression vector, Spr.2+tag: cells transfected with the full-length 6xHis/c-myc-tagged Spred-2 expression vector. Left panel probed with anti-Spred-1 antibody, right panel probed with anti-Spred-2 antibody. No cross-reactivity of the Spred-1-specific antibody with Spred-2 (left panel) and no cross-reactivity of the Spred-2-specific antibody with Spred-1 (right panel) was observed. Longer exposure revealed low expression levels of both proteins in untransfected HEK cells.

5.12.2. Spred-1/-2 protein expression pattern in fetal and adult mice

Western blot analyzes detected the strongest Spred-1 protein expression in whole brain and cerebellum, whereas Spred-2 protein expression was observed predominantly in lung, liver, and testis. After long exposure times, Spred-1 was also detectable in lung and colon, and Spred-2 was observed in all examined tissues (Engelhardt et al., 2004).

In order to test whether the expression patterns of the Spred proteins change during development, the immunoreactivity of mouse fetal tissues was examined. Spred-1 was expressed in fetal liver, brain, and heart at E16, whereas no Spred-2 immunoreactivity was detectable in these three fetal organs (Engelhardt et al., 2004).

5.13. Generation of *Spred-1* and *Spred-2* knockout mice using gene targeting vectors

To identify the chromosomal location and the genomic *Spred-1* and *Spred-2* sequences, the murine cDNA sequences were “blasted” to the EBI database of the Sanger Institute (<http://www.ensembl.org>). *Spred-1* was localized at chromosome 2 (E5), *Spred-2* at chromosome 11 (A3.2), and *Spred-3* at chromosome 7 (A3) (Fig. 26). Comparing the cDNAs with the genomic sequences, the exon-intron boundaries were detected, and thereby the gene organization defined. *Spred-1* consists of 7 and *Spred-2* of 6 exons. A detailed diagram with corresponding protein structures is illustrated in Figure 27.

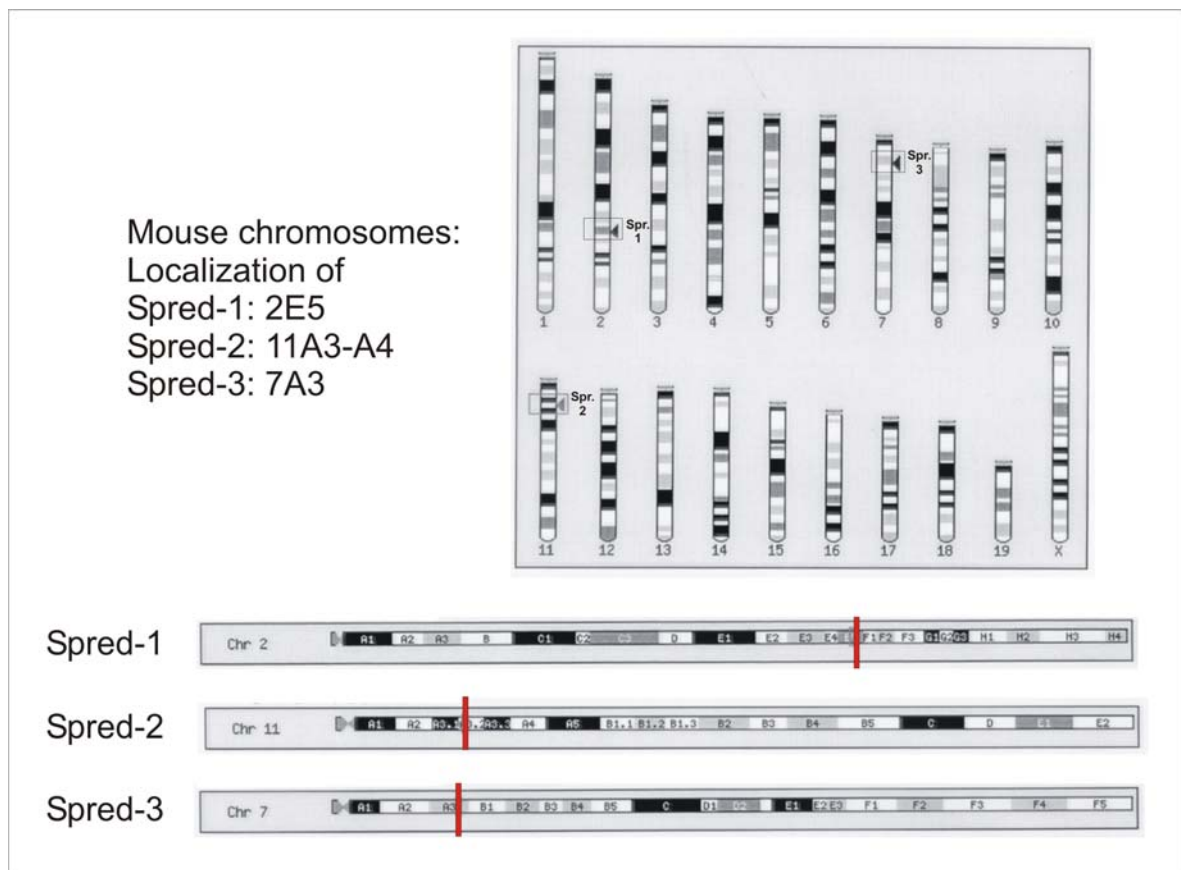


Figure 26.
Gene localization of *Spred-1*, -2, and -3 in the mouse genome (EBI database, Sanger Institute)

The upper part illustrates the 20 mouse chromosomes with the localization of *Spred-1* on chromosome 2 (E5), *Spred-2* on chromosome 11 (A3.2), and *Spred-3* on chromosome 7 (A3).

The lower part shows higher magnifications of the three chromosome areas with a more detailed gene location (red bars). (Spr.: *Spred*).

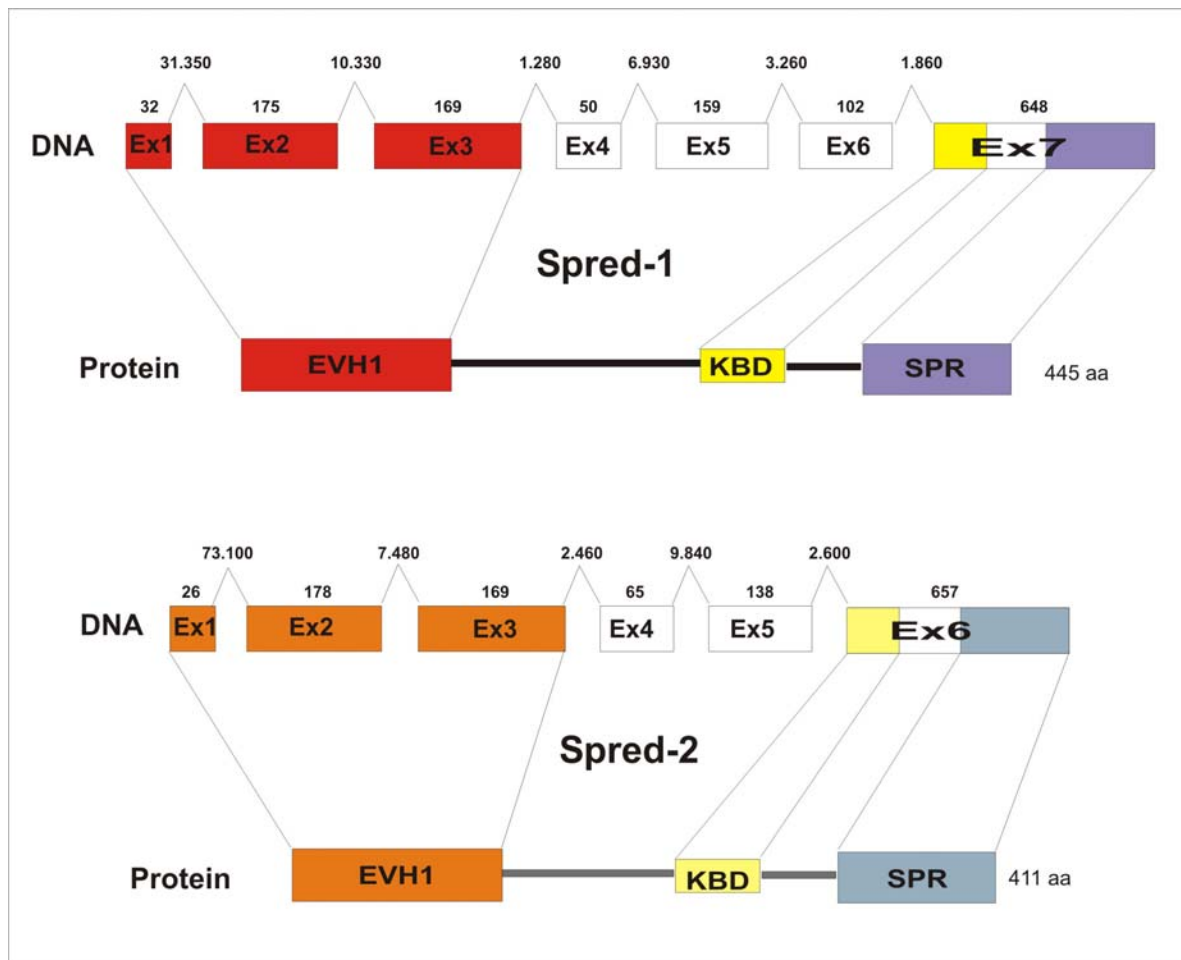


Figure 27.

Diagram of the genomic organization and correlated protein structure of Spred-1 and Spred-2.

The upper lines illustrate the exon lengths (numbers indicate the base pairs of each exon) and organization. Intron lengths were calculated from the EBI mouse database. The lower lines present the correlated protein structures. Spred-1 DNA consists of 7 exons and the protein has 445 amino acids. *Spred-2* DNA consists of 6 exons and the protein has 411 amino acids. (Ex: Exon; EVH-1: Ena/VASP homology 1 domain; KBD: c-Kit binding domain; SPR: Sprouty related domain; aa: amino acids).

In order to generate Spred-1 and Spred-2 knockout mice, gene targeting vectors with a Cre-lox and Flp-frt system were designed. Both targeting vectors were designed with almost the same cloning strategy, giving the opportunity to generate conventional as well as conditional knockout mice. Aim of this strategy was to flank exons 2 on both sides with a loxP site, to delete this exon completely (“conventional knockout”) or tissue-specific (“conditional knockout”). Conditional knockouts can be obtained by mating this mice with mice containing the Cre-recombinase under control of a tissue specific promoter. If exon 2 is deleted, only a very short remaining exon 1 coding for 10 amino acids (Spred-1) and 8 amino acids (Spred-2), respectively, could be expressed. Furthermore, this strategy excludes any theoretically possible splicing

events because, in any case, a frame shift, resulting in a nonsense protein, would occur. Both, Spred-1 and Spred-2 targeting vectors were cloned as documented in Figure 4 and Figure 5 and described in detail in the Methods section. The gene targeting vectors were linearized and electroporated in E14.1 embryonic stem cells, and screened by PCR for homologous recombination (Fig. 28).

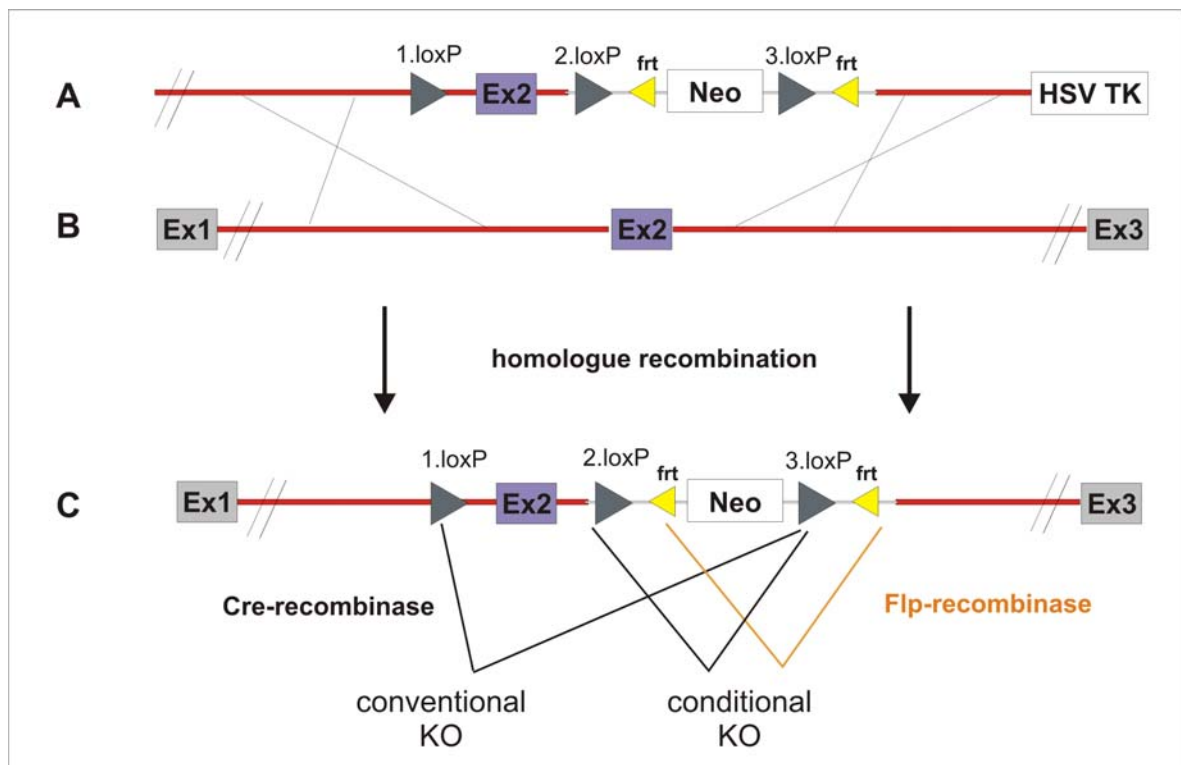


Figure 28.

Spred-1/ Spred-2 knockout strategy using gene targeting vectors.

(A) Organization of the cloned part of the gene targeting vector. (For Spred-1 and Spred-2 the same strategy was used). Spred DNA sequences are marked in red, exon (Ex) 2 is flanked by loxP sites, and the neomycin resistance cassette (Neo) is flanked by loxP (green) and frt sites (yellow). The short homologous sequence is followed by two Herpes simplex virus-thymidin kinase cassettes (HSV-TK).

(B) One Allele of the corresponding homologous Spred gene region is shown.

(C) Spred DNA structure after appropriate homologous recombination of the gene targeting vector. In a further step, Cre-mediated recombination can lead to a conventional (1. and 3. loxP site) or a conditional (2. and 3. loxP site) knockout (KO) construct. Additionally, Flp-mediated recombination can lead to a conditional knockout construct as well (orange).

For each construct, one clone with homologous recombination was identified. For Spred-1, clone III9E (2. electroporation) and for Spred-2, clone VI7E (1. electroporation), were positive (Fig. 29).

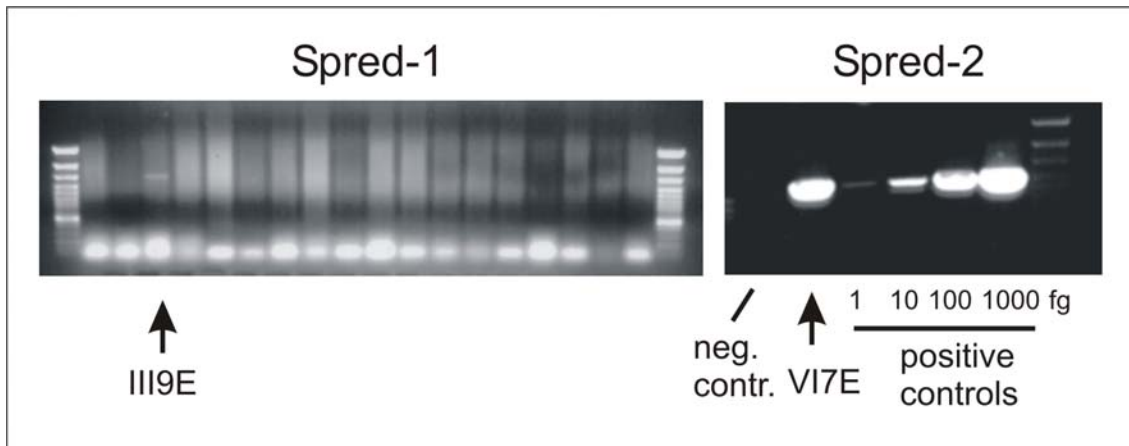


Figure 29.

Positive ES cell clones for Spred-1 and Spred-2.

Left: Spred-1 ES cell screening PCR with one positive clone in lane 3 (clone III9E). Right: Spred-2 ES cell screening PCR with one positive clone in lane 2 (clone VI7E), a negative control, and dilution row of positive controls (1 fg, 10 fg, 100 fg, 1 pg of the control plasmid).

Both ES cell clones are now ready for further use. These ES cells offer different opportunities:

1. Electroporation with a Cre-recombinase expression vector, which can lead to the following 4 recombination events (Fig. 30):

A) no recombination, resulting in the original clone;

B) recombination with deletion of the part between the 1. and 3. loxP site, resulting in a conventional knockout, where exon 2 and the neo cassette is deleted;

C) recombination with deletion of the part between the 2. and 3. loxP site, resulting in a conditional knockout, where exon 2 is flanked by loxP sites (floxed) and the neo cassette is deleted;

D) recombination with deletion of the part between the 1. and 2. loxP site, resulting in a nonsense product, where exon 2 is deleted but the neo cassette is still present.

Subsequently, the conventional (Fig. 30B) and conditional (Fig. 30C) ES cells could be used directly for blastocyst injection to generate chimeras and, therefore, the mouse strain of interest.

2. Electroporation with a Flp-recombinase expression vector, which can lead to conditional knockouts. After successful recombination, the neo cassette is deleted and a floxed exon 2 remains (Fig. 30E).

3. Generation of a mouse strain by direct blastocyst injection of the clone and then mating with Cre- or Flp-recombinase deleter mice to obtain conditional knockout mice.

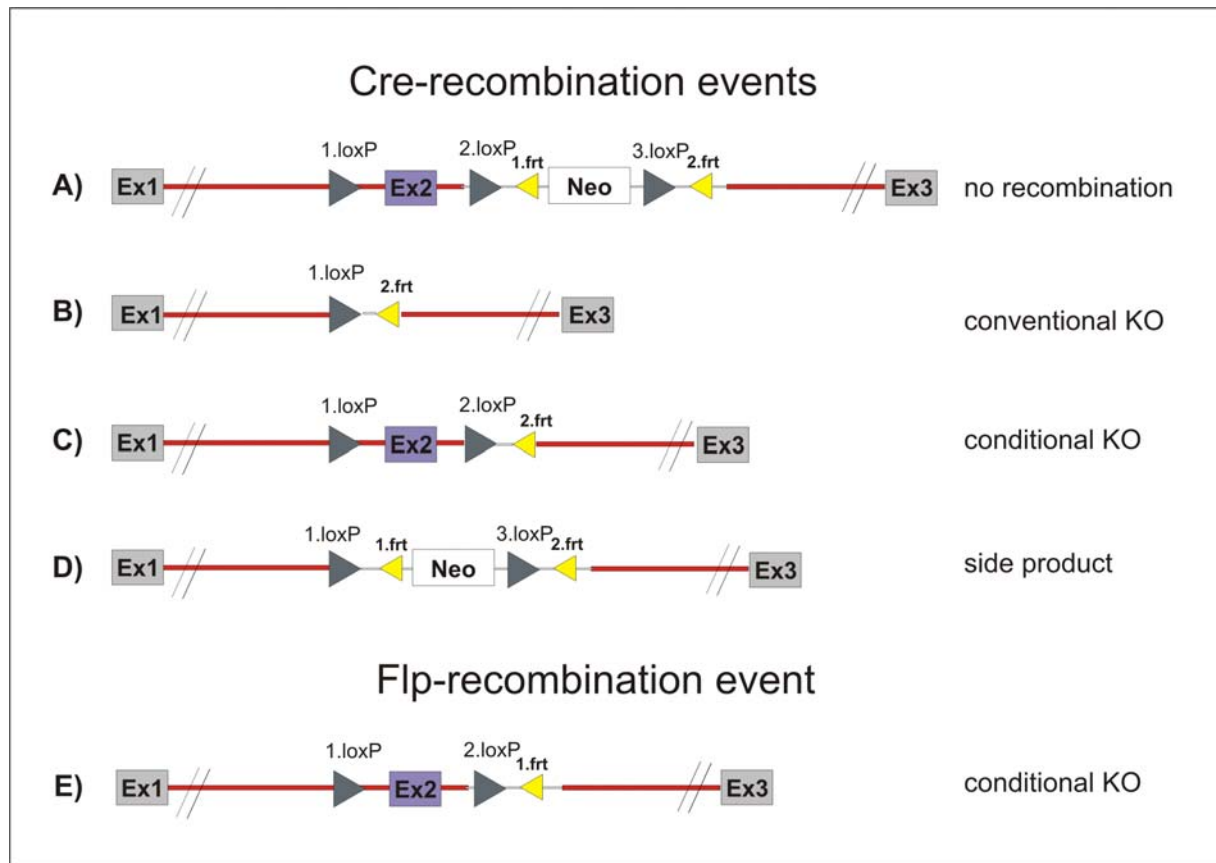


Figure 30.

Cre- and Flp-recombination events.

- (A) Spred (-1 or -2) gene after appropriate homologous recombination of the gene targeting vector without any further Cre- or Flp-recombination event.
- (B) Cre-mediated recombination event using the 1. and 3. loxP site, resulting in a conventional knockout construct.
- (C) Cre-mediated recombination event using the 2. and 3. loxP site, resulting in a conditional knockout construct.
- (D) Cre-mediated recombination event using the 1. and 2. loxP site, resulting in a nonsense side product.
- (E) Flp-mediated recombination event using the 1. and 2. frt site, resulting in a conditional knockout construct.

6. Discussion

6.1. Domain structure of Spred-2

Beside the *Drosophila* *AE33* gene, cloned as a probable *rough* transcription factor target regulating photoreceptor cell development in the fly (DeMille et al., 1996), three mammalian Spred proteins have been described as negative regulators of growth factor-induced mitogen-activated protein kinase (MAPK) pathways (Kato et al., 2003; Wakioka et al., 2001). They consist of three distinct domains, namely the N-terminal EVH-1 (Ena/Vasodilator-stimulated phosphoprotein (VASP) homology 1) domain, a unique KBD (c-Kit kinase binding) domain and a C-terminal SPR (Sprouty-related) domain. EVH-1 domains are protein interaction modules, which target their multi-domain host proteins to specific sites of action where they are involved in regulating cellular processes as diverse as cytoskeletal re-organization, synaptic transmission, proliferation and differentiation (reviewed in (Ball et al., 2002; Reinhard et al., 2001)). The c-Kit binding domain (KBD) is not related to any previously identified tyrosine kinase interaction domain, such as SH2, PTB, or c-Met-binding domain and efficient phosphorylation of Spred-1 required this domain consisting of about 50 amino acids (Wakioka et al., 2001). The cysteine-rich SPR domain involved in membrane localization was first described in the context of Sprouty proteins, which have been shown to be both positive and negative regulators of MAP kinase pathways (for review see Christofori, 2003), and the efficient suppression of ERK activation by Spred requires this SPR domain (Kato et al., 2003). Here, at the DNA level the organization of the six exons encoding Spred-2 and the correlated domain structure at the protein level is shown. The mouse *Spred-2* was found to be located on chromosome 11 (Fig. 26), (Kato et al., 2003); exon 1 to exon 3 code for the EVH-1 domain, exon 4 and exon 5 code for the middle part and exon 6 is responsible for the KBD and SPR domain (Fig. 8A, Fig. 27).

6.2. Physiological function of Spred

Sproutys selectively inhibit FGF-induced ERK activation but do not inhibit EGF-induced ERK activation (Sasaki et al., 2001). In contrast, overexpression of Spred-1 and Spred-2 efficiently suppressed ERK activation induced by several stimuli, including EGF, FGF, VEGF, PDGF, SCF, serum, and LPA. Spred constitutively associates with Ras and inhibits the activation of MAP kinase by suppressing

phosphorylation and activation of Raf (Wakioka et al., 2001). So far, only some rare data of isolated hematopoietic cells derived from midgestation *Spred-2*^{-/-} mice indicate an increased number of granulocyte and macrophage colonies (Nobuhisa et al., 2004). In bone marrow-derived mast cells of *Spred-1*^{-/-} mice, an augmentation of ERK activation and proliferation in response to IL-3 was observed (Nonami et al., 2004). Recently, it has been shown that *Spred-1* is expressed in eosinophils and negatively regulates allergen-induced airway eosinophilia and hyperresponsiveness (Inoue et al., 2005). Except of these data, all functional information about *Spred* was gained by overexpression of full-length constructs or deletion mutants in different cell culture systems. Therefore, the observed general inhibitory effects of *Spred* proteins on the Ras/Raf/MAP kinase pathway might be due to high levels of overexpressed proteins and may not necessarily reflect the in vivo situation, in which functional interaction is strongly dependent on specific expression levels and affinity of interacting proteins. So far, no comprehensive in vivo data of *Spred* function were available. Therefore, the in this work established *Spred-2*^{-/-} mouse line represents a new in vivo model to investigate *Spred-2* function in the entire organism.

6.3. The *Spred-2* gene trap model

In this work, the ES cell line XB228, harboring a gene trap vector insertion between exons 4 and 5 of the *Spred-2* gene, was used. Previously, it has been described in different knockout strategies that exons in front of the vector insertion were still used as an RNA template and a truncated protein was expressed. Expression of read-through products containing exon and vector information or truncated splice variants has also been reported. As *Spred-2* was interrupted downstream of exon 4, expression of the first four exons, basically representing the EVH-1 domain, could not be excluded. Based on sequence comparisons, four different subclasses of EVH-1/WH-1 domains have been identified. High resolution structures of three classes, comprising the cytoskeletal Ena/VASP proteins, the synaptic terminal Homer/Vesl proteins, and the Wiskott-Aldrich syndrome (WAS) proteins have been solved (for reviews see (Ball et al., 2002; Callebaut et al., 1998). Recently, the 3D-structure of the *Spred* EVH-1 domain has also been enlightened (Harmer et al., 2005; Zimmermann et al., 2004). The EVH-1 domain of VASP was shown to act as a dominant negative form, when overexpressed in cardiac myocytes (Eigenthaler et al., 2003). Overexpression of a ΔC -mutant of *Spred-1*, missing the Sprouty domain but

still containing the EVH-1 and the c-Kit binding domain, demonstrated the dominant negative behavior of Spred-EVH1, as well (Nonami et al., 2004). Immunoblot analyzes of Spred-2^{-/-} mice brains, the organ with the highest natural Spred-2 expression, failed to detect the full-length Spred-2, a truncated Spred-2 protein, or an enlarged read-through product (Fig. 9C). These results were confirmed by Northern blots in which Spred-2 mRNAs in tissues of wildtype mice but no full-length or truncated transcripts in samples of Spred-2^{-/-} mice were detectable (Fig. 9B). Based on these findings, it can be concluded that in this work Spred-2 knockout mice were generated, which do not express truncated, potentially dominant negative Spred-2 forms.

6.4. Spred-2 knockout mice

Spred-1 overexpression in osteosarcoma cells inhibited tumor proliferation, metastasis, cell migration, and Rho-dependent actin-stress fiber remodelling (Miyoshi et al., 2004). Therefore, one could speculate about a phenotype with hyperproliferative cell populations in different organs and tumor development with a forced metastatic situation in Spred-2-deficient mice. In a monitored time period of more than 12 months, none of these phenomena appeared in Spred-2-deficient mice. Histology indicated unaltered tissue structures without any tumor formations. Males and females were fertile, were born healthy, and did not display any strange behavior. However, the altered Mendelian distribution of offspring resulting from heterozygous Spred-2^{+/-} matings pointed towards developmental restraints in some knockout and heterozygous mice but the mechanisms underlying this phenomenon have to be investigated further.

In the spleen of adult Spred-2-deficient mice, an increased number of megakaryocytes was observed (Fig. 17). This underlines the results, which have been observed in Spred-2^{-/-} and Spred-1^{-/-} mice generated by a different knockout strategy (Nobuhisa et al., 2004; Nonami et al., 2004). In VASP^{-/-} mice, a moderate hyperplasia of megakaryocytes has been observed and VASP-deficient platelets have an increased aggregation response to known stimulants and partial resistance to cAMP and cGMP effects in vitro (Aszodi et al., 1999; Hauser et al., 1999) and in vivo (Massberg et al., 2004). Similar to Spred proteins, VASP contains an EVH-1 domain at the N-terminus, suggesting that this type of domain might also be important in megakaryocyte function.

6.5. Spred-2 loss of function causes dwarfism

In this work, the Spred-2^{-/-} mice exhibited an obvious dwarf phenotype. They were born smaller and lighter and stayed smaller throughout their whole life span as compared to wildtype littermates (Fig. 10A, C-F). In males, growth differences were more pronounced than in females, which might be an X-chromosomal compensatory effect. Database analyzes revealed a genomic sequence similar to *Spred-2* on the mouse X-chromosome (NCBI Gene database, Loc213280, Chromosome X A4, Contig NT_039702), which might be a putative “*Spred-4*” or just a pseudogene and has to be investigated further.

Peripheral steroid and thyroid hormones as well as blood glucose levels were not altered (Fig. 11). Therefore, the most common causes of metabolic dwarfism could be excluded. X-ray exposures and tibia lengths measurements revealed that the growth difference was probably due to a defect in skeletal development (Fig. 10B, Fig. 12M, N). Whereas Spred-3 is expressed exclusively in brain, Spred-1 and Spred-2 were found to have an overlapping expression pattern in various tissues (Engelhardt et al., 2004; Kato et al., 2003). Here, it is shown that Spred-2, the most ubiquitously expressed isoform, was also found to be expressed in chondrocytes of bones, growing by secondary ossification, suggesting a specific role of Spred-2 in these cells (Fig. 12, Fig. 13E-H). In growth plates of long bones, where endochondral ossification regulates bone growth, Spred-2 expression was detected in resting, proliferating, and hypertrophic chondrocytes (Fig. 12A, C, M, Fig. 13E, G). In tibiae of P6, P10, 1 week, 4 weeks, and 12 weeks old Spred-2-deficient mice, the epiphyseal growth plate showed a predominantly narrower zone of hypertrophic chondrocytes and a reduction in size of hypertrophic chondrocytes as compared to wildtype littermates (Fig. 13I-L, Fig. 14), indicating a chondrocyte dysfunction at the growth plate during endochondral ossification.

Overexpression of FGFs (Coffin et al., 1995; Garofalo et al., 1999), activating FGFR3 mutants (Chen et al., 2001a; Iwata et al., 2000; Iwata et al., 2001; Li et al., 1999; Naski and Ornitz, 1998; Segev et al., 2000; Wang et al., 1999), or constitutive activation of MEK1 in chondrocytes (Murakami et al., 2004) caused achondroplasia-like dwarfism in mice. This indicates that FGF signaling through the FGFR3 and MAPK pathway plays a major role in the regulation of bone growth. Therefore, it can be regarded as an important negative regulator of skeletal growth. Spred is known to be an inhibitor of FGF-induced MAPK signaling by binding to Ras and inhibiting

phosphorylation of Raf-1 (Kato et al., 2003; Sasaki et al., 2001; Wakioka et al., 2001). Therefore, lack of functional Spred-2 may accelerate MAPK signaling because an inhibitor of the system was removed. In this study, stimulation of cultured Spred-2^{-/-} chondrocytes with different FGF concentrations demonstrated an earlier and increased ERK phosphorylation as compared to wildtype chondrocytes, whereas unspecific stimulation with FCS revealed no differences between wildtype and knockout cells (Fig. 16). Here, a similar achondroplasia-like dwarfism phenotype in Spred-2^{-/-} mice, as described for other factors activating the MAPK pathway, was observed. So far, information about downstream events through which FGFs influence the proliferation or differentiation of osteogenic chondrocytes is rare.

In this study, it is demonstrated that Spred-2 is an important modulator of bone morphogenesis by inhibiting the FGF-induced MAPK pathway, and loss of Spred-2 causes dwarfism by activating the MAPK pathway in chondrocytes. These observations support the model in which FGFR3 signaling inhibits bone growth by inhibiting chondrocyte differentiation through the MAPK pathway.

Contrary functions in bone growth have been published for Sprouty protein family members, which have also been identified as inhibitors of the MAPK pathway and contain, like Spred, a SPR domain at the C-terminus. In contrast to Spred-2, overexpression of vertebrate Sproutys in limbs caused reduction in size of skeletal elements due to an inhibition of chondrocyte differentiation (Minowada et al., 1999). Therefore, Sproutys could act as negative feedback regulators (Minowada et al., 1999), whereas Spred-2 appears to play a role as a downstream inhibitor of FGF-induced MAPK signaling in chondrocytes.

The fairly mild phenotype of Spred-2 knockout mice is probably due to compensatory effects of Spred-1, which is co-expressed in various organs (Engelhardt et al., 2004). Even in brain, the organ normally showing the highest expression of Spred-2, Spred-2 deficiency has not caused dramatic disturbances, suggesting compensation by Spred-1 and/or Spred-3.

A comparable situation was described for gene-ablation of Mena or VASP proteins. In vertebrates, genetic analysis of Ena/VASP function was hindered by the broad and overlapping expression of the three highly related family members Mena (Mammalian enabled), VASP, and EVL (Ena-VASP like). Mice deficient in either Mena or VASP exhibit subtle defects in forebrain commissure formation and platelet activation, respectively (Aszodi et al., 1999; Hauser et al., 1999; Lanier et al., 1999; Massberg et

al., 2004). $Mena^{-/-}/VASP^{-/-}$ double mutants die perinatally and display defects in neurulation, in development of craniofacial structures, and in the formation of several fiber tracts in the CNS and peripheral nervous system (Menzies et al., 2004). It is likely that the expression of the third family member, EVL, masks the requirement for $Ena/VASP$ function in other cell types of $Mena^{-/-}/VASP^{-/-}$ animals. In another mouse model, specific transgenic overexpression of a C-terminal fragment of VASP in keratinocytes resulted in skin defects (Vasioukhin et al., 2000). However, cortical lamination and skin defects were not detected in $Mena^{-/-}/VASP^{-/-}$ mice, suggesting that continued expression of EVL alone is likely sufficient for proper development of many tissues in these mice. Therefore, it is certainly of interest to generate $Spred-1^{-/-}$ and $Spred-2^{-/-}$ double knockout mice, or even triple knockout mice for all three known *Spred* family members to study the general *in vivo* function of *Spred*.

6.6. *Spred-2* promoter activity

The *Spred-2* promoter is supposed to be a region upstream of exon 1 of the *Spred-2* gene on chromosom 11. So far, nothing was known about its organisation, regulation, and activity. In this study, the physiological *Spred-2* promoter activity pattern in newborn and adult mice revealed by a gene trap approach is demonstrated for the first time.

A gene trap approach has the big advantage of an inserted reporter element directly under control of the physiological promoter. Other systems, examining the promoter activity pattern in mice, usually use a random integration approach to generate transgenic mice. Most of the times, the insertion vector consists of the promoter of interest followed by a detection element, e.g., a luciferase or *lacZ* gene. These transgenic models maintain the problem that the vector inserts randomly in an artificial position anywhere in the genome. Therefore, the external promoter is placed into a complete different chromosomal and genomic environment and might be influenced by other non-physiological regulatory elements. This can be due to an integration of the vector close to another promoter region, a silencer, or enhancer region, respectively. An additional problem is the multiple vector integration in the genome. Therefore, the expression level of the detection element is not necessarily comparable with the physiological promoter activity in these systems. In contrast, this gene trap approach offers the opportunity to examine the promoter activity under

physiological conditions and the β -galactosidase expression level is directly correlated to the endogenous *Spred-2* promoter activity.

To date, the *Spred-2* expression pattern has been examined already in different studies on RNA level by Northern blots, RT-PCR, and in situ hybridisation analyzes. On protein level, the *Spred-2* expression has been studied by Western blots, and immunohistochemical analyzes. One Northern blot analysis revealed a ubiquitous *Spred-2* expression pattern. In this experiment, *Spred-2* RNA was found to be predominantly expressed in brain, kidney, colon, small intestine, lung and to a lower extent in heart, liver, stomach, skeletal muscle, spleen, and thymus (Kato et al., 2003). The Northern blot data and RT-PCR analyzes of this work showed an almost ubiquitous *Spred-2* mRNA distribution in adult mice (Fig. 23A, Fig. 24) (Engelhardt et al., 2004) with a comparable expression pattern to the Northern blot analysis of Kato et al. (2003). Except of the high RNA expression in lung (Kato et al., 2003), these expression profiles were as well compatible with the promoter activity pattern demonstrated in this study.

In mouse embryonic organs, *Spred-2* mRNA was detected by RT-PCR in heart, lung, liver, brain, and bone (Fig, 23B) (Engelhardt et al., 2004). Furthermore, RT-PCR analyzes of E16 and adult rats demonstrated *Spred-2* mRNA expression in lung (Hashimoto et al., 2002). Additionally, in situ hybridization studies of E14 rat embryos detected *Spred-2* mRNA expression in brain, spinal cord, heart, intestine, skin, and mesenchymal lung cells (Hashimoto et al., 2002).

Western blot analyzes of various adult mouse organs confirmed the ubiquitous *Spred-2* expression pattern (Engelhardt et al., 2004), whereas the protein levels in some organs differed markedly as compared to the RT-PCR and promoter activity results of this work. On one hand, in lung, liver, and testis, a strong *Spred-2* protein signal was detectable (Engelhardt et al., 2004), whereas in this study, a rather weak *Spred-2* promoter activity was seen. On the other hand, the *Spred-2* Western blot data show a moderate signal in brain (Engelhardt et al., 2004), whereas in this work, a very strong promoter activity was found. But in heart, kidney, stomach, small intestine, colon, spleen, and skin the protein expression levels are comparable with the promoter activity levels in this study.

Immunohistochemical experiments showed staining of *Spred-2* in murine spermatids of testicular tubules and in human hepatocytes (Engelhardt et al., 2004). This is not in line with the present observations, where no *Spred-2* promoter activity was detected

in such cells. Compatible with the results of this work were the strong immunohistochemical Spred-2 protein signals in skin, salivary glands, prostate, and the mucosal layer and apical pole of endothelial cells in organs of the human intestinal tract (Engelhardt et al., 2004).

These discrepancies are probably due to different methods, different species, and cell type-dependent turnover of Spred-2 mRNA and protein in the cell. The quantitative relevance of RT-PCR analyzes is certainly dependent on the amount of cycles, binding affinity of primers, and RNA quality and should therefore be interpreted carefully. Western blot and immunohistochemical experiments are extremely dependent on the affinity and specificity of antibodies and different expression levels in mouse, rat, and human tissues are possible. But the most important point is probably the different stability, modification, and turn over of RNAs and proteins in different cell types. In contrast, X-Gal staining intensity is directly correlated with the physiological promoter activity level, therefore, providing an ideal method to monitor promoter activity in situ.

In this work, it is shown that Spred-2 plays an important role in the appropriate regulation of bone growth. Lack of Spred-2 causes achondroplasia-like dwarfism in mice, due to an FGF-induced up-regulation of the MAPK pathway in chondrocytes. Furthermore, Spred-2 has a potential function in the regulation of vesicle transport and the secretion processes of glands. Spred-2 is highly expressed in the apical pole of secretory glandular cells and is co-localized with Rab11; a small GTPase that regulates vesicle transport (Engelhardt et al., 2004). Moreover, Spred-2 is expressed in midgestation mouse embryos in the aorto-gonad-mesonephros region, and is supposed to function there as a negative regulator of embryonic hematopoiesis (Nobuhisa et al., 2004). Distinct functions of Spred-2 in brain, eye, skin, kidney, and smooth muscle cells of the intestinal tract, uterus, and blood vessels -all tissues with a high *Spred-2* promoter activity- are not known yet and have to be investigated further.

6.7. Enhanced bleeding of *Spred-2*^{-/-} mice

An additional phenotype of the *Spred-2*^{-/-} mice was an increased bleeding after injuries. The bleeding volume was extremely enlarged and the bleeding time was significantly prolonged (Fig. 17). So far, an increased bleeding resulted by hypertension was excluded by blood pressure measurements (Fig. 17). To examine

the physiological reasons for this phenotype, the different steps of the clotting cascade have to be investigated further. Therefore, following studies have to examine the contractility of vascular smooth muscle cells, blood clotting factors, platelet functions, and endothel functions.

Very interesting is certainly the examination of vascular smooth muscle cell contractility, because the *Spred-2* promoter activity studies of this work demonstrated that *Spred-2* is specifically expressed in smooth muscle cells of blood vessels (Fig. 22). Recently, it has been shown that *Spred-2* associates with RhoA and suppresses constitutively activated RhoA-induced stress fiber formations (Miyoshi et al., 2004). Since RhoA is a key regulator of vascular smooth muscle contraction (for review see (Lee et al., 2004; Somlyo and Somlyo, 2003), the investigation of physical and functional interaction of *Spred* and RhoA in vascular smooth muscle cells is of major interest and should be a focus of future studies employing *Spred*-deficient mouse models.

Another interesting candidate for this bleeding phenotype is the examination of platelet function, because the number of megakaryocytes in spleen and the amount of platelets in the peripheral blood of *Spred-2* knockout mice are increased (Fig. 17). This could be due to a compensatory upregulation, if the physiological function of platelets is altered.

6.8. Outlook

In summary, these studies provide new insights into the in vivo function of *Spred-2* during bone development and, potentially, for the regulation of coagulation processes. Especially the examination of the bleeding phenotype should be a focus of the future work. Moreover, the *Spred-2* RNA expression and *Spred-2* promoter activity levels gave a first clue which organs or cells might be additionally affected by the *Spred-2* deficiency.

Because the fairly mild phenotype of *Spred-2* knockout mice is probably due to the compensatory effects of the other *Spred* family members, it is certainly of interest to generate *Spred-1*^{-/-} and *Spred-2*^{-/-} double knockout mice or even triple knockout mice for all three known *Spred* family members to study the general physiological functions. A feasible option to generate *Spred-1* knockout mice is the use of the AD429 ES cells line (Baygenomics), in which a gene trap vector has inserted between exons 4 and 5 of the *Spred-1* gene. This construct is very similar to the

XB228 ES cell line - used in this work to generate the *Spred-2*^{-/-} mice - and, therefore, could be explored in the same manner as described here. To examine the *Spred-1* function, the in this work generated *Spred-1* specific antibody will be certainly of essential help.

One may speculate that double or latest triple knockout mice will not survive the embryonic period or are not viable for a long time. However, it is possible to study tissue specific functions of the *Spred* family members by using conditional knockout mice. For this purpose, the in this work generated gene targeted ES cell lines - with a floxed exon 2 of the *Spred-1* and *Spred-2* gene, respectively - will be perfect tools.

7. References

- Amling, M., Priemel, M., Holzmann, T., Chapin, K., Rueger, J. M., Baron, R. and Demay, M. B.** (1999). Rescue of the skeletal phenotype of vitamin D receptor-ablated mice in the setting of normal mineral ion homeostasis: formal histomorphometric and biomechanical analyses. *Endocrinology* **140**, 4982-7.
- Aszodi, A., Pfeifer, A., Ahmad, M., Glauner, M., Zhou, X. H., Ny, L., Andersson, K. E., Kehrel, B., Offermanns, S. and Fassler, R.** (1999). The vasodilator-stimulated phosphoprotein (VASP) is involved in cGMP- and cAMP-mediated inhibition of agonist-induced platelet aggregation, but is dispensable for smooth muscle function. *Embo J* **18**, 37-48.
- Austin, C. P., Battey, J. F., Bradley, A., Bucan, M., Capecchi, M., Collins, F. S., Dove, W. F., Duyk, G., Dymecki, S., Eppig, J. T. et al.** (2004). The knockout mouse project. *Nat Genet* **36**, 921-4.
- Bai, R. Y., Koester, C., Ouyang, T., Hahn, S. A., Hammerschmidt, M., Peschel, C. and Duyster, J.** (2002). SMIF, a Smad4-interacting protein that functions as a co-activator in TGFbeta signalling. *Nat Cell Biol* **4**, 181-90.
- Ball, L. J., Jarchau, T., Oschkinat, H. and Walter, U.** (2002). EVH1 domains: structure, function and interactions. *FEBS Lett* **513**, 45-52.
- Bashaw, G. J., Kidd, T., Murray, D., Pawson, T. and Goodman, C. S.** (2000). Repulsive axon guidance: Abelson and Enabled play opposing roles downstream of the roundabout receptor. *Cell* **101**, 703-15.
- Basilico, C. and Moscatelli, D.** (1992). The FGF family of growth factors and oncogenes. *Adv Cancer Res* **59**, 115-65.
- Bellus, G. A., McIntosh, I., Smith, E. A., Aylsworth, A. S., Kaitila, I., Horton, W. A., Greenhaw, G. A., Hecht, J. T. and Francomano, C. A.** (1995). A recurrent mutation in the tyrosine kinase domain of fibroblast growth factor receptor 3 causes hypochondroplasia. *Nat Genet* **10**, 357-9.
- Beneken, J., Tu, J. C., Xiao, B., Nuriya, M., Yuan, J. P., Worley, P. F. and Leahy, D. J.** (2000). Structure of the Homer EVH1 domain-peptide complex reveals a new twist in polyproline recognition. *Neuron* **26**, 143-54.
- Bultman, S. J., Michaud, E. J. and Woychik, R. P.** (1992). Molecular characterization of the mouse agouti locus. *Cell* **71**, 1195-204.
- Callebaut, I.** (2002). An EVH1/WH1 domain as a key actor in TGFbeta signalling. *FEBS Lett* **519**, 178-80.
- Callebaut, I., Cossart, P. and Dehoux, P.** (1998). EVH1/WH1 domains of VASP and WASP proteins belong to a large family including Ran-binding domains of the RanBP1 family. *FEBS Lett* **441**, 181-5.
- Casci, T., Vinos, J. and Freeman, M.** (1999). Sprouty, an intracellular inhibitor of Ras signaling. *Cell* **96**, 655-65.
- Chambers, D. and Mason, I.** (2000). Expression of sprouty2 during early development of the chick embryo is coincident with known sites of FGF signalling. *Mech Dev* **91**, 361-4.
- Chen, L., Li, C., Qiao, W., Xu, X. and Deng, C.** (2001a). A Ser(365)-->Cys mutation of fibroblast growth factor receptor 3 in mouse downregulates Ihh/PTHrP signals and causes severe achondroplasia. *Hum Mol Genet* **10**, 457-65.
- Chen, R. Z., Akbarian, S., Tudor, M. and Jaenisch, R.** (2001b). Deficiency of methyl-CpG binding protein-2 in CNS neurons results in a Rett-like phenotype in mice. *Nat Genet* **27**, 327-31.

- Chen, W. V., Delrow, J., Corrin, P. D., Frazier, J. P. and Soriano, P.** (2004). Identification and validation of PDGF transcriptional targets by microarray-coupled gene-trap mutagenesis. *Nat Genet* **36**, 304-12.
- Choi, D. Y., Toledo-Aral, J. J., Lin, H. Y., Ischenko, I., Medina, L., Safo, P., Mandel, G., Levinson, S. R., Halegoua, S. and Hayman, M. J.** (2001). Fibroblast growth factor receptor 3 induces gene expression primarily through Ras-independent signal transduction pathways. *J Biol Chem* **276**, 5116-22.
- Christofori, G.** (2003). Split personalities: the agonistic antagonist Sprouty. *Nat Cell Biol* **5**, 377-9.
- Coffin, J. D., Florkiewicz, R. Z., Neumann, J., Mort-Hopkins, T., Dorn, G. W., 2nd, Lightfoot, P., German, R., Howles, P. N., Kier, A. and O'Toole, B. A.** (1995). Abnormal bone growth and selective translational regulation in basic fibroblast growth factor (FGF-2) transgenic mice. *Mol Biol Cell* **6**, 1861-73.
- Colavita, A. and Culotti, J. G.** (1998). Suppressors of ectopic UNC-5 growth cone steering identify eight genes involved in axon guidance in *Caenorhabditis elegans*. *Dev Biol* **194**, 72-85.
- Colvin, J. S., Bohne, B. A., Harding, G. W., McEwen, D. G. and Ornitz, D. M.** (1996). Skeletal overgrowth and deafness in mice lacking fibroblast growth factor receptor 3. *Nat Genet* **12**, 390-7.
- D'Arcangelo, G., Miao, G. G., Chen, S. C., Soares, H. D., Morgan, J. I. and Curran, T.** (1995). A protein related to extracellular matrix proteins deleted in the mouse mutant reeler. *Nature* **374**, 719-23.
- de Maximy, A. A., Nakatake, Y., Moncada, S., Itoh, N., Thiery, J. P. and Bellusci, S.** (1999). Cloning and expression pattern of a mouse homologue of drosophila sprouty in the mouse embryo. *Mech Dev* **81**, 213-6.
- DeMille, M. M., Kimmel, B. E. and Rubin, G. M.** (1996). A *Drosophila* gene regulated by rough and glass shows similarity to ena and VASP. *Gene* **183**, 103-8.
- Deng, C., Wynshaw-Boris, A., Zhou, F., Kuo, A. and Leder, P.** (1996). Fibroblast growth factor receptor 3 is a negative regulator of bone growth. *Cell* **84**, 911-21.
- Dikic, I. and Giordano, S.** (2003). Negative receptor signalling. *Curr Opin Cell Biol* **15**, 128-35.
- D'Orleans-Juste, P., Honore, J. C., Carrier, E. and Labonte, J.** (2003). Cardiovascular diseases: new insights from knockout mice. *Curr Opin Pharmacol* **3**, 181-5.
- Egan, J. E., Hall, A. B., Yatsula, B. A. and Bar-Sagi, D.** (2002). The bimodal regulation of epidermal growth factor signaling by human Sprouty proteins. *Proc Natl Acad Sci U S A* **99**, 6041-6.
- Eigenthaler, M., Engelhardt, S., Schinke, B., Kobsar, A., Schmitteckert, E., Gambaryan, S., Engelhardt, C. M., Krenn, V., Eliava, M., Jarchau, T. et al.** (2003). Disruption of cardiac Ena-VASP protein localization in intercalated disks causes dilated cardiomyopathy. *Am J Physiol Heart Circ Physiol* **285**, H2471-81.
- Engelhardt, C. M., Bundschu, K., Messerschmitt, M., Renne, T., Walter, U., Reinhard, M. and Schuh, K.** (2004). Expression and subcellular localization of Spred proteins in mouse and human tissues. *Histochem Cell Biol* **122**, 527-38.
- Freeman, M., Kimmel, B. E. and Rubin, G. M.** (1992). Identifying targets of the rough homeobox gene of *Drosophila*: evidence that rhomboid functions in eye development. *Development* **116**, 335-46.
- Garofalo, S., Klinger-Spatz, M., Cooke, J. L., Wolstin, O., Lunstrum, G. P., Moshkovitz, S. M., Horton, W. A. and Yayon, A.** (1999). Skeletal dysplasia and defective chondrocyte differentiation by targeted overexpression of fibroblast growth factor 9 in transgenic mice. *J Bone Miner Res* **14**, 1909-15.

- Gertler, F. B., Niebuhr, K., Reinhard, M., Wehland, J. and Soriano, P.** (1996). Mena, a relative of VASP and Drosophila Enabled, is implicated in the control of microfilament dynamics. *Cell* **87**, 227-39.
- Glienke, J., Fenten, G., Seemann, M., Sturz, A. and Thierauch, K. H.** (2000). Human SPRY2 inhibits FGF2 signalling by a secreted factor. *Mech Dev* **96**, 91-9.
- Goldfarb, M.** (1996). Functions of fibroblast growth factors in vertebrate development. *Cytokine Growth Factor Rev* **7**, 311-25.
- Goldstein, J. L.** (2001). Laskers for 2001: knockout mice and test-tube babies. *Nat Med* **7**, 1079-80.
- Gross, I., Bassit, B., Benezra, M. and Licht, J. D.** (2001). Mammalian sprouty proteins inhibit cell growth and differentiation by preventing ras activation. *J Biol Chem* **276**, 46460-8.
- Hacohen, N., Kramer, S., Sutherland, D., Hiromi, Y. and Krasnow, M. A.** (1998). sprouty encodes a novel antagonist of FGF signaling that patterns apical branching of the Drosophila airways. *Cell* **92**, 253-63.
- Haffner, C., Jarchau, T., Reinhard, M., Hoppe, J., Lohmann, S. M. and Walter, U.** (1995). Molecular cloning, structural analysis and functional expression of the proline-rich focal adhesion and microfilament-associated protein VASP. *Embo J* **14**, 19-27.
- Halbrugge, M. and Walter, U.** (1989). Purification of a vasodilator-regulated phosphoprotein from human platelets. *Eur J Biochem* **185**, 41-50.
- Hall, A. B., Jura, N., DaSilva, J., Jang, Y. J., Gong, D. and Bar-Sagi, D.** (2003). hSpry2 is targeted to the ubiquitin-dependent proteasome pathway by c-Cbl. *Curr Biol* **13**, 308-14.
- Hanafusa, H., Torii, S., Yasunaga, T. and Nishida, E.** (2002). Sprouty1 and Sprouty2 provide a control mechanism for the Ras/MAPK signalling pathway. *Nat Cell Biol* **4**, 850-8.
- Hansen, J., Floss, T., Van Sloun, P., Fuchtbauer, E. M., Vauti, F., Arnold, H. H., Schnutgen, F., Wurst, W., von Melchner, H. and Ruiz, P.** (2003). A large-scale, gene-driven mutagenesis approach for the functional analysis of the mouse genome. *Proc Natl Acad Sci U S A* **100**, 9918-22.
- Harmer, N. J., Sivak, J. M., Amaya, E. and Blundell, T. L.** (2005). 1.15Å Crystal structure of the X. tropicalis Spred1 EVH1 domain suggests a fourth distinct peptide-binding mechanism within the EVH1 family. *FEBS Lett* **579**, 1161-6.
- Hart, K. C., Robertson, S. C., Kanemitsu, M. Y., Meyer, A. N., Tynan, J. A. and Donoghue, D. J.** (2000). Transformation and Stat activation by derivatives of FGFR1, FGFR3, and FGFR4. *Oncogene* **19**, 3309-20.
- Hashimoto, S., Nakano, H., Singh, G. and Katyal, S.** (2002). Expression of Spred and Sprouty in developing rat lung. *Mech Dev* **119 Suppl 1**, S303-9.
- Hauser, W., Knobloch, K. P., Eigenthaler, M., Gambaryan, S., Krenn, V., Geiger, J., Glazova, M., Rohde, E., Horak, I., Walter, U. et al.** (1999). Megakaryocyte hyperplasia and enhanced agonist-induced platelet activation in vasodilator-stimulated phosphoprotein knockout mice. *Proc Natl Acad Sci U S A* **96**, 8120-5.
- Impagnatiello, M. A., Weitzer, S., Gannon, G., Compagni, A., Cotten, M. and Christofori, G.** (2001). Mammalian sprouty-1 and -2 are membrane-anchored phosphoprotein inhibitors of growth factor signaling in endothelial cells. *J Cell Biol* **152**, 1087-98.
- Inoue, H., Kato, R., Fukuyama, S., Nonami, A., Taniguchi, K., Matsumoto, K., Nakano, T., Tsuda, M., Matsumura, M., Kubo, M. et al.** (2005). Spred-1 negatively regulates allergen-induced airway eosinophilia and hyperresponsiveness. *J Exp Med* **201**, 73-82.
- Iwata, T., Chen, L., Li, C., Ovchinnikov, D. A., Behringer, R. R., Francomano, C. A. and Deng, C. X.** (2000). A neonatal lethal mutation in FGFR3 uncouples proliferation and differentiation of growth plate chondrocytes in embryos. *Hum Mol Genet* **9**, 1603-13.

- Iwata, T., Li, C. L., Deng, C. X. and Francomano, C. A.** (2001). Highly activated Fgfr3 with the K644M mutation causes prolonged survival in severe dwarf mice. *Hum Mol Genet* **10**, 1255-64.
- Kanai, M., Goke, M., Tsunekawa, S. and Podolsky, D. K.** (1997). Signal transduction pathway of human fibroblast growth factor receptor 3. Identification of a novel 66-kDa phosphoprotein. *J Biol Chem* **272**, 6621-8.
- Kato, A., Ozawa, F., Saitoh, Y., Fukazawa, Y., Sugiyama, H. and Inokuchi, K.** (1998). Novel members of the Ves1/Homer family of PDZ proteins that bind metabotropic glutamate receptors. *J Biol Chem* **273**, 23969-75.
- Kato, R., Nonami, A., Taketomi, T., Wakioka, T., Kuroiwa, A., Matsuda, Y. and Yoshimura, A.** (2003). Molecular cloning of mammalian Spred-3 which suppresses tyrosine kinase-mediated Erk activation. *Biochem Biophys Res Commun* **302**, 767-72.
- Kerkhoff, E. and Rapp, U. R.** (2001). The Ras-Raf relationship: an unfinished puzzle. *Adv Enzyme Regul* **41**, 261-7.
- Klostermann, A., Lutz, B., Gertler, F. and Behl, C.** (2000). The orthologous human and murine semaphorin 6A-1 proteins (SEMA6A-1/Sema6A-1) bind to the enabled/vasodilator-stimulated phosphoprotein-like protein (EVL) via a novel carboxyl-terminal zyxin-like domain. *J Biol Chem* **275**, 39647-53.
- Koike, M., Yamanaka, Y., Inoue, M., Tanaka, H., Nishimura, R. and Seino, Y.** (2003). Insulin-like growth factor-1 rescues the mutated FGF receptor 3 (G380R) expressing ATDC5 cells from apoptosis through phosphatidylinositol 3-kinase and MAPK. *J Bone Miner Res* **18**, 2043-51.
- Kong, M., Wang, C. S. and Donoghue, D. J.** (2002). Interaction of fibroblast growth factor receptor 3 and the adapter protein SH2-B. A role in STAT5 activation. *J Biol Chem* **277**, 15962-70.
- Kramer, S., Okabe, M., Hacohen, N., Krasnow, M. A. and Hiromi, Y.** (1999). Sprouty: a common antagonist of FGF and EGF signaling pathways in *Drosophila*. *Development* **126**, 2515-25.
- Krause, M., Sechi, A. S., Konradt, M., Monner, D., Gertler, F. B. and Wehland, J.** (2000). Fyn-binding protein (Fyb)/SLP-76-associated protein (SLAP), Ena/vasodilator-stimulated phosphoprotein (VASP) proteins and the Arp2/3 complex link T cell receptor (TCR) signaling to the actin cytoskeleton. *J Cell Biol* **149**, 181-94.
- Kronenberg, H. M.** (2003). Developmental regulation of the growth plate. *Nature* **423**, 332-6.
- Kunath, T., Gish, G., Lickert, H., Jones, N., Pawson, T. and Rossant, J.** (2003). Transgenic RNA interference in ES cell-derived embryos recapitulates a genetic null phenotype. *Nat Biotechnol* **21**, 559-61.
- Lander, E. S., Linton, L. M., Birren, B., Nusbaum, C., Zody, M. C., Baldwin, J., Devon, K., Dewar, K., Doyle, M., FitzHugh, W. et al.** (2001). Initial sequencing and analysis of the human genome. *Nature* **409**, 860-921.
- Lanier, L. M., Gates, M. A., Witke, W., Menzies, A. S., Wehman, A. M., Macklis, J. D., Kwiatkowski, D., Soriano, P. and Gertler, F. B.** (1999). Mena is required for neurulation and commissure formation. *Neuron* **22**, 313-25.
- Lanier, L. M. and Gertler, F. B.** (2000). From Abl to actin: Abl tyrosine kinase and associated proteins in growth cone motility. *Curr Opin Neurobiol* **10**, 80-7.
- Lee, D. L., Webb, R. C. and Jin, L.** (2004). Hypertension and RhoA/Rho-kinase signaling in the vasculature: highlights from the recent literature. *Hypertension* **44**, 796-9.
- Lee, S. H., Schloss, D. J., Jarvis, L., Krasnow, M. A. and Swain, J. L.** (2001). Inhibition of angiogenesis by a mouse sprouty protein. *J Biol Chem* **276**, 4128-33.
- Leeksa, O. C., Van Achterberg, T. A., Tsumura, Y., Toshima, J., Eldering, E., Kroes, W. G., Mellink, C., Spaargaren, M., Mizuno, K., Pannekoek, H. et al.** (2002). Human

- sprouty 4, a new ras antagonist on 5q31, interacts with the dual specificity kinase TESK1. *Eur J Biochem* **269**, 2546-56.
- Legeai-Mallet, L., Benoist-Lasselien, C., Delezoide, A. L., Munnich, A. and Bonaventure, J.** (1998). Fibroblast growth factor receptor 3 mutations promote apoptosis but do not alter chondrocyte proliferation in thanatophoric dysplasia. *J Biol Chem* **273**, 13007-14.
- Li, C., Chen, L., Iwata, T., Kitagawa, M., Fu, X. Y. and Deng, C. X.** (1999). A Lys644Glu substitution in fibroblast growth factor receptor 3 (FGFR3) causes dwarfism in mice by activation of STATs and ink4 cell cycle inhibitors. *Hum Mol Genet* **8**, 35-44.
- Lim, J., Wong, E. S., Ong, S. H., Yusoff, P., Low, B. C. and Guy, G. R.** (2000). Sprouty proteins are targeted to membrane ruffles upon growth factor receptor tyrosine kinase activation. Identification of a novel translocation domain. *J Biol Chem* **275**, 32837-45.
- Lim, J., Yusoff, P., Wong, E. S., Chandramouli, S., Lao, D. H., Fong, C. W. and Guy, G. R.** (2002). The cysteine-rich sprouty translocation domain targets mitogen-activated protein kinase inhibitory proteins to phosphatidylinositol 4,5-bisphosphate in plasma membranes. *Mol Cell Biol* **22**, 7953-66.
- Liu, Z., Xu, J., Colvin, J. S. and Ornitz, D. M.** (2002). Coordination of chondrogenesis and osteogenesis by fibroblast growth factor 18. *Genes Dev* **16**, 859-69.
- Lowy, D. R. and Willumsen, B. M.** (1993). Function and regulation of ras. *Annu Rev Biochem* **62**, 851-91.
- Machesky, L. M.** (2000). Putting on the brakes: a negative regulatory function for Ena/VASP proteins in cell migration. *Cell* **101**, 685-8.
- Martinez-Quiles, N., Rohatgi, R., Anton, I. M., Medina, M., Saville, S. P., Miki, H., Yamaguchi, H., Takenawa, T., Hartwig, J. H., Geha, R. S. et al.** (2001). WIP regulates N-WASP-mediated actin polymerization and filopodium formation. *Nat Cell Biol* **3**, 484-91.
- Massberg, S., Gruner, S., Konrad, I., Garcia Arguinzonis, M. I., Eigenthaler, M., Hemler, K., Kersting, J., Schulz, C., Muller, I., Besta, F. et al.** (2004). Enhanced in vivo platelet adhesion in vasodilator-stimulated phosphoprotein (VASP)-deficient mice. *Blood* **103**, 136-42.
- Menzies, A. S., Aszodi, A., Williams, S. E., Pfeifer, A., Wehman, A. M., Goh, K. L., Mason, C. A., Fassler, R. and Gertler, F. B.** (2004). Mena and vasodilator-stimulated phosphoprotein are required for multiple actin-dependent processes that shape the vertebrate nervous system. *J Neurosci* **24**, 8029-38.
- Minowada, G., Jarvis, L. A., Chi, C. L., Neubuser, A., Sun, X., Hacoheh, N., Krasnow, M. A. and Martin, G. R.** (1999). Vertebrate Sprouty genes are induced by FGF signaling and can cause chondrodysplasia when overexpressed. *Development* **126**, 4465-75.
- Miyoshi, K., Wakioka, T., Nishinakamura, H., Kamio, M., Yang, L., Inoue, M., Hasegawa, M., Yonemitsu, Y., Komiya, S. and Yoshimura, A.** (2004). The Sprouty-related protein, Spred, inhibits cell motility, metastasis, and Rho-mediated actin reorganization. *Oncogene* **23**, 5567-76.
- Morrison, D. K. and Cutler, R. E.** (1997). The complexity of Raf-1 regulation. *Curr Opin Cell Biol* **9**, 174-9.
- Moses, K., Ellis, M. C. and Rubin, G. M.** (1989). The glass gene encodes a zinc-finger protein required by Drosophila photoreceptor cells. *Nature* **340**, 531-6.
- Murakami, S., Balmes, G., McKinney, S., Zhang, Z., Givol, D. and de Crombrughe, B.** (2004). Constitutive activation of MEK1 in chondrocytes causes Stat1-independent achondroplasia-like dwarfism and rescues the Fgfr3-deficient mouse phenotype. *Genes Dev* **18**, 290-305.
- Murakami, S., Kan, M., McKeehan, W. L. and de Crombrughe, B.** (2000). Up-regulation of the chondrogenic Sox9 gene by fibroblast growth factors is mediated by the mitogen-activated protein kinase pathway. *Proc Natl Acad Sci U S A* **97**, 1113-8.

- Nadeau, J. H., Balling, R., Barsh, G., Beier, D., Brown, S. D., Bucan, M., Camper, S., Carlson, G., Copeland, N., Eppig, J. et al.** (2001). Sequence interpretation. Functional annotation of mouse genome sequences. *Science* **291**, 1251-5.
- Naski, M. C. and Ornitz, D. M.** (1998). FGF signaling in skeletal development. *Front Biosci* **3**, D781-94.
- Niebuhr, K., Ebel, F., Frank, R., Reinhard, M., Domann, E., Carl, U. D., Walter, U., Gertler, F. B., Wehland, J. and Chakraborty, T.** (1997). A novel proline-rich motif present in ActA of *Listeria monocytogenes* and cytoskeletal proteins is the ligand for the EVH1 domain, a protein module present in the Ena/VASP family. *Embo J* **16**, 5433-44.
- Nobuhisa, I., Kato, R., Inoue, H., Takizawa, M., Okita, K., Yoshimura, A. and Taga, T.** (2004). Spred-2 suppresses aorta-gonad-mesonephros hematopoiesis by inhibiting MAP kinase activation. *J Exp Med* **199**, 737-42.
- Nonami, A., Kato, R., Taniguchi, K., Yoshiga, D., Taketomi, T., Fukuyama, S., Harada, M., Sasaki, A. and Yoshimura, A.** (2004). Spred-1 negatively regulates interleukin-3-mediated ERK/MAP kinase activation in hematopoietic cells. *J Biol Chem*.
- Oberklaid, F., Danks, D. M., Jensen, F., Stace, L. and Rosshandler, S.** (1979). Achondroplasia and hypochondroplasia. Comments on frequency, mutation rate, and radiological features in skull and spine. *J Med Genet* **16**, 140-6.
- Ohbayashi, N., Shibayama, M., Kurotaki, Y., Imanishi, M., Fujimori, T., Itoh, N. and Takada, S.** (2002). FGF18 is required for normal cell proliferation and differentiation during osteogenesis and chondrogenesis. *Genes Dev* **16**, 870-9.
- Peters, K., Ornitz, D., Werner, S. and Williams, L.** (1993). Unique expression pattern of the FGF receptor 3 gene during mouse organogenesis. *Dev Biol* **155**, 423-30.
- Petit, M. M., Fradelizi, J., Golsteyn, R. M., Ayoubi, T. A., Menichi, B., Louvard, D., Van de Ven, W. J. and Friederich, E.** (2000). LPP, an actin cytoskeleton protein related to zyxin, harbors a nuclear export signal and transcriptional activation capacity. *Mol Biol Cell* **11**, 117-29.
- Ramesh, N., Anton, I. M., Hartwig, J. H. and Geha, R. S.** (1997). WIP, a protein associated with wiskott-aldrich syndrome protein, induces actin polymerization and redistribution in lymphoid cells. *Proc Natl Acad Sci U S A* **94**, 14671-6.
- Rechsteiner, M. and Rogers, S. W.** (1996). PEST sequences and regulation by proteolysis. *Trends Biochem Sci* **21**, 267-71.
- Reich, A., Sapir, A. and Shilo, B.** (1999). Sprouty is a general inhibitor of receptor tyrosine kinase signaling. *Development* **126**, 4139-47.
- Reinhard, M., Jarchau, T. and Walter, U.** (2001). Actin-based motility: stop and go with Ena/VASP proteins. *Trends Biochem Sci* **26**, 243-9.
- Reinhard, M., Jouvenal, K., Tripier, D. and Walter, U.** (1995). Identification, purification, and characterization of a zyxin-related protein that binds the focal adhesion and microfilament protein VASP (vasodilator-stimulated phosphoprotein). *Proc Natl Acad Sci U S A* **92**, 7956-60.
- Reinhard, M., Rudiger, M., Jockusch, B. M. and Walter, U.** (1996). VASP interaction with vinculin: a recurring theme of interactions with proline-rich motifs. *FEBS Lett* **399**, 103-7.
- Reinhard, M., Zumbunn, J., Jaquemar, D., Kuhn, M., Walter, U. and Trueb, B.** (1999). An alpha-actinin binding site of zyxin is essential for subcellular zyxin localization and alpha-actinin recruitment. *J Biol Chem* **274**, 13410-8.
- Renfranz, P. J. and Beckerle, M. C.** (2002). Doing (F/L)PPPPs: EVH1 domains and their proline-rich partners in cell polarity and migration. *Curr Opin Cell Biol* **14**, 88-103.
- Robinson, M. J. and Cobb, M. H.** (1997). Mitogen-activated protein kinase pathways. *Curr Opin Cell Biol* **9**, 180-6.

- Rousseau, F., Bonaventure, J., Legeai-Mallet, L., Pelet, A., Rozet, J. M., Maroteaux, P., Le Merrer, M. and Munnich, A. (1994). Mutations in the gene encoding fibroblast growth factor receptor-3 in achondroplasia. *Nature* **371**, 252-4.
- Rubin, C., Litvak, V., Medvedovsky, H., Zwang, Y., Lev, S. and Yarden, Y. (2003). Sprouty fine-tunes EGF signaling through interlinked positive and negative feedback loops. *Curr Biol* **13**, 297-307.
- Sahni, M., Ambrosetti, D. C., Mansukhani, A., Gertner, R., Levy, D. and Basilico, C. (1999). FGF signaling inhibits chondrocyte proliferation and regulates bone development through the STAT-1 pathway. *Genes Dev* **13**, 1361-6.
- Sala, C., Piech, V., Wilson, N. R., Passafaro, M., Liu, G. and Sheng, M. (2001). Regulation of dendritic spine morphology and synaptic function by Shank and Homer. *Neuron* **31**, 115-30.
- Sasaki, A., Taketomi, T., Kato, R., Saeki, K., Nonami, A., Sasaki, M., Kuriyama, M., Saito, N., Shibuya, M. and Yoshimura, A. (2003). Mammalian Sprouty4 suppresses Ras-independent ERK activation by binding to Raf1. *Nat Cell Biol* **5**, 427-32.
- Sasaki, A., Taketomi, T., Wakioka, T., Kato, R. and Yoshimura, A. (2001). Identification of a dominant negative mutant of Sprouty that potentiates fibroblast growth factor- but not epidermal growth factor-induced ERK activation. *J Biol Chem* **276**, 36804-8.
- Schlessinger, J. (2000). Cell signaling by receptor tyrosine kinases. *Cell* **103**, 211-25.
- Segev, O., Chumakov, I., Nevo, Z., Givol, D., Madar-Shapiro, L., Sheinin, Y., Weinreb, M. and Yayon, A. (2000). Restrained chondrocyte proliferation and maturation with abnormal growth plate vascularization and ossification in human FGFR-3(G380R) transgenic mice. *Hum Mol Genet* **9**, 249-58.
- Shiang, R., Thompson, L. M., Zhu, Y. Z., Church, D. M., Fielder, T. J., Bocian, M., Winokur, S. T. and Wasmuth, J. J. (1994). Mutations in the transmembrane domain of FGFR3 cause the most common genetic form of dwarfism, achondroplasia. *Cell* **78**, 335-42.
- Skarnes, W. C., von Melchner, H., Wurst, W., Hicks, G., Nord, A. S., Cox, T., Young, S. G., Ruiz, P., Soriano, P., Tessier-Lavigne, M. et al. (2004). A public gene trap resource for mouse functional genomics. *Nat Genet* **36**, 543-4.
- Snapper, S. B., Rosen, F. S., Mizoguchi, E., Cohen, P., Khan, W., Liu, C. H., Hagemann, T. L., Kwan, S. P., Ferrini, R., Davidson, L. et al. (1998). Wiskott-Aldrich syndrome protein-deficient mice reveal a role for WASP in T but not B cell activation. *Immunity* **9**, 81-91.
- Somlyo, A. P. and Somlyo, A. V. (2003). Ca²⁺ sensitivity of smooth muscle and nonmuscle myosin II: modulated by G proteins, kinases, and myosin phosphatase. *Physiol Rev* **83**, 1325-58.
- Stanford, W. L., Cohn, J. B. and Cordes, S. P. (2001). Gene-trap mutagenesis: past, present and beyond. *Nat Rev Genet* **2**, 756-68.
- Sternberg, P. W. and Alberola-Ila, J. (1998). Conspiracy theory: RAS and RAF do not act alone. *Cell* **95**, 447-50.
- Stryke, D., Kawamoto, M., Huang, C. C., Johns, S. J., King, L. A., Harper, C. A., Meng, E. C., Lee, R. E., Yee, A., L'Italien, L. et al. (2003). BayGenomics: a resource of insertional mutations in mouse embryonic stem cells. *Nucleic Acids Res* **31**, 278-81.
- Su, W. C., Kitagawa, M., Xue, N., Xie, B., Garofalo, S., Cho, J., Deng, C., Horton, W. A. and Fu, X. Y. (1997). Activation of Stat1 by mutant fibroblast growth-factor receptor in thanatophoric dysplasia type II dwarfism. *Nature* **386**, 288-92.
- Symons, M., Derry, J. M., Karlak, B., Jiang, S., Lemahieu, V., McCormick, F., Francke, U. and Abo, A. (1996). Wiskott-Aldrich syndrome protein, a novel effector for the GTPase CDC42Hs, is implicated in actin polymerization. *Cell* **84**, 723-34.
- Tavormina, P. L., Shiang, R., Thompson, L. M., Zhu, Y. Z., Wilkin, D. J., Lachman, R. S., Wilcox, W. R., Rimoin, D. L., Cohn, D. H. and Wasmuth, J. J. (1995). Thanatophoric

- dysplasia (types I and II) caused by distinct mutations in fibroblast growth factor receptor 3. *Nat Genet* **9**, 321-8.
- Tefft, D., Lee, M., Smith, S., Crowe, D. L., Bellusci, S. and Warburton, D.** (2002). mSprouty2 inhibits FGF10-activated MAP kinase by differentially binding to upstream target proteins. *Am J Physiol Lung Cell Mol Physiol* **283**, L700-6.
- Tefft, J. D., Lee, M., Smith, S., Leinwand, M., Zhao, J., Bringas, P., Jr., Crowe, D. L. and Warburton, D.** (1999). Conserved function of mSpry-2, a murine homolog of Drosophila sprouty, which negatively modulates respiratory organogenesis. *Curr Biol* **9**, 219-22.
- Tomlinson, A.** (1989). Short-range positional signals in the developing Drosophila eye. *Development* **107 Suppl**, 59-63.
- Tomlinson, A., Kimmel, B. E. and Rubin, G. M.** (1988). rough, a Drosophila homeobox gene required in photoreceptors R2 and R5 for inductive interactions in the developing eye. *Cell* **55**, 771-84.
- Treisman, J. E. and Rubin, G. M.** (1996). Targets of glass regulation in the Drosophila eye disc. *Mech Dev* **56**, 17-24.
- Valenzuela, D. M., Murphy, A. J., Friendewey, D., Gale, N. W., Economides, A. N., Auerbach, W., Poueymirou, W. T., Adams, N. C., Rojas, J., Yasenchak, J. et al.** (2003). High-throughput engineering of the mouse genome coupled with high-resolution expression analysis. *Nat Biotechnol* **21**, 652-9.
- Vasioukhin, V., Bauer, C., Yin, M. and Fuchs, E.** (2000). Directed actin polymerization is the driving force for epithelial cell-cell adhesion. *Cell* **100**, 209-19.
- Venter, J. C. Adams, M. D. Myers, E. W. Li, P. W. Mural, R. J. Sutton, G. G. Smith, H. O. Yandell, M. Evans, C. A. Holt, R. A. et al.** (2001). The sequence of the human genome. *Science* **291**, 1304-51.
- Wakioka, T., Sasaki, A., Kato, R., Shouda, T., Matsumoto, A., Miyoshi, K., Tsuneoka, M., Komiya, S., Baron, R. and Yoshimura, A.** (2001). Spred is a Sprouty-related suppressor of Ras signalling. *Nature* **412**, 647-51.
- Wallace, D. C.** (2001). Mouse models for mitochondrial disease. *Am J Med Genet* **106**, 71-93.
- Wang, Y., Spatz, M. K., Kannan, K., Hayk, H., Avivi, A., Gorivodsky, M., Pines, M., Yayon, A., Lonai, P. and Givol, D.** (1999). A mouse model for achondroplasia produced by targeting fibroblast growth factor receptor 3. *Proc Natl Acad Sci U S A* **96**, 4455-60.
- Waterston, R. H. Lindblad-Toh, K. Birney, E. Rogers, J. Abril, J. F. Agarwal, P. Agarwala, R. Ainscough, R. Alexandersson, M. An, P. et al.** (2002). Initial sequencing and comparative analysis of the mouse genome. *Nature* **420**, 520-62.
- Weksler, N. B., Lunstrum, G. P., Reid, E. S. and Horton, W. A.** (1999). Differential effects of fibroblast growth factor (FGF) 9 and FGF2 on proliferation, differentiation and terminal differentiation of chondrocytic cells in vitro. *Biochem J* **342 Pt 3**, 677-82.
- Wiles, M. V., Vauti, F., Otte, J., Fuchtbauer, E. M., Ruiz, P., Fuchtbauer, A., Arnold, H. H., Lehrach, H., Metz, T., von Melchner, H. et al.** (2000). Establishment of a gene-trap sequence tag library to generate mutant mice from embryonic stem cells. *Nat Genet* **24**, 13-4.
- Wong, E. S., Fong, C. W., Lim, J., Yusoff, P., Low, B. C., Langdon, W. Y. and Guy, G. R.** (2002). Sprouty2 attenuates epidermal growth factor receptor ubiquitylation and endocytosis, and consequently enhances Ras/ERK signalling. *Embo J* **21**, 4796-808.
- Wong, E. S., Lim, J., Low, B. C., Chen, Q. and Guy, G. R.** (2001). Evidence for direct interaction between Sprouty and Cbl. *J Biol Chem* **276**, 5866-75.
- Xiao, B., Tu, J. C. and Worley, P. F.** (2000). Homer: a link between neural activity and glutamate receptor function. *Curr Opin Neurobiol* **10**, 370-4.

- Yasoda, A., Komatsu, Y., Chusho, H., Miyazawa, T., Ozasa, A., Miura, M., Kurihara, T., Rogi, T., Tanaka, S., Suda, M. et al.** (2004). Overexpression of CNP in chondrocytes rescues achondroplasia through a MAPK-dependent pathway. *Nat Med* **10**, 80-6.
- Yigzaw, Y., Cartin, L., Pierre, S., Scholich, K. and Patel, T. B.** (2001). The C terminus of sprouty is important for modulation of cellular migration and proliferation. *J Biol Chem* **276**, 22742-7.
- Yusoff, P., Lao, D. H., Ong, S. H., Wong, E. S., Lim, J., Lo, T. L., Leong, H. F., Fong, C. W. and Guy, G. R.** (2002). Sprouty2 inhibits the Ras/MAP kinase pathway by inhibiting the activation of Raf. *J Biol Chem* **277**, 3195-201.
- Zambrowicz, B. P., Abuin, A., Ramirez-Solis, R., Richter, L. J., Piggott, J., BeltrandelRio, H., Buxton, E. C., Edwards, J., Finch, R. A., Friddle, C. J. et al.** (2003). Wnk1 kinase deficiency lowers blood pressure in mice: a gene-trap screen to identify potential targets for therapeutic intervention. *Proc Natl Acad Sci U S A* **100**, 14109-14.
- Zambrowicz, B. P., Friedrich, G. A., Buxton, E. C., Lilleberg, S. L., Person, C. and Sands, A. T.** (1998). Disruption and sequence identification of 2,000 genes in mouse embryonic stem cells. *Nature* **392**, 608-11.
- Zhang, Y., Proenca, R., Maffei, M., Barone, M., Leopold, L. and Friedman, J. M.** (1994). Positional cloning of the mouse obese gene and its human homologue. *Nature* **372**, 425-32.
- Zigmond, S. H.** (2000). In vitro actin polymerization using polymorphonuclear leukocyte extracts. *Methods Enzymol* **325**, 237-54.
- Zimmermann, J., Jarchau, T., Walter, U., Oschkinat, H. and Ball, L. J.** (2004). ¹H, ¹³C and ¹⁵N resonance assignment of the human Spred2 EVH1 domain. *J Biomol NMR* **29**, 435-6.

8. Abbreviations

Aa	Amino acids
Arp2/3	Actin-related protein 2/3 complex
β-geo	Beta-galactosidase and neomycin resistance fusion gene
bp	Basepair(s)
BSA	Bovine serum albumin
cAMP	Cyclic adenosine-3',5'-monophosphate
c-Cbl	Casitas B-lineage lymphoma proto-oncogene
cDNA	Coding DNA
cGMP	Cyclic guanosine-3',5'-monophosphate
CNP	C-type natriuretic peptide
CNS	Central nervous system
Cre	Cyclization recombination enzyme
CSF-1	Colony-stimulating-factor-1
DMEM	Dulbecco's modified eagle medium
DMSO	Dimethylsulfoxid
dNTP	Desoxyribonucleosidtriphosphates
dSprouty	Drosophila Sprouty
E2	Estradiol
E.coli	Escherichia coli
ECL	Enhanced chemiluminescence
EDTA	Ethylendiamine tetraacetic acid
EGF	Epidermal growth factor
En2	Engrailed2
Ena	Enabled
ERK	Extracellular stimulus-activated protein kinases
ES cells	Embryonic stem cells
EVH-1	Ena/vasodilator-stimulated phosphoprotein homology-1
Evl	Enabled/vasodilator-stimulated phosphoprotein-like protein
F-actin	Filamentous actin
FCS	Fetal calf serum
FGF	Fibroblast growth factor
Fig.	Figure
Flp	Flipase-recombinase
frt site	Flipase-recombinase targeting site
Fyb/SLAP	Fyn-binding protein/SLP-76-associated protein
GAPDH	Glyceraldehyde-3-phosphate dehydrogenase
Gap1	GTPase activating protein 1
Grb2	Growth factor receptor-bound protein 2
GSH	Glutathione
GST	Glutathione-S-transferase
Hb	Hemoglobin
HE	Hematoxylin/eosin staining
HEPES	N-2-hydroxyethylpiperazin-N'-2'-ethansulfonacid
Hk	Hematokrit
HMG-box	High mobility group box
HSV-TK	Herpes simplex virus-thymidine kinase
IGF-1	Insulin-like growth factor 1
IgG	Immunglobulin G
IL-3	Interleukin-3
IP3	Inositol-1,4,5-triphosphate
IPTG	Isopropyl β-D-thiogalactopyranoside
KBD	C-Kit binding domain
ko	Knockout

Abbreviations

LA-PCR	Long and accurate PCR
LB	Luria Bertani medium
loxP	Locus of X-over of P1
LPP	Lipoma-preferred partner
MAPK	Mitogen-activated protein kinase
MEK1	Mitogen-activated protein kinase (MAPK) kinase
Mena	Mammalian enabled
Neo	Neomycin
OD	Optical density
PAGE	Polyacrylamid gel electrophoresis
PBS	Phosphate-buffered saline
PCR	Polymerase Chain Reaction
PDGF	Platelet-derived growth factor
PEST	Proline (P), glutamic acid (E), serine (S), and threonine (T) domain
PFA	Paraformaldehyde
Pr.	Primer
RNase	Ribonuclease
Robo	Roundabout
RT-PCR	Reverse transcription-polymerase chain reaction
RTKs	Receptor tyrosin kinases
PTP1B	Protein-tyrosine-phosphatase 1B
SA	Splice acceptor
SAP	Shrimp alkaline phosphatase
SCF	Stem cell factor
SD	Splice donor
SDS	Sodiumdodecylsulfate
Sema6A-1	Semaphorin 6A-1
SMIF	Smad4-interacting transcriptional co-activator
Sos	Son of sevenless
SPR	Sprouty domain
Spred	Sprouty-related protein with an EVH1 domain
Spry	Sprouty
STAT	Signal transducer and activator of a transcription
T3	3,5,3'-triiodothyronine
T4	Thyroxin
TEMED	N,N,N',N'-Tetramethyldiamine
TGF- β	Transforming growth factor beta
Tris	Trishydroxymethylaminomethan
TSH	Thyroid-stimulating hormone
VASP	Vasodilatator-stimulated phosphoprotein
VEGF	Vascular epithelial growth factor
Vesl	<u>V</u> ASP/ <u>e</u> na-related gene up-regulated during <u>s</u> eizure and <u>L</u> TTP
WASP	Wiskott-Aldrich syndrome protein
WH1	WASP homology 1
WIP	WASP interacting protein
wt	Wildtype
X-Gal	4-chloro-5-bromo-3-indolyl- β -galactosidase

9. Acknowledgments

First, I would like to address my gratitude to **Prof. Ulrich Walter** for giving me the possibility to do my PhD work in his group, and supporting me in all critical situations.

Furthermore, I thank **Prof. Georg Krohne** for his time and kindness to examine this work as 2. expert.

I specially thank **Dr. Kai Schuh** for his engagement supervising my work and all the long discussions, good ideas, helpful advises, and pleasant hours in the lab.

A lot of thanks to **Dr. Catherine Engelhardt** and **Constanze Blume**, who were very helpful with their discussions and made –together with a lot of other people- the work in the lab amusing. Thanks as well to **Dr. Thomas Renne**, who gave me the opportunity to work in the team of his NWG (Nachwuchsforschergruppe).

Moreover, I thank **Lilo Fischer** and **Heidi Runknagel** for their kind help with technical assistance.

I thank Baygenomics, San Francisco, USA (<http://baygenomics.ucsf.edu>), for providing the XB228 ES-cell line, and Dr. K.-P. Knobeloch of the Institute of Molecular Pharmacology, Berlin, for blastocyst injection of the XB228 ES cells and providing the resulting chimeras.

I thank Prof. J. Herz and Jochen Brich, Dallas, for providing the backbone gene targeting vector (KO/lox/frt pJB1).

Moreover, I thank Prof. Sendtner, Dr. S. Wiese, and K. Kalus of the Department of Neurobiology, University of Wuerzburg, for electroporation and cultivation of mouse ES cells. Furthermore, I thank Prof. Hahn, J. Hemmerich, A. Sauter, and D. Kurre of the Department for Radiology, University of Wuerzburg, for performing the X-ray exposures; Prof. Dietl, S. Blissing, and H. Blaut of the Department for Gynaecology, University of Wuerzburg, for steroid hormone measurements; A. Luthe of the Department for Endocrinology, University of Wuerzburg, for thyroid hormone measurements; Christoph Renne, Institute of Pathology, University of Frankfurt, and Stefan Gattenlöhner, Institute of Pathology, University of Würzburg, for evaluation of histological sections; and T. Schinke and M. Amling of the Department for Experimental Surgery, University of Hamburg, for performing the toluidine staining of tibia and growth plate measurements.

My work was supported by grants of the IZKF Wuerzburg (MD/PhD Stipendium) and the “Deutsche Vereinigte Gesellschaft für Klinische Chemie und Laboratoriumsmedizin“ (“DGKL Scherer-Stipendium”).

Very special thanks are addressed to my husband **Christoph** and our son **Sebastian**, who were extremely patient with me and accepted and supported my work whenever it was possible and underlined it with a happy and satisfied private life.

Additionally, I thank **my parents** for their great support during my whole education and all the thousands of little things to make this work possible for me.

10. Curriculum Vitae

Personal details

Name Karin Andrea Bundschu (maiden name: Geis)
Date and place of birth 30.12.1973, Frankfurt/Main
Nationality German
Marital Status Married, 1 son (*27.08.2003)

University

10/1993-3/2002 **Humanmedizin Studium**, University of Ulm
4/1999-3/2000 Praktisches klinisches Jahr (PJ): Gynaecology and Obstetrics, Surgery, Internal Medicine; University of Ulm
10/2001-3/2002 **Biologie Studium**, University of Würzburg (MD/PhD Program)
(Abschluss: Zulassung zur Promotion in der Biologischen Fakultät)

Studies abroad

2-4/1996 Gynaecology, Obstetrics and Paediatrics „Medfem Clinic“;
Johannesburg/ South Africa
7-8/1997 Orthopaedic surgery „The Toronto Hospital Western Division“;
Toronto/ Canada
8-9/1998 General Medicine „Family Practice Care Team of the George
Washington University“; Washington DC/ USA

Medical Dissertation

8/1996-11/1998 Experimental scientific work, Department of Biochemistry, group of Prof. Dr. D. Wedlich, University of Ulm
Topic: “Functional analyzes of murine p120CAS1B and PAR-1 in Xenopus embryos” (Summa cum laude)
7/2001 “Promotionspreis für hervorragende Promotionsleistung“; University of Ulm

Clinical work

8/2000-1/2002 Department of Gynaecology and Obstetrics, University of Würzburg
2/2002 Approbation

Additional scientific work

2/1998-8/2000 Experimental scientific work (DFG project) in the Department of Biochemistry, group of Prof. Dr. D. Wedlich; University of Ulm
Topic: “Molecular regulation of cell migration during gastrulation of Xenopus embryos by different members of the Xwnt family.”
12/2000-4/2001 Building and presentation of an interactive model for the „Science Street 2001“ in Leipzig (Pojekt im Jahr der Lebenswissenschaften des Bundesministeriums für Bildung und Forschung: Das Wunder Schwangerschaft. Warum akzeptiert der Körper der Mutter das Baby?)
11/2002-3/2005 Teaching (Anatomy and Physiology) at the „Berufsfachschule für Hebammen“, University of Würzburg

MD/PhD Program

10/2001 Candidate of the MD/PhD Program; IZKF, University of Würzburg
3/2002 Permission for scientific work to obtain the “Dr. rer. nat.” degree of the Biological Faculty of the University of Würzburg
4/2002-3/2005 Dissertation project in the Institute of Clinical Biochemistry and Pathobiochemistry, group of Prof. Dr. U. Walter, University of Würzburg
(*Topic:* “Generation and characterization of Spred-2 knockout mice”)

11. Publications

Geis K., Aberle H., Kühl M., Kemmler R., Wedlich D. (1998) Expression of murine p120CAS1B in *Xenopus* embryos effects head differentiation but not axis formation. *Development, Genes and Evolution* 207, 471-481

Kühl M., **Geis K.**, Sheldahl LC., Pukrop T., Moon RT., Wedlich D. (2001) Antagonistic regulation of convergent extension movements in *Xenopus* by Wnt/ β -catenin and Wnt/ Ca^{2+} signaling. *Mechanisms of Development* 106, 61-76

Geis K., Dietl J. (2001) The role of cytokines at the fetomaternal interface. *Zentralbl Gynakol* 123, 609-618

Geis K., Kämmerer U. (2001) Das Wunder Schwangerschaft. *Gynäkologische Nachrichten* 11, 24

Steck T., Kämmerer U., **Geis K.**, Dietl J. (2001) Störungen des intrauterinen Immunsystems bei Frauen mit wiederholten Aborten. *Reproduktionsmedizin* 17, 206-213

Geis K., Dietl J. (2002) Ilioinguinal nerve entrapment after Tension-free vaginal tape (TVT) procedure. *Int Urogynecol J* 13;136-138

Schuh K., Cartwright E. J., Jankevics E., **Bundschu K.**, Liebermann J., Williams J. C., Armesilla A. L., Emerson M., Oceandy D., Knobloch K. P., Neyses, L (2004). Plasma membrane Ca^{2+} ATPase 4 is required for sperm motility and male fertility. *J Biol Chem* 279, 28220-6

Engelhardt C. M., **Bundschu K.**, Messerschmitt M., Renne T., Walter U., Reinhard M., Schuh K. (2004). Expression and subcellular localization of Spred proteins in mouse and human tissues. *Histochem Cell Biol* 122, 527-538

Bundschu K., Knobloch K.-P., Ullrich M., Schinke T., Amling M., Engelhardt C.M., Renné T., Walter U., Schuh K. (2005). Gene disruption of *Spred-2* causes achondroplasia-like dwarfism in mice. *submitted*

Bundschu K., Gattenlöhner S., Knobloch K.-P., Walter U., Schuh K. (2005). Tissue-specific *Spred-2* promoter activity characterized by a gene trap approach. *submitted*